Determination of Lepton Flavor Mixing Parameters by Reactor Neutrinos

Hiroaki Sugiyama

Department of Physics, Graduate School of Science,
Tokyo Metropolitan University,
1-1 Minami-Osawa, Hachioji, Tokyo 192-0397, Japan

A dissertation submitted to
Graduate School of Science, Tokyo Metropolitan University

February 2004

Contents

1 Introduction and Summary **3**

2 Massive Neutrinos in a Minimal Extension of the Standard Model **7**

2.1 Massless Neutrinos in the Standard Model of Particle Physics 7

2.2 Physics of Massive Neutrinos 11

2.2.1 Neutrino oscillations in vacuum 11

2.2.2 Neutrino oscillations in matter 13

2.2.3 Majorana neutrinos 16

2.3 Number of Light Active Neutrinos 17

2.4 Direct measurement of Neutrino Mass 18

2.5 Neutrinoless Double Beta Decay 19

3 Recent Status of Neutrino Oscillation Experiments **23**

3.1 The 2-3 Sector 23

3.1.1 Atmospheric neutrino measurement 23

3.1.2 K2K experiment 24

3.2 The 1-2 Sector 26

3.2.1 Solar neutrino measurement 26

3.2.2 KamLAND experiment 30

3.3 The 1-3 Sector 32

3.3.1 CHOOZ experiment 32

3.3.2 Bugey experiment 34

4 Future Long Baseline Experiments and the Problem of Parameter Degeneracy **37**

4.1 Future Long Baseline Experiments 37

4.1.1 An overview 37

4.1.2 J-PARC to Kamioka experiment 39

4.2 The Problem of Parameter Degeneracy 45

4.2.1 An overview of the problem 45
4.2.2 Another viewpoint of the problem 49

5 Reactor Measurement of θ_{13} and Its Complementarity to Long Baseline Experiments 52

5.1 Possibility to Measure θ_{13} by the Future Reactor Experiment 52
5.1.1 Reactor experiment as a clean laboratory for θ_{13} measurement . . . 52
5.1.2 Near-far detector complex: basic concepts and estimation of sensitivity 54
5.2 Resolving the Parameter Degeneracy by Reactor Measurement of θ_{13} 60
5.2.1 Illustration of how reactor measurement helps resolve the $\{\theta_{13}, \theta_{23}\}$ degeneracy 61
5.2.2 Resolving power of the $\{\theta_{13}, \theta_{23}\}$ degeneracy by a reactor measurement 65

6 Exploring Leptonic CP Violation by Reactor and Neutrino Superbeam Experiments 68

6.1 Measurement of CP Violation in Long Baseline Experiments 68
6.2 Reactor-LBL Combined Measurement of CP Violation 69
6.3 Treatment of Errors in LBL and Reactor Experiments 70
6.3.1 Treatment of errors in the JPARC-HK experiment 70
6.3.2 Treatment of errors in the reactor experiment 75
6.4 Estimation of Sensitivity of Reactor-LBL Combined Detection of CP Violation 77
6.4.1 CP sensitivity in the case of known sign of Δm^2_{31} 79
6.4.2 CP sensitivity in the case of unknown sign of Δm^2_{31} 82

7 Conclusion 84

A Statistical Analysis 88

A.1 χ^2 Analysis 88
A.2 Cancellation of Errors by Near-Far Detector Comparison 90

Chapter 1

Introduction and Summary

The standard model of particle physics is one of the most successful theory in physics. It is consistent with almost all results of experiments up to now. It does not, however, seem to be ultimate one because, for example, the standard model does not include the gravity. Furthermore, the standard model has many parameters such as the Yukawa coupling constants between Higgs and each of the fermions; The values of the coupling constants are not predicted in the model but only tuned to produce observed masses of fermions. Thus, we crave to uncover phenomena which can not be explained in the natural way by the model as the hints for the physics beyond the standard model.

The neutrino is rather strange particle in the standard model. It had been regarded as unique massless fermion in the standard electro-weak model [1] which constitutes the standard model. Even after the discovery of the neutrino mass by the atmospheric neutrino measurement with Super-Kamiokande [2], the neutrino is unnaturally light compared with other fermions. It is interesting because smallness of the mass can be an indication of the existence of very large energy scale [3] where the physics beyond the standard model will unfold itself. On the other hand, the existence of neutrino masses leads to the lepton flavor mixing similarly to the quark mixing. However, it turned out that the structure of the flavor mixing in the lepton sector is quite different from that in the quark sector. Neutrino oscillation experiments have shown that the lepton sector has two large mixing angle in contrast to the small mixing nature of the quark sector. From those points of view, neutrino physics is interesting field, and exploring its properties is very important. In this thesis, the subject is how to determine their mixing parameters precisely.

The lepton flavor mixing is expressed with the Maki-Nakagawa-Sakata (MNS) matrix [4]. In the three neutrino scheme, the MNS matrix is parameterized by three mixing angles (θ_{12}, θ_{23}, and θ_{13}), two differences of squared masses (Δm^2_{21} and Δm^2_{31}), and a CP violating phase δ. The values of those parameters can be determined by the measurement of the neutrino oscillation due to the lepton flavor mixing. By measuring the deficit of

μ-flavor neutrinos produced in the atmosphere, Super-Kamiokande has shown that the neutrino oscillation occurs and neutrinos have their masses in 1998 [2]. Since nothing happened for e-flavor atmospheric neutrinos, the deficit of μ-flavor ones is understood as the oscillation to τ-flavor ones. Since the oscillation is characterized by the mixing of the 2-3 sector, the parameters in the sector have been explored by the measurement of atmospheric neutrinos. The consistent result is exhibited by the K2K experiment [5] which is the first long baseline experiment of the neutrino oscillation with the accelerator neutrino. On the other hand, the parameters in the 1-2 mixing sector have been determined as the solution of the solar neutrino problem. The solar neutrino problem, namely the remarkable deficiency of ν_e from the sun, was first recognized in the late 1960's [6, 7] and had been long-term problem. The deficiency is explained by the oscillation of ν_e characterized by the 1-2 mixing. Recently, the solution of the problem was pinned down by combining solar neutrino measurements [6, 8, 9, 10, 11] and the long baseline reactor neutrino measurement [12]. The atmospheric and solar neutrino measurements disclosed that the mixings of 2-3 and 1-2 sectors are both large.

The 1-3 mixing sector which includes CP violating phase have not been determined yet because of the smallness of the mixing. We have only an upper bound on the mixing $\sin^2 2\theta_{13} < 0.15$ imposed by the CHOOZ reactor experiment [13]. Measuring θ_{13} is very important because the value is directly related with the possibility of observing leptonic CP violation. The experiments for the observation of CP violation can not be started without finding that θ_{13} is not extremely small.

We discuss in this thesis the possibility to measure θ_{13} by the future reactor experiment with Kashiwazaki-Kariwa nuclear power plant [14] which is the most powerful ($24.3\mathrm{GW_{th}}$) in the world. Reducing systematic errors is crucial to improve the CHOOZ bound significantly. For this purpose, we develop two detector method by placing identical detectors at near and far from a reactor. It is estimated that the systematic error can be reduced from 2.7% of the CHOOZ experiment to 1% level by virtue of the cancellation of correlated systematic errors between the measurements with near and far detectors; Examples of correlated errors are the error on neutrino flux, the error on the cross section for the detection, and so on. Then, we find that the sensitivity to $\sin^2 2\theta_{13}$ is improved by about one order of magnitude. It is emphasized that the reactor measurement of $\sin^2 2\theta_{13}$ is the pure one without any ambiguity caused by other neutrino mixing parameters. We discuss also the application of the measurement of $\sin^2 2\theta_{13}$ with reactor $\overline{\nu}_e$.

The other way to measure $\sin^2 2\theta_{13}$ is the utilization of the long baseline (LBL) oscillation experiment of the accelerator neutrino. The appearance measurement by the LBL experiment is, however, afflicted with the problem of the so-called parameter degeneracy [15, 16, 17, 18] while the experiment potentially has high sensitivities to θ_{13} and

δ. There can be eight sets of parameter values that explain $P(\nu_\mu \to \nu_\mu)$, $P(\nu_\mu \to \nu_e)$, and $P(\overline{\nu}_\mu \to \overline{\nu}_e)$ because of the problem. Hence, studying how to resolve the problem is important for the determination of parameter values. Throughout this thesis, we focus on the J-PARC (Japan Proton Accelerator Research Complex) neutrino project [19] as the LBL experiment. In the J-PARC experiment with the beam of the first oscillation maximum energy $E = |\Delta m^2_{31}|L/2\pi$, eight solutions of $\sin^2 2\theta_{13}$ are effectively reduced to two solutions which correspond to the ambiguity of $\theta_{23} \leftrightarrow \pi/2 - \theta_{23}$[18, 20]; The ambiguity of θ_{23} is caused by the fact that the information of θ_{23} is obtained as $\sin^2 2\theta_{23}$ by ν_μ disappearance measurement: $\sin 2\theta_{23} = \sin(\pi - 2\theta_{23})$. We investigate the possibility of resolving the $\{\theta_{23}, \theta_{13}\}$ degeneracy in this thesis by combining the reactor experiment of θ_{13} with the J-PARC experiment [14]. The analysis is based on the comparison between the sensitivity of reactor experiment and the split of two $\sin^2 2\theta_{13}$ due to the degeneracy problem. If the reactor sensitivity is enough to exclude the fake solution, the θ_{23} degeneracy is resolved, and then the precise determination of unique values of θ_{13} and θ_{23} will be achieved.

We quest for also the leptonic CP violation. The conventional way to search for the CP violation is combining measurements of $P(\nu_\mu \to \nu_e)$ and $P(\overline{\nu}_\mu \to \overline{\nu}_e)$ in the LBL experiment. We consider, as a new possibility, combining $P(\nu_\mu \to \nu_e)$ measurement in the J-PARC phase II, where 4MW beam and Hyper-Kamiokande of 540kt fiducial mass are assumed, with $P(\overline{\nu}_e \to \overline{\nu}_e)$ measurement in the reactor experiment [21]. It is fruitful because the reactor experiment does not need to wait the completion of ν mode measurement of $P(\nu_\mu \to \nu_e)$ while $\overline{\nu}$ mode measurement must do. Thus, the reactor-LBL combined method can provide the first indication of the leptonic CP violation. We examine also the possibility of detecting CP violation by combining the reactor experiment with the J-PARC experiment without upgraded beam nor Hyper-Kamiokande, namely very long exposure with 0.75MW beam and Super-Kamiokande of 22.5kt fiducial mass.

This thesis is composed as follows. First of all, we overview the theory of neutrinos and their masses in Chapter 2. The theory of the neutrino oscillation is explained also in the chapter. Chapter 3 is devoted to a review of the recent status of neutrino oscillation experiments. We survey the future long baseline accelerator experiments in Chapter 4 with particular emphasis on the J-PARC neutrino project. The problem of parameter degeneracy, from which LBL experiments suffer, is also described in this chapter. The reactor experiment for θ_{13} measurement with Kashiwazaki-Kariwa nuclear power plant, which plays the most important role in this thesis, is addressed in Chapter 5. Then, we discuss about the possibility of resolving the parameter degeneracy problem by combining reactor and the J-PARC (ν mode and $\overline{\nu}$ mode) experiments. The discussion in this chapter is based on [14]. Finally, we investigate the possibility of observing the leptonic CP

violation by combining reactor and J-PARC (ν mode) experiments in Chapter 6. The work in this chapter rests on [21]. We conclude in Chapter 7. The prescription for statistical analysis is explained briefly in Appendix.

Throughout this thesis, we use the data summarized in the reference [22] and the natural unit in which each of the reduced Planck constant ($\hbar \equiv h/2\pi = 6.6 \times 10^{-22}\mathrm{MeV}\cdot\mathrm{s}$) and the speed of light ($c = 3 \times 10^{8}\mathrm{m}\cdot\mathrm{s}^{-1}$) is regarded as unity. I mention also an useful website [23] on neutrinos.

Chapter 2

Massive Neutrinos in a Minimal Extension of the Standard Model

2.1 Massless Neutrinos in the Standard Model of Particle Physics

The standard model of the particle physics is so powerful that it explains most of the results of existing experiments. It is made up of the Quantum ChromoDynamics (QCD) and the standard electroweak model [1] which includes neutrinos. In this section, only the standard electroweak model is overviewed with emphasis on neutrinos. The standard electroweak model is based on the $SU(2)_L \times U(1)_Y$ gauge symmetry. The gauge bosons are denoted as $W^i_\mu (i = 1, 2, 3)$ and B_μ for $SU(2)_L$ and $U(1)_Y$, respectively. All of fermion fields ψ can be projected to the left-handed and right-handed ones as

$$\psi_L \equiv \frac{1}{2}\left(1-\gamma^5\right)\psi,\ \psi_R \equiv \frac{1}{2}\left(1+\gamma^5\right)\psi,\quad \gamma^5 \equiv \begin{pmatrix} -1 & 0 \\ 0 & 1 \end{pmatrix}. \tag{2.1}$$

The left-handed leptons and quarks form the doublets with respect to $SU(2)_L$:

$$L_1,\, L_2,\, L_3 \ \equiv\ \begin{pmatrix} \nu'_{eL} \\ e'_L \end{pmatrix},\ \begin{pmatrix} \nu'_{\mu L} \\ \mu'_L \end{pmatrix},\ \begin{pmatrix} \nu'_{\tau L} \\ \tau'_L \end{pmatrix}, \tag{2.2}$$

$$Q_1,\, Q_2,\, Q_3 \ \equiv\ \begin{pmatrix} u'_L \\ d'_L \end{pmatrix},\ \begin{pmatrix} c'_L \\ s'_L \end{pmatrix},\ \begin{pmatrix} t'_L \\ b'_L \end{pmatrix}, \tag{2.3}$$

where the "prime" is used for convenience in the following part. On the other hand, the right-handed fermions are regarded as the singlets under $SU(2)_L$ transformation:

$$e'_R, \cdots,\ u'_R, \cdots,\ d'_R, \cdots. \tag{2.4}$$

Note that the right-handed neutrinos are not included because neutrinos are assumed to be massless in the model. We deal with only the particles of the first generation for the time being for simplicity. The gauge symmetries forbid not only the gauge bosons but also the fermions to have their mass terms because ψ_L and ψ_R belong to different representations of $SU(2)_L$; The mass terms $m\overline{\psi_R}\psi_L$ are not invariant with respect to the gauge transformations. The Higgs mechanism enable us to get over the difficulty. We introduce Higgs bosons as a $SU(2)_L$ doublet

$$\phi \equiv \begin{pmatrix} \phi^+ \\ \phi^0 \end{pmatrix}, \tag{2.5}$$

and their potential

$$V(\phi) \equiv -\lambda^2 v^2 \phi^\dagger \phi + \frac{\lambda^2}{2}\left(\phi^\dagger \phi\right)^2. \tag{2.6}$$

The potential has the minimum (vacuum) at non-zero ϕ, and we choose it as

$$\phi_0 \equiv \frac{1}{\sqrt{2}} \begin{pmatrix} 0 \\ v \end{pmatrix}. \tag{2.7}$$

Any other choice of the vacuum can be made to the above one by an appropriate $SU(2)_L$ transformation. Once we have chosen a vacuum, the symmetry $SU(2)_L \times U(1)_Y$ is spontaneously broken in the theory constructed on the ground state. Then, the mass terms of the gauge bosons arise from the kinetic term for the Higgs boson

$$\begin{aligned} |D_\mu \phi|^2 &\equiv \left| \left(\partial_\mu - igW_\mu^i \hat{T}^i - ig' \frac{\hat{Y}}{2} B_\mu \right) \phi \right|^2 \\ &= \left| \frac{1}{\sqrt{2}} \left(-igW_\mu^i \frac{\sigma^i}{2} - ig' \frac{1}{2} B_\mu \right) \begin{pmatrix} 0 \\ v \end{pmatrix} \right|^2 + \cdots \\ &= \frac{1}{2}\frac{v^2}{4} \left\{ g^2 (W_\mu^1)^2 + g^2 (W_\mu^2)^2 + (-gW_\mu^3 + g' B_\mu)^2 \right\} + \cdots, \end{aligned} \tag{2.8}$$

where $\hat{T}^i = \sigma^i/2$ and $\hat{Y}/2$ represent the generators of $SU(2)_L$ and $U(1)_Y$, respectively; The charge assignments for each particles are listed in the Table 2.1. We can identify the three massive bosons in (2.8) as $W^\pm$ and Z bosons:

$$\begin{aligned} W_\mu^\pm &= \frac{1}{\sqrt{2}} \left(W_\mu^1 \mp i W_\mu^2 \right), \qquad m_W = g\frac{v}{2}, \\ Z_\mu &= \frac{1}{\sqrt{g^2 + (g')^2}} \left(g W_\mu^3 - g' B_\mu \right), \quad m_Z = \sqrt{g^2 + (g')^2}\, \frac{v}{2} \end{aligned} \tag{2.9}$$

The fourth gauge boson A_μ, which is orthogonal to Z, is massless and identified as the photon:

$$\begin{pmatrix} Z_\mu \\ A_\mu \end{pmatrix} = \begin{pmatrix} \cos\theta_w & -\sin\theta_w \\ \sin\theta_w & \cos\theta_w \end{pmatrix} \begin{pmatrix} W_\mu^3 \\ B_\mu \end{pmatrix},$$

	u_L	d_L	ν_{eL}	e_L	u_R	d_R	e_R	ϕ^+	ϕ^0
T^3 for $SU(2)_L$	$1/2$	$-1/2$	$1/2$	$-1/2$	0	0	0	$1/2$	$-1/2$
$Y/2$ for $U(1)_Y$	$1/6$	$1/6$	$-1/2$	$-1/2$	$2/3$	$-1/3$	-1	$1/2$	$1/2$
$Q_{\rm EM}$ for $U(1)_{\rm EM}$	$2/3$	$-1/3$	0	-1	$2/3$	$-1/3$	-1	1	0

Table 2.1: Listed are the charge assignments for the particles in the standard electroweak model of $SU(2)_L \times U(1)_Y$. The electro-magnetic charges are obtained by $Q_{\rm EM} = T^3 + Y/2$.

$$\cos\theta_w \equiv \frac{g}{\sqrt{g^2 + (g')^2}}, \quad \sin\theta_w \equiv \frac{g'}{\sqrt{g^2 + (g')^2}}. \tag{2.10}$$

Note that m_W and m_Z have the relation

$$m_W = m_Z \cos\theta_w. \tag{2.11}$$

The experimental results, which are $m_Z = 91$GeV [24] and $m_W = 80$GeV [24, 25], show $\cos\theta_w = 0.88$; It is consistent completely with the result $\sin^2\theta_w = 0.23$ obtained by the measurement of $\nu_\mu e$ and $\overline{\nu}_\mu e$ elastic scatterings [26]. Eventually, the original $SU(2)_L \times U(1)_Y$ is spontaneously broken by the Higgs boson to $U(1)_{\rm EM}$ which conserves the electro-magnetic charge. In terms of those massive gauge bosons, the covariant derivative becomes

$$\begin{aligned} D_\mu &= \partial_\mu - igW_\mu^i \hat{T}^i - ig'\frac{\hat{Y}}{2}B_\mu \\ &= \partial_\mu - i\frac{g}{\sqrt{2}}\left(W_\mu^+ \hat{T}^+ + W_\mu^- \hat{T}^-\right) \\ &\quad - i\frac{g}{\cos\theta_w}Z_\mu \left\{\hat{T}^3 - \left(\hat{T}^3 + \frac{\hat{Y}}{2}\right)\sin^2\theta_w\right\} \\ &\quad - ig\sin\theta_w A_\mu \left(\hat{T}^3 + \frac{\hat{Y}}{2}\right), \end{aligned} \tag{2.12}$$

where $\hat{T}^\pm \equiv \hat{T}^1 \pm i\hat{T}^2$. It is found by the last term in (2.12) that the coupling constant of the electro-magnetic interaction, which is the electron charge e, is

$$e = g\sin\theta_w \simeq 0.47\, g, \tag{2.13}$$

and the generator $\hat{Q}_{\rm EM}$ for $U(1)_{\rm EM}$ is

$$\hat{Q}_{\rm EM} = \hat{T}^3 + \frac{\hat{Y}}{2}. \tag{2.14}$$

It is seen in Table 2.1 that T_3 and Y are assigned to each particle so that the values of the charge $Q_{\rm EM}$ are consistent with the measurement. The fermions couple with those gauge

bosons as

$$\begin{aligned}\sum_j \overline{\psi}_j (i\not{D}) \psi_j &= \overline{L}\,(i\not{\partial}) L + \overline{e'_R}\,(i\not{\partial}) e'_R + \cdots \\ &\quad + g\left(W^+_\mu J^{\mu+}_{\rm CC} + W^-_\mu J^{\mu-}_{\rm CC} + Z_\mu J^\mu_{\rm NC}\right) + eA_\mu J^\mu_{\rm EM}, \end{aligned} \tag{2.15}$$

where

$$J^{\mu+}_{\rm CC} = (J^{\mu-}_{\rm CC})^\dagger \equiv \frac{1}{\sqrt{2}}\left(\overline{\nu'_{eL}}\,\gamma^\mu e'_L + \overline{u'_L}\,\gamma^\mu d'_L\right), \tag{2.16}$$

$$J^\mu_{\rm NC} \equiv \frac{1}{\cos\theta_w}\left\{\overline{\nu'_{eL}}\,\gamma^\mu\left(\hat{T}^3 - \hat{Q}\sin^2\theta_w\right)\nu'_{eL} + \cdots\right\}, \tag{2.17}$$

$$J^\mu_{\rm EM} \equiv \overline{e'_L}\,\gamma^\mu\,\hat{Q}\,e'_L + \cdots. \tag{2.18}$$

On the other hand, the fermion mass terms emerge out of the Yukawa interaction terms with ϕ:

$$\begin{aligned}&-y_{ee}\,\overline{L}\,\phi\,e'_R - y_{uu}\,\epsilon^{\alpha\beta}\,\overline{Q}_\alpha\,\phi^\dagger_\beta\,u'_R - y_{dd}\,\overline{Q}\,\phi\,d'_R \\ &\quad = -\frac{1}{\sqrt{2}} y_{ee}\,v\,\overline{e'_R}\,e'_L + \frac{1}{\sqrt{2}} y_{uu}\,v\,\overline{u'_R}\,u'_L + \frac{1}{\sqrt{2}} y_{dd}\,v\,\overline{d'_R}\,d'_L + \cdots. \end{aligned} \tag{2.19}$$

The omitted terms are the Yukawa interaction terms with the physical Higgs boson h which is the fluctuation around the vacuum (2.7). Since the Yukawa coupling constants are the free parameters of the model, the fermion masses are not predicted but just explained.

Now, let us consider multiple generation case. In general, the matrix of the Yukawa coupling constants is not diagonal with respect to generation index, namely off-diagonal elements y_{uc} etc. are allowed. The matrix Y_u for up-type quarks is diagonalized as

$$U^\dagger_{uL} Y_u\,U_{uR} = \sqrt{2}\;v\,{\rm diag}(m^j_u), \tag{2.20}$$

where U_{uL} and U_{uR} are unitary matrices, and m^j_u (> 0) denote the masses of up-type quarks. In the similar way, the matrix for down-type quarks is also diagonalized as

$$U^\dagger_{dL} Y_d\,U_{dR} = \sqrt{2}\;v\,{\rm diag}(m^j_d). \tag{2.21}$$

The unitary matrices are eliminated from the mass matrix by the redefinition of the quarks

$$\begin{aligned}&(u'_R)^j \equiv U^{jk}_{uR}\,u^k_R, \quad (u'_L)^j \equiv U^{jk}_{uL}\,u^k_L, \\ &(d'_R)^j \equiv U^{jk}_{dR}\,d^k_R, \quad (d_L\prime)^j \equiv U^{jk}_{dL}\,d^k_L. \end{aligned} \tag{2.22}$$

This redefinitions affect only the terms of the charged-current weak interaction (2.16) because each of those includes both up-type and down-type quarks:

$$\overline{(u'_L)^i}\;\gamma^\mu\,(d'_L)^i = \overline{(u_L)^j}\;\gamma^\mu\,V^{jk}(d_L)^k, \quad V \equiv U^\dagger_{uL} U_{dL}. \tag{2.23}$$

The matrix V is what we call the Cabibbo-Kobayashi-Maskawa (CKM) mixing matrix [27, 28]. Since neutrinos are massless in the standard model, there is no mixing in the lepton sector.

2.2 Physics of Massive Neutrinos

2.2.1 Neutrino oscillations in vacuum

When neutrinos have their masses, the mass eigenstates are not necessarily the same as the flavor eigenstates. Then, we can introduce the neutrino mixing

$$|\nu_\alpha\rangle = \sum_i U_{\alpha i}|\nu_i\rangle, \quad |\nu_i\rangle = \sum_\alpha U^*_{\alpha i}|\nu_\alpha\rangle, \tag{2.24}$$

where $|\nu_\alpha\rangle$ ($|\nu_i\rangle$) represents the flavor (mass) eigenstate and U denotes the Maki-Nakagawa-Sakata (MNS) matrix [4] which is similar to the CKM matrix in the quark sector. The propagation of the mass eigenstates are controlled by the Schrödinger equation

$$i\frac{d}{dt}|\nu_i(t)\rangle = E_i|\nu_i(t)\rangle, \tag{2.25}$$

where $E_i = \sqrt{p^2 + m_i^2}$. Assuming that the neutrinos are relativistic, the equation becomes

$$i\frac{d}{dL}|\nu_i(L)\rangle \simeq \left(P + \frac{m_i^2}{2p}\right)|\nu_i(L)\rangle, \tag{2.26}$$

where L is the variable of the distance. Here, suppose that a neutrino was born as ν_α: $|\nu_\alpha(0)\rangle = \sum_i U_{\alpha i}|\nu_i(0)\rangle$. Then, after the propagation for a distance L, the neutrino becomes

$$|\nu_\alpha(0)\rangle = \sum_i U_{\alpha i}\, e^{i\frac{m_i^2 L}{2E}}|\nu_i(L)\rangle \tag{2.27}$$

$$= \sum_\beta \sum_i U_{\alpha i}\, e^{i\frac{m_i^2 L}{2E}} U^*_{\beta i}|\nu_\beta(L)\rangle, \tag{2.28}$$

where we used $p \simeq E$ and ignored an irrelevant common phase $\exp(-ipL)$. The transition probability $P(\nu_\alpha \to \nu_\beta)$ is obtained as

$$\begin{aligned} P(\nu_\alpha \to \nu_\beta) &= |\langle\nu_\beta(L)|\nu_\alpha(0)\rangle|^2 \\ &= \delta_{\alpha\beta} - 4\sum_{j>k} \mathrm{Re}\left(U_{\alpha j}U^*_{\beta j}U^*_{\alpha k}U_{\beta k}\right) \sin^2\left(\frac{\Delta m^2_{jk}L}{4E}\right) \\ &\quad - 2\sum_{j>k} \mathrm{Im}\left(U_{\alpha j}U^*_{\beta j}U^*_{\alpha k}U_{\beta k}\right) \sin\left(\frac{\Delta m^2_{jk}L}{2E}\right), \end{aligned} \tag{2.29}$$

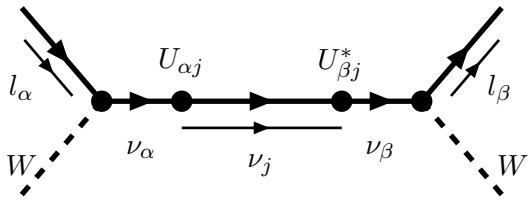

Figure 2.1: Flavor transition of neutrinos.

where $\Delta m^2_{jk} \equiv m^2_j - m^2_k$. We can find that the probability oscillates with respect to the distance L, and that is the neutrino oscillation. Note that the oscillation probabilities depend on not m_j but Δm^2_{jk}. Thus, the neutrino masses themselves can not be measured by oscillation experiments though an evidence for oscillation implies that at least one of the neutrino masses is non-vanishing.

When CPT is conserving, the oscillation probabilities in vacuum obey the following relation

$$\begin{aligned} P(\bar{\nu}_\alpha \to \bar{\nu}_\beta; U) = CPT\left[P(\bar{\nu}_\alpha \to \bar{\nu}_\beta; U)\right] &= P(\nu_\beta \to \nu_\alpha; U) \\ &= P(\nu_\alpha \to \nu_\beta; U^*). \end{aligned} \tag{2.30}$$

Therefore, non-real U leads the CP violation $P(\bar{\nu}_\alpha \to \bar{\nu}_\beta; U) \neq P(\nu_\alpha \to \nu_\beta; U)$. It is clear that the CP violating effect, which is the effect of non-real U, comes out from the last term in eq. (2.29). Since the term vanishes for $\alpha = \beta$, disappearance probabilities $1 - P(\nu_\alpha \to \nu_\alpha)$ are CP invariant. The number of phase (non-real) parameters of the mixing matrix are obtained as follows. A general $N \times N$ unitary matrix has N^2 parameters. $N(N-1)/2$ of those are angle (real) parameters, where the number is of the parameters of a general $N \times N$ orthogonal matrix. Furthermore, the redefinition of the relative phases of $2N$ fermions can eliminate $2N - 1$ of phase parameters, excluding an overall phase. Eventually, the mixing matrix includes $N(N-1)/2$ angle parameters and $(N-1)(N-2)/2$ phase parameters. It is found that $N \geq 3$ is necessary for CP violation [28].

In the case of two neutrinos, the neutrino mixing can be described as

$$\begin{pmatrix} \nu_e \\ \nu_\mu \end{pmatrix} = \begin{pmatrix} \cos\theta & \sin\theta \\ -\sin\theta & \cos\theta \end{pmatrix} \begin{pmatrix} \nu_1 \\ \nu_2 \end{pmatrix}. \tag{2.31}$$

The explicit forms of the oscillation probabilities are

$$P(\nu_\alpha \to \nu_\beta) = P(\bar{\nu}_\alpha \to \bar{\nu}_\beta) = \sin^2 2\theta \, \sin^2\left(\frac{\Delta m^2 L}{4E}\right), \tag{2.32}$$

$$P(\nu_\alpha \to \nu_\alpha) = P(\bar{\nu}_\alpha \to \bar{\nu}_\alpha) = 1 - \sin^2 2\theta \, \sin^2\left(\frac{\Delta m^2 L}{4E}\right), \tag{2.33}$$

where $\alpha \neq \beta$. Although the actual number of neutrinos is not two, those probabilities are useful enough because two neutrino approximation is applicable for many experiments. For such a case, the value of $\sin^2 2\theta$ and Δm^2 can be measured by a single oscillation experiment. Even if Δm^2_{jk} is tiny, the effect of the oscillation can be observed by performing experiments at long enough L or low enough E so that $\Delta m^2_{jk} L/(4E)$ is of order unity. It is worth to remember that it can be expressed as

$$\frac{\Delta m^2_{jk} L}{4E} \simeq 1.27 \frac{\Delta m^2_{jk}(\mathrm{eV}^2)\ L(\mathrm{km})}{E(\mathrm{GeV})} \tag{2.34}$$

in the natural unit $c\hbar = 197\mathrm{MeV}\cdot\mathrm{fm} = 1$.

In the case of three neutrinos, the mixing matrix has three angles and one phase parameters. Throughout this thesis, we use the standard parametrization [29, 30] of the mixing matrix

$$\begin{aligned} U &\equiv \begin{pmatrix} 1 & 0 & 0 \\ 0 & c_{23} & s_{23} \\ 0 & -s_{23} & c_{23} \end{pmatrix} \begin{pmatrix} c_{13} & 0 & s_{13}\, e^{-i\delta} \\ 0 & 1 & 0 \\ -s_{13}\, e^{i\delta} & 0 & c_{13} \end{pmatrix} \begin{pmatrix} c_{12} & s_{12} & 0 \\ -s_{12} & c_{12} & 0 \\ 0 & 0 & 1 \end{pmatrix} \\ &= \begin{pmatrix} c_{12}\, c_{13} & s_{12}\, c_{13} & s_{13}\, e^{-i\delta} \\ -s_{12}\, c_{23} - c_{12}\, s_{23}\, s_{13}\, e^{i\delta} & c_{12}\, c_{23} - s_{12}\, s_{23}\, s_{13}\, e^{i\delta} & s_{23}\, c_{13} \\ s_{12}\, s_{23} - c_{12}\, c_{23}\, s_{13}\, e^{i\delta} & -c_{12}\, s_{23} - s_{12}\, c_{23}\, s_{13}\, e^{i\delta} & c_{23}\, c_{13} \end{pmatrix}, \end{aligned} \tag{2.35}$$

where $s_{jk} \equiv \sin\theta_{jk}$ and $c_{jk} \equiv \cos\theta_{jk}$, and δ is the CP violating phase. We can choose those parameters as $0 \leq \theta_{jk} \leq \pi/2$ and $0 \leq \delta \leq 2\pi$ without loss of the generality [30]. Note that CP invariance holds for $\theta_{13} = 0$ because the CP violating phase δ lives with s_{13}. The explicit formula of $\mathrm{Im}(U_{\alpha j} U^*_{\beta j} U^*_{\alpha k} U_{\beta k})$, which controls the CP violation, is expressed simply with the Jarlskog factor J as

$$\left|\mathrm{Im}(U_{\alpha j} U^*_{\beta j} U^*_{\alpha k} U_{\beta k})\right| = J \equiv \frac{1}{4}\, c^2_{13}\, s_{13}\, \sin 2\theta_{12} \sin 2\theta_{23} \sin\delta, \tag{2.36}$$

where $\alpha \neq \beta$ and $j \neq k$ are assumed.

2.2.2 Neutrino oscillations in matter

So far we dealt with the neutrino oscillations in vacuum. The oscillations in matter are, however, different from that in vacuum due to the matter effect, which is the so-called Mikheev-Smirnov-Wolfenstein (MSW) effect [31]. This section is devoted to the discussion about the oscillations in matter. Although all active neutrinos interact with matter by exchange of Z boson, only electron-flavor neutrinos have the charged-current interaction with matter because electrons are the unique leptons that are contained in ordinary matter. The effect of the flavor-symmetric interactions such as Z exchange gives the

flavor-symmetric potential which is irrelevant to the neutrino oscillation. Therefore, the relevant potential comes from the charged-current interaction of electron-flavor neutrinos. The interaction is described by neglecting the momentum of W boson as

$$2\sqrt{2}G_{\rm F}\left(\overline{\nu_{eL}}\gamma^{\mu}e_L\right)\left(\overline{e_L}\gamma_{\mu}\nu_{eL}\right) = -2\sqrt{2}G_{\rm F}\left(\overline{\nu_{eL}}\gamma^{\mu}\nu_{eL}\right)\left(\overline{e_L}\gamma_{\mu}e_L\right), \tag{2.37}$$

where $G_{\rm F}$ ($\equiv \sqrt{2}g^2/8M_W^2 \simeq 1.2\times 10^{-5}{\rm GeV}^{-2}$) denotes the Fermi coupling constant and we used the Fierz identity

$$\left(\overline{\sigma}^{\mu}\right)_{\alpha\beta}\left(\overline{\sigma}_{\mu}\right)_{\gamma\delta} = 2\epsilon_{\alpha\gamma}\epsilon_{\beta\delta}, \quad \overline{\sigma}^{\mu} \equiv \left(1, -\sigma^i\right). \tag{2.38}$$

In the rest frame of matter, we obtain

$$\langle\overline{e_L}\gamma^{\mu}e_L\rangle = \frac{1}{2}\delta^{0\mu}N_e, \tag{2.39}$$

where N_e denotes the electron number density which is $\sim 10^{24}{\rm cm}^{-3}$ in the Earth crust. It is found that ν_{eL} feels the potential

$$a \equiv \sqrt{2}G_{\rm F}N_e. \tag{2.40}$$

Then, the propagation of mass eigenstates in matter is determined by

$$i\frac{d}{dL}|\nu_{\alpha}(L)\rangle = \left(U_{\alpha i}\frac{\Delta m_{i1}^2}{2E}U_{\beta i}^{*} + \sqrt{2}G_{\rm F}N_e\delta_{e\alpha}\delta_{e\beta}\right)|\nu_{\beta}(L)\rangle. \tag{2.41}$$

For 2ν case, the matrix in the right-hand side of (2.41) is described as

$$\frac{1}{2E}\begin{pmatrix} \Delta m^2\sin^2\theta + A & \Delta m^2\sin\theta\cos\theta \\ \Delta m^2\sin\theta\cos\theta & \Delta m^2\cos^2\theta \end{pmatrix}, \quad A \equiv 2\sqrt{2}EG_{\rm F}N_e. \tag{2.42}$$

The matrix is diagonalized by the effective mixing matrix in matter

$$U_{\rm M} \equiv \begin{pmatrix} \cos\theta_{\rm M} & \sin\theta_{\rm M} \\ -\sin\theta_{\rm M} & \cos\theta_{\rm M} \end{pmatrix}, \tag{2.43}$$

$$\sin^2 2\theta_{\rm M} \equiv \frac{\left(\Delta m^2\right)^2\sin^2 2\theta}{\left(\Delta m^2\cos 2\theta - A\right)^2 + \left(\Delta m^2\right)^2\sin^2 2\theta}. \tag{2.44}$$

Then, the eigenvalues (effective mass in matter) are

$$m_{\rm M\pm}^2 \equiv \frac{1}{2}\left\{\Delta m^2 + A \pm \sqrt{\left(\Delta m^2\cos 2\theta - A\right)^2 + \left(\Delta m^2\right)^2\sin^2 2\theta}\right\}. \tag{2.45}$$

It is interesting that the effective mixing becomes maximal, $\sin 2\theta_{\rm M} = 1$, for $A = \Delta m^2\cos 2\theta$ even if the original mixing is very small.[1] (See Fig. 2.2.) If the matter density is constant,

[1] If $A > 2\Delta m^2\cos 2\theta$, $\sin 2\theta_{\rm M}$ becomes smaller than $\sin 2\theta$.

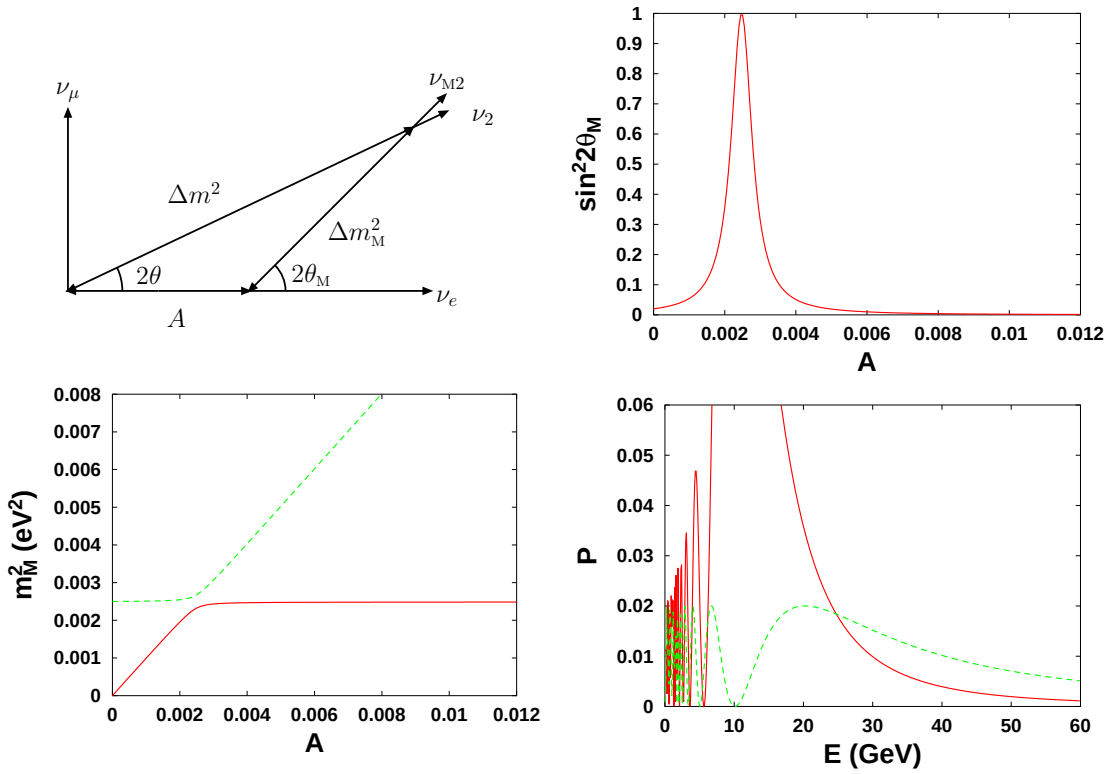

Figure 2.2: Left top: The figure shows the relation between vacuum parameters (Δm^2 and θ) and those in matter ($\Delta m^2_{\rm M}$ and $\theta_{\rm M}$). Right top: An example of $\sin^2 2\theta_{\rm M}$ is presented as a function of $A = 2\sqrt{2}EG_{\rm F}N_e$. The mixing in vacuum is assumed as $\sin^2 2\theta = 0.02$. Left bottom: An example of $m^2_{\rm M\pm}$ is presented as a function of A. Solid and dashed lines are of $m^2_{\rm M-}$ and $m^2_{\rm M+}$, respectively. Right bottom: Oscillation probabilities in matter (solid line) and in vacuum (dashed line). Parameter values are chosen so that $E = 60$GeV corresponds to $A = 0.012$.

the oscillation probability in matter is obtained by simply replacing θ and Δm^2 with θ_M and $\Delta m^2_{\rm M} \equiv m^2_{\rm M+} - m^2_{\rm M-}$ as

$$P(\nu_e \to \nu_\mu) = \sin^2 2\theta_{\rm M} \, \sin^2 \left(\frac{\Delta m^2_{\rm M} L}{4E} \right). \tag{2.46}$$

The calculation for 3ν case is much more complicated, but a smart derivation of exact 3ν oscillation probabilities in matter was presented recently [32].

2.2.3 Majorana neutrinos

Similarly to other fermions, massive neutrinos can have the Dirac mass term

$$\overline{\nu_R} \, m_{\rm D} \, \nu_L \tag{2.47}$$

with new particle ν_R which is neglected but not be prohibited in the standard model. Since neutrinos have no electro-magnetic charge differently from other fermions in the standard model, the neutrinos can be identified as their anti-particles: $\overline{\nu} = \nu$. Then, it is possible to have another mass term (Majorana mass term)

$$\overline{(\nu_L)^C} M \nu_L, \quad \psi^C \equiv -i\gamma^2 \psi^*. \tag{2.48}$$

Therefore, the left-handed neutrinos can have their mass terms without the right-handed neutrinos. The neutrinos with the Majorana mass term are referred to as the Majorana neutrinos, and ones without the term are called the Dirac neutrinos. Note that the Majorana mass term prohibit us redefining the phase of the neutrino. Then, the $N-1$ extra phases, which are called the Majorana phases, remain in the MNS matrix for N generation case as

$$U \;\longrightarrow\; U \times {\rm diag}\left(1, e^{-i\beta}, e^{-i\gamma}, \cdots\right). \tag{2.49}$$

The oscillation probability (2.29) is independent of the Majorana phases because

$$U_{\alpha i} U^*_{\beta i} \;\longrightarrow\; U_{\alpha i} e^{-i\beta_i} e^{i\beta_i} U^*_{\beta i} = U_{\alpha i} U^*_{\beta i}. \tag{2.50}$$

Conversely, it means that we can not know by oscillation experiments whether the neutrinos are Majorana or Dirac particles. Distinguishing them is possible, for example, by observation of neutrinoless double beta decay which does not occur for Dirac neutrinos.

In general, the neutrino mass term should be

$$\left(\overline{(\nu_L)^C}, \overline{\nu_R} \right) \begin{pmatrix} M_L & m_{\rm D} \\ m_{\rm D} & M_R \end{pmatrix} \begin{pmatrix} \nu_L \\ (\nu_R)^C \end{pmatrix}, \tag{2.51}$$

where $m_{\rm D}$ represents the Dirac mass, and M_L and M_R the Majorana masses for the left-handed and right-handed neutrinos, respectively. The general mass term can be diagonalized and the absolute values of the eigenvalues give the masses of the physical neutrinos. The eigenvalues of the mass matrix are

$$m_\pm = \frac{1}{2}\left\{ M_R + M_L \pm \sqrt{(M_R + M_L)^2 + 4m_{\rm D}^2} \right\}. \tag{2.52}$$

Here, we assume $1 \gg m_{\rm D}/M_R > M_L/m_{\rm D}$ because M_R can be very large while large M_L interferes with experimental results which agree with the standard electroweak model. Then, the eigenvalues are approximated as

$$m_+ \simeq M_R, \quad m_- \sim \frac{m_{\rm D}^2}{M_R}, \tag{2.53}$$

where we pushed the minus sign of m_- on to the eigenstate. Although the Dirac mass $m_{\rm D}$ is expected to be $\gtrsim$ MeV as for other fermions, it is suppressed by the small factor $m_{\rm D}/M_R$ and the result can be $\lesssim$ eV. The neutrino that corresponds to the small eigenvalue $m_{\rm D}^2/M_R$ can be identified as the light neutrino we observe, and the remaining heavy neutrino is decoupled from the standard model. This is the so-called seesaw mechanism [3] which can give a reason for the smallness of neutrino masses. The smallness of neutrino masses may be an indication of very high energy ($\sim M_R$) physics where the heavy Majorana neutrinos live. Since the Majorana mass term plays the crucial role for the mechanism, it is important to confirm that neutrinos are Majorana particles.

2.3 Number of Light Active Neutrinos

The measurement of decay width of Z produced in e^+e^- collisions gives the most stringent constraint on the number n_ν of light active neutrinos. The light active neutrinos are what can be produced by Z decay, namely their masses are less than $m_Z/2$ and they receive the electroweak interaction. n_ν is determined by comparing the predicted Z decay width into a neutrino pair, $(\Gamma_\nu^{(1)})_{\rm SM}$, with the invisible width $\Gamma_{\rm inv}$. The width $\Gamma_{\rm inv}$ is obtained by subtracting the contribution of quark pairs and charged lepton pairs from the total width. The width $\Gamma_{\rm inv}$ will be proportional to the number of light active neutrinos. (See Fig. 2.3.) In order to reduce uncertainties, the ratio to the decay width into the charged lepton pairs is used:

$$n_\nu = \frac{\Gamma_{\rm inv}}{\Gamma_l}\left(\frac{\Gamma_l}{\Gamma_\nu^{(1)}}\right)_{\rm SM}. \tag{2.54}$$

The combined result from four LEP experiments [24] (the ALEPH, DELPHI, L3, and OPAL experiments) is

$$n_\nu = 2.9841 \pm 0.0083. \tag{2.55}$$

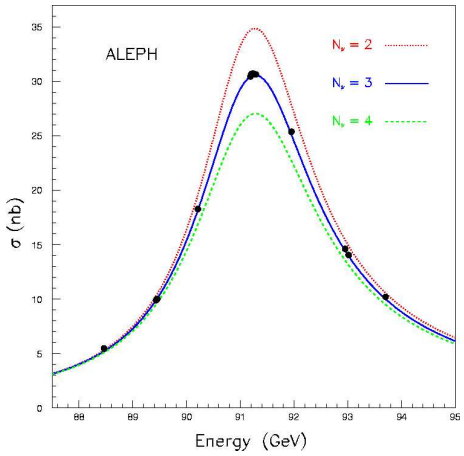

Figure 2.3: The ALEPH result of hadronic cross section of Z boson decay as function of center of mass energy. Expectations for 2, 3, and 4 neutrinos are superimposed. You can find this figure in [33].

2.4 Direct measurement of Neutrino Mass

The neutrino is originally introduced in 1930 by W. Pauli to explain the energy loss in the beta decay without laying aside the energy conservation law. The energy loss was understood as the energy took away by the unobserved particle "neutrino". From the present point of view, the neutrino take away the energy correspond to not only its momentum but also its mass. Thus, the neutrino mass can be measured in principle by the precise measurement of the beta decay. Although the possibility have been well known, this is a typical example of the proverb "saying is one thing and doing another" because the neutrino mass is so small. Nevertheless, the precise measurement of the beta decay is extremely important because the absolute mass can not be determined by oscillation experiments which can, however, probe smaller mass scale; The oscillation probabilities depend on the mass squared difference Δm^2 as we observed in the previous discussion.

Although the neutrino from the beta decay is $\overline{\nu}_e$ and it is the mixed state of the mass eigenstates, we can approximate those masses as a degenerate one m_ν because the mass splitting are much smaller than the energy scale probed by recent beta decay measurements. Then, the neutrino moves the endpoint of the energy spectrum of the emitted electrons by just m_ν. The recent bounds on the neutrino mass are obtained by ^{3}H (tritium) beta decay measurement. The results of Mainz group [34] is

$$m_\nu < 2.2\text{eV } (95\%\text{CL}), \tag{2.56}$$

and that of Troitsk group [35] is

$$m_\nu < 2.5\text{eV } (95\%\text{CL}). \tag{2.57}$$

The future KATRIN experiment [36] (KArlsruhe TRItium Neutrino experiment) is expected to probe the mass down to

$$m_\nu \simeq 0.3\text{eV}. \tag{2.58}$$

2.5 Neutrinoless Double Beta Decay

Double beta decay is a rare decay of a nucleus described as

$$(Z, A) \to (Z+2, A) + 2e^- + 2\overline{\nu}_e, \tag{2.59}$$

where Z and A denote the atomic number and the mass number. The decay occur for some even-even nuclei for which the beta decay to the odd-odd nuclei is energetically forbidden by the pairing energy. Here, if neutrinos are Majorana particles, the neutrinoless double beta decay ($0\nu\beta\beta$) is also possible:

$$(Z, A) \to (Z+2, A) + 2e^-. \tag{2.60}$$

This process is interesting because it does not conserve the lepton number which is protected in the standard model. In order to know whether neutrinos are Majorana or Dirac particles, $0\nu\beta\beta$ searches are very important because oscillation experiments can not give the answer. If the decay is dominated by the exchange of Majorana neutrinos, the leptonic part of the interaction is

$$\begin{aligned}
&\sum_j \overline{e_L}\,\gamma^\rho\, U_{ej} \left\langle \nu_{jL}\, \overline{(\nu_{jL})^C} \right\rangle U_{ej}\, \gamma^\sigma\, (e_L)^C \\
&\quad = \sum_j \overline{e_L}\,\gamma^\rho\, \frac{1}{2}\left(1-\gamma^5\right) U_{ej}^2\, \frac{i(\not{q}+m_j)}{q^2-m_j^2}\, \frac{1}{2}\left(1-\gamma^5\right)\, \gamma^\sigma\, (e_L)^C \\
&\quad = \sum_j U_{ej}^2\, m_j\, \overline{e_L}\,\gamma^\rho\, \frac{i}{q^2-m_j^2}\, \gamma^\sigma\, (e_L)^C.
\end{aligned} \tag{2.61}$$

For light neutrinos ($m_j \lesssim 10\text{MeV}$), m_j in the denominator of (2.61) can be neglected and (2.61) is simply proportional to $\sum_j U_{ej}^2 m_j$. Then, we obtain the half life (the observable)

$$\left(T_{1/2}^{0\nu}\right)^{-1} = G^{0\nu} |M^{0\nu}|^2 \langle m \rangle_{\beta\beta}^2, \tag{2.62}$$

$$\langle m \rangle_{\beta\beta} \equiv \left| \sum_j m_j U_{ej}^2 \right|, \tag{2.63}$$

where $G^{0\nu}$ represents the phase space integral, $M^{0\nu}$ is the nuclear matrix element which has the information of the nucleus and of the neutrino propagator, and $\langle m \rangle_{\beta\beta}$ is the effective mass of the electron neutrino for $0\nu\beta\beta$. Note that (2.63) depend on not $|U|^2$ but U^2 because the C transformation includes taking complex conjugate.

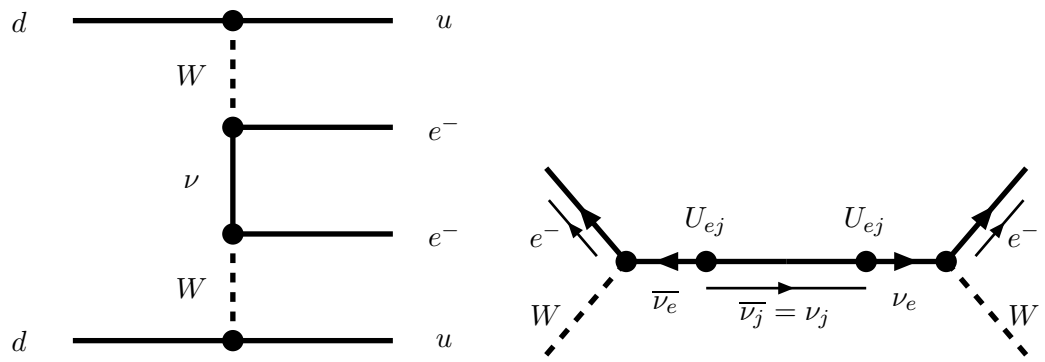

Figure 2.4: Left: The diagram for the neutrinoless double beta decay by the exchange of light Majorana neutrinos. Right: Detail of the leptonic part of the left figure.

The most stringent bounds to date on the half-life $T^{0\nu}_{1/2}$ were obtained by the Heidelberg-Moscow [37] and IGEX [38] collaborations. The Heidelberg-Moscow group used 125.5 moles ($\simeq$ 10kg) of enriched[2] germanium (86% ^{76}Ge) as the $0\nu\beta\beta$ source and detector, and the IGEX group 90 moles ($\simeq$ 7kg). If $0\nu\beta\beta$ occurs in ^{76}Ge, a peak appears at 2039keV (Q value of the double beta decay) in the spectrum for the total energy of two emitted electrons. The negative results of the observation of the peak lead to the upper bounds on $T^{0\nu}_{1/2}$:

$$T^{0\nu}_{1/2} > 1.9 \times 10^{25}\,\mathrm{yr} \quad \text{(Heidelberg-Moscow)}, \tag{2.64}$$

$$T^{0\nu}_{1/2} > 1.57 \times 10^{25}\,\mathrm{yr} \quad \text{(IGEX)}. \tag{2.65}$$

Those are translated to the bounds on $\langle m\rangle_{\beta\beta}$ by (2.62) as

$$\langle m\rangle_{\beta\beta} < 0.35\,\mathrm{eV} \quad \text{(Heidelberg-Moscow)}, \tag{2.66}$$

$$\langle m\rangle_{\beta\beta} < 0.33\text{-}1.31\,\mathrm{eV} \quad \text{(IGEX)}. \tag{2.67}$$

Note that the translation of the lifetime limit to mass limit involves the value of $G^{0\nu}|M^{0\nu}|^2$. (Examples are listed in Table 2.2.) Thus, it is important to obtain the precise value of $G^{0\nu}|M^{0\nu}|^2$ for utilization of $\langle m\rangle_{\beta\beta}$ which has the information of neutrino masses and mixing.

On the other hand, an evidence of the $0\nu\beta\beta$ signal was announced in late 2002 [45]. The result at 95% CL and the best fit value are

$$T^{0\nu}_{1/2} = 0.8\text{-}18.3 \times 10^{25}\,\mathrm{yr}, \quad \left(T^{0\nu}_{1/2}\right)^{\mathrm{best}} = 1.5 \times 10^{25}\,\mathrm{yr}, \tag{2.68}$$

and those are interpreted as

$$\langle m\rangle_{\beta\beta} = 0.05\text{-}0.84\,\mathrm{eV}, \quad \langle m\rangle^{\mathrm{best}}_{\beta\beta} = 0.39\,\mathrm{eV}, \tag{2.69}$$

[2]Natural Ge consists of 36.5% ^{74}Ge, 27.4% ^{72}Ge, 20.5% ^{70}Ge, 73% ^{73}Ge, and 7.8% ^{76}Ge.

	bound on $\langle m \rangle_{\beta\beta}$ (eV)	
	Heidelberg-Moscow	IGEX
$G^{0\nu}\|M^{0\nu}\|^2$ $(\mathrm{eV}^{-2} \cdot \mathrm{yr}^{-1})$	$T^{0\nu}_{1/2} > 1.9 \times 10^{25}\,\mathrm{yr}$	$T^{0\nu}_{1/2} > 1.57 \times 10^{25}\,\mathrm{yr}$
5.97×10^{-25} [39]	< 0.30	< 0.33
4.63×10^{-25} [40]	< 0.34	< 0.37
4.37×10^{-25} [41]	< 0.35	< 0.38
4.29×10^{-25} [42]	< 0.35	< 0.39
5.40×10^{-26} [43]	< 0.99	< 1.09
3.70×10^{-26} [44]	< 1.19	< 1.31

Table 2.2: Upper bounds on $\langle m \rangle_{\beta\beta}$ by the results of Heidelberg-Moscow and IGEX group with several values of translation factor $G^{0\nu}|M^{0\nu}|^2$.

where $\pm 50\%$ error due to the uncertainty of the nuclear matrix element is taken into account.[3]

After the announcement, a comment paper was written by several authors [46], and the replies also appeared [47, 48]. Since it seems to be not conclusive yet, it is important to probe the region of the announced evidence by other experiments. The future experiments are listed in Table 2.3, and some of them will be able to inspect the announced evidence. Note that precise values of $G^{0\nu}|M^{0\nu}|^2$ for each $0\nu\beta\beta$ nuclei are necessary for also the consistency check of results obtained by some different nuclei. More detailed review is found in [60]. For a review of theoretical aspects of $0\nu\beta\beta$, see e.g. [61] and the references therein.

[3]The $+50\%$ (-50%) error in $\langle m \rangle_{\beta\beta}$ corresponds to -33% ($+100\%$) error in $|M^{0\nu}|^2$.

experiment	source	detector size	sensitivity to $T^{0\nu}_{1/2}$ (yr)	sensitivity to $\langle m \rangle_{\beta\beta}$ (eV)
COBRA[49]	^{130}Te	10kg CdTe	1.2×10^{24} (5yr run)	6.5×10^{-1}
	^{116}Cd		3×10^{23} (5yr run)	1.26
DCBA[50]	^{150}Nd	20kg enriched Nd	2×10^{25}	3.5×10^{-2}
NEMO[51]	^{100}Mo	10kg $0\nu\beta\beta$ isotopes (7kg ^{100}Mo)	4×10^{24} (5yr run, 90% CL)	5.6×10^{-1}
	^{82}Se	(1kg ^{82}Se)	1.5×10^{24} (5yr run, 90% CL)	6.3×10^{-1}
CAMEO[52]	^{116}Cd	65-1000kg $CdWO_4$	$\simeq 10^{26}$-10^{27}	2.2-6.9 $\times 10^{-2}$
CANDLES[53]	^{48}Ca	$\sim$ t enriched (2%) CaF_2	2-4 $\times 10^{26}$ (5yr run)	
CUORE[54]	^{130}Te	750kg TeO_2	1.1-3.6 $\times 10^{26}$ (1yr run)	3.7-6.7 $\times 10^{-2}$
EXO[55]	^{136}Xe	1t enriched (65%) Xe	8.3×10^{26} (5yr run)	5.1×10^{-2}
GENIUS[56]	^{76}Ge	1t enriched (86%) Ge	5.8×10^{27} (1yr run, 68% CL)	2.0×10^{-2}
Majorana[57]	^{76}Ge	0.5t enriched (86%) Ge	4.2×10^{27} (10yr run, 90% CL)	2.4×10^{-2}
MOON[58]	^{100}Mo	1t enriched (80%) Mo	1.6×10^{27} (10yr run)	2.8×10^{-2}
XMASS[59]	^{136}Xe	10t liquid Xe	3.3×10^{26} (5yr run)	8.2×10^{-2}

Table 2.3: Listed are future experiments of neutrinoless double beta decay search. Sensitivities to $\langle m \rangle_{\beta\beta}$ are calculated with $G^{0\nu}|M^{0\nu}|^2$ obtained in [42] for each isotope: $(T^{0\nu}_{1/2})^{-1} = G^{0\nu}|M^{0\nu}|^2 \langle m \rangle^2_{\beta\beta}$.

Chapter 3

Recent Status of Neutrino Oscillation Experiments

3.1 The 2-3 Sector

3.1.1 Atmospheric neutrino measurement

The atmosphere is a source of ∼GeV-TeV neutrinos. The cosmic rays, which are mainly composed of protons, produce pions in collision on nuclei in the atmosphere. The pions then decay as

$$\pi^+ (\pi^-) \to \mu^+ \nu_\mu \, (\mu^- \, \overline{\nu}_\mu). \tag{3.1}$$

The muons decay also into neutrinos subsequently:

$$\mu^+ (\mu^-) \to e^+ \nu_e \overline{\nu}_\mu \, (e^- \overline{\nu}_e \nu_\mu). \tag{3.2}$$

Thus, the ratio $N_{\nu_\mu + \overline{\nu}_\mu} / N_{\nu_e + \overline{\nu}_e}$ is predicted to be 2 for $E_\nu \lesssim 1\text{GeV}$.[1] The measured values of the ratio, however, were significantly smaller than the prediction in Kamiokande (Kamioka Nucleon Decay Experiment) [62, 63]. Although the anomaly indicated the neutrino oscillation, the result seemed to be insufficient to be regarded as the evidence. It was because that IMB (Irvine-Michigan-Brookhaven) [64] experiment excluded almost all the region allowed by Kamiokande in the oscillation parameter space though the experiment also observed the deficit of μ-flavor neutrinos. Moreover, there were negative results of the deficit (with rather low statistics) in Fréjus [65] and NUSEX (NUcleon Stability EXperiment) [66] experiments.

In 1998 the Super-Kamiokande (Super Kamioka Neutrino Detection Experiment. Hereafter it is referred to as SK.) [2] proved with high statistics that the atmospheric neutrino

[1] For higher E_ν, the ratio becomes larger because the high energy parent muon reaches to the ground before the decay to high energy e-flavor neutrino.

events (535 days) depends on the zenith angle, which was first observed in Kamiokande [63]. Fig. 3.1 is the recent SK result for 1489 day exposure [67]. The SK detector (22.5kt fiducial mass) has an advantage for reconstruction of neutrino direction because the larger detector can investigate higher energy final state leptons whose directions correlate more to those of initial neutrinos. The result shows the significant up-down asymmetry of μ-flavor neutrino events which would be up-down symmetric if nothing happened during the flight of the neutrinos. The asymmetry is a clear evidence for the atmospheric neutrino anomaly without ambiguities of initial fluxes because the initial flux is probably radial symmetric. Since the zenith angle dependence of the deficit is the dependence on the flight length of neutrinos, the result convinced us that the deficit was the evidence for neutrino oscillation. The reason why the downward going ν_μ do not disappear is understood that the travel distance L to the detector ($\sim$ 20km) is too short for neutrinos to oscillate while the distance for upward going ones ($\sim$ 10000km) is enough. In 3ν framework, the disappearance of μ-flavor neutrino is regarded as the effect of the oscillation to τ-flavor neutrino because there was no anomaly in e-flavor events. Actually, vanishingly small $P(\mu_\mu \to \nu_e)$ is consistent with vary small value of θ_{13} which is constrained by reactor experiments (See Sect. 3.3). The smallness of θ_{13} enables us to use the simple 2ν framework for the analysis of the atmospheric neutrino oscillation. Fig. 3.2(left) presents the allowed region obtained for 2ν case in the most recent analysis. For 3ν case, Δm^2 and θ of atmospheric neutrino oscillation are understood approximately as Δm^2_{32} and θ_{23} of the standard parametrization (2.35), and the parameters are constrained at 90% CL as

$$|\Delta m^2_{32}| = 1.3\text{-}3.0 \times 10^{-3}\text{eV}^2, \quad |\Delta m^2_{32}|^{\text{best}} = 2.0 \times 10^{-3}\text{eV}^2, \tag{3.3}$$

$$\sin^2 2\theta_{23} = 0.9\text{-}1, \qquad \sin^2 2\theta_{23}^{\text{best}} = 1. \tag{3.4}$$

Consistent results were obtained by MACRO (Monopole, Astrophysics, and Cosmic Ray Observatory) [68] and Soudan2 [69] experiments.

3.1.2 K2K experiment

The KEK to Kamioka experiment (K2K) [5], which is the first long baseline accelerator neutrino experiment, started in 1999 to confirm the SK result of atmospheric neutrino measurement by using an accelerator ν_μ beam. The neutrino source is the KEK proton synchrotron whose power is 5kW producing every 2.2 seconds about 6×10^{12} protons of 12GeV within a 1.1μs beam spill. The neutrino beam is a wide band beam whose peak energy is about 1.3GeV, and the beam spectrum is measured by the 1t near detector at 300m baseline length. The detector is SK and the baseline length is 250km. Therefore,

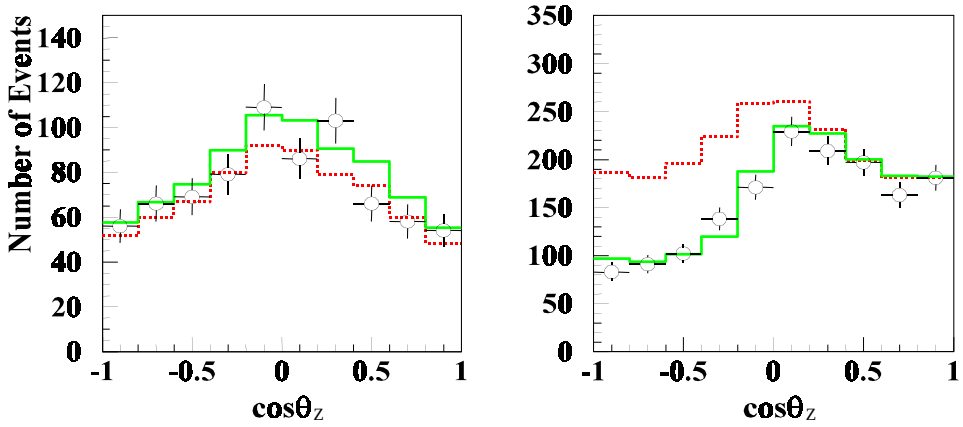

Figure 3.1: Zenith angle θ_z dependence of multi-GeV events whose visible energy is grater than 1.33GeV. $\cos\theta_z = 1$ corresponds to downward direction. The left and right figures are for e- and μ-flavor neutrinos, respectively. Dashed (solid) line is the expectation with no oscillation (best fit $\nu_\mu \to \nu_\tau$ oscillation). The excess around $\cos\theta_z = 0$ of expected value is because that longer flight length in the atmosphere enable also high energy muons to decay before arrival to the ground. μ-like events include also partially contained events (PC) which have exiting particles from the inner detector.

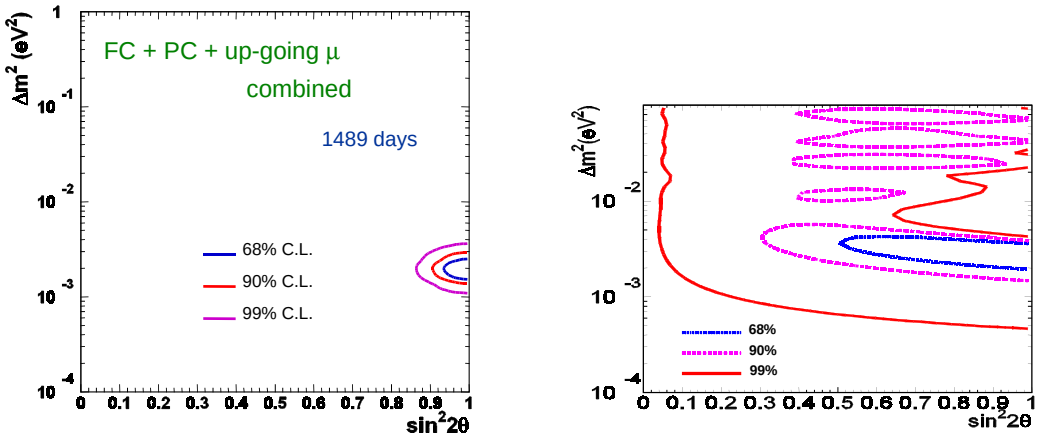

Figure 3.2: Allowed region for 2ν oscillation parameters which are understood in a good approximation as $|\Delta m^2_{32}|$ and $\sin^2 2\theta_{23}$ for 3ν case. Left figure is for SK and right one is for K2K.

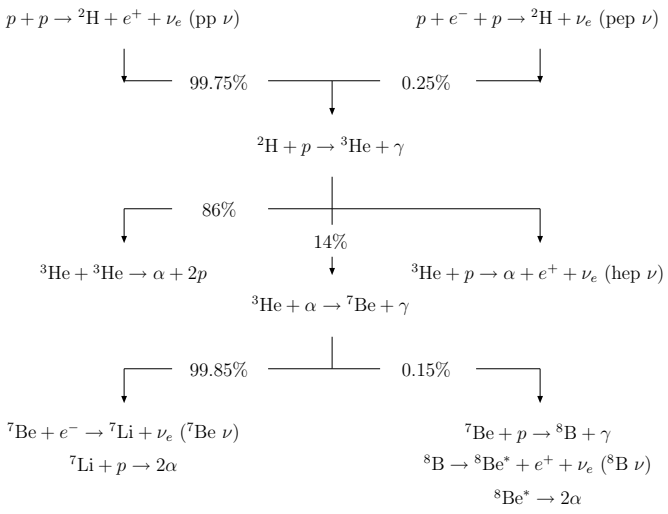

Figure 3.3: The chain of nuclear fusion reactions in the sun. The branching ratios are shown also. The neutrinos of each reaction are referred to as pp neutrino etc. which are presented in parentheses.

the experiment focuses on

$$\Delta m^2 = \frac{\pi}{2} \frac{1.3(\mathrm{GeV})}{1.27 \times 250(\mathrm{km})} \simeq 6 \times 10^{-3}\mathrm{eV}^2, \tag{3.5}$$

and it is possible to probe the region around the SK atmospheric neutrino result. The neutrino events at SK due to the KEK neutrino beam are distinguished precisely from backgrounds such as atmospheric neutrinos by timing synchronization with the Global Positioning System (GPS). The result that was obtained with 4.8×10^{19} protons on target (POT) is presented also in Fig. 3.2(right) for 2ν case at 90% CL. At $\sin^2 2\theta = 1$, the result shows $|\Delta m^2_{32}| = 1.5\text{-}3.9 \times 10^{-3}\mathrm{eV}^2$ which is consistent with the SK result of atmospheric neutrino measurement. The best fit values in K2K are $\sin^2 2\theta^{\mathrm{best}}_{23} = 1.0$ and $|\Delta m^2_{32}|^{\mathrm{best}} = 2.8 \times 10^{-3}\mathrm{eV}^2$.

3.2 The 1-2 Sector

3.2.1 Solar neutrino measurement

The sun shines due to the nuclear fusion reaction, $4\mathrm{p} \rightarrow \alpha + 2e^+ + 2\nu_e$. (See Fig. 3.3.) Thus, we are in the neutrino window from the sun. In 1968, the solar neutrino observation

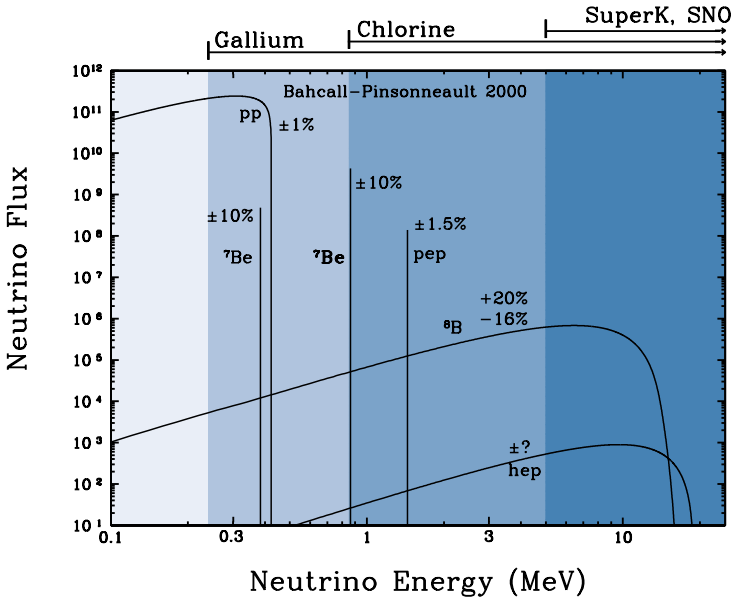

Figure 3.4: Solar ν_e spectra at the Earth (taken from the second reference of [7]). The unit for pp, ^{8}B, and hep neutrinos is cm^{-2}s^{-1}MeV. The lines for ^{7}Be and pep neutrinos show the peak energies and the fluxes in the unit of cm^{-2}s^{-1}. Estimated uncertainties are also presented. The lightly shadowed energy range is probed by gallium experiments, the shadowed one by also chlorine experiment, and the dark shadowed one by also SK and SNO.

started by using a radiochemical method with liquid C_2Cl_4 (tetrachloroethylen) [6]. The solar neutrino produces ^{37}Ar, which is not a natural isotope, in the detector by the inverse beta decay $^{37}\mathrm{Cl} + \nu_e \rightarrow {}^{37}\mathrm{Ar} + e^-$ whose threshold energy is 0.814MeV. Since argon is a light noble gas, it is not chemically attached to tetrachloroethylen and it can be easily removed with helium gas. The number of recovered ^{37}Ar is counted after a few month exposure by the decay which emits Auger electrons of 2.82keV (K shell) total energy. Curiously, the result showed that the solar $\overline{\nu}_e$ flux is no more than about 1/3 of the theoretical prediction with the Standard Solar Model (SSM) [7]. (See Fig. 3.4 as recent prediction.)

As we see in Figs. 3.3 and 3.4, the chlorine experiment can not observe the pp neutrino which dominates the fusion reactions in the sun. The result of the chlorine experiment is controlled by ^{8}B neutrino which covers only 0.02% of the nuclear fusion reaction in the sun. Therefore, the deficit of solar neutrino observed by the chlorine experiment might be explained by small changes of the Standard Solar Model. The possibility was eliminated by SAGE (Russian-American Gallium Experiment[2]) [8], GALLEX (GALLium

[2]It had been Soviet-American Gallium Experiment.

EXperiment) [9] and its successor GNO (Gallium Neutrino Observatory) [70]. Those experiments employ the similar radiochemical method with ^{71}Ga. The reaction used in those experiments is $^{71}\mathrm{Ga} + \nu_e \to {}^{71}\mathrm{Ge} + e^-$ whose threshold energy is 0.233MeV. SAGE used Ga metal, and GALLEX did the solution of $GaCl_3$ in water. By virtue of the low energy threshold, they could observe the pp neutrinos and the deficit was presented. If we modify the Standard Solar Model to explain the results, it becomes inconsistent with the luminosity of the sun.

Solar neutrino was observed also by Kamiokande [71] and SK [10] water Cherenkov detectors with the total mass of 3 and 50kt, respectively. Those experiments observed the Cherenkov lights of electrons scattered elastically by the solar neutrinos: $e^- + \nu_e \to e^- + \nu_e$. Note that ν_μ and ν_τ also scatter e^- with about 6 times smaller cross sections than that for ν_e. The energy thresholds of signal detection are $E_\nu \simeq 7$MeV and 5MeV for Kamiokande and SK, respectively. The experiments can determine the direction from which the neutrino comes. It is due to the relation

$$\cos\theta_{\mathrm{ES}} = \frac{2E_\nu\sqrt{m_e^2 + p_e^2} - m_e^2}{2E_\nu p_e} \simeq 1 \tag{3.6}$$

at relativistic energy $p_e \gg m_e$, where θ_{ES} denotes the angle of recoiled electron to the direction where the initial neutrino comes, and p_e is the momentum of the recoil electron whose mass $m_e = 0.511$MeV is smaller enough than detectably large E_ν. Thus, they can identify the neutrinos whose direction point back to the sun. The directionality provides the powerful selection criterion for signal events against radioactive background. It was found that the solar neutrino flux on the Earth is about 1/2 times the expectation of the Standard Solar Model with high statistics. Furthermore, neutrino energy can be reconstructed and no significant distortion was observed. Those experiments investigated the day-night variation of the energy spectrum also. There is, however, no significant variation.

The results of the Cl and Ga experiments are analyzed together with SK experiment within the framework of two flavor mixing. As a result of such analysis, the allowed regions are obtained in the mixing parameter space spanned by $\sin^2 2\theta$ and Δm^2, and presented in Fig. 3.5. In the context of three neutrino mixing, these parameters can be interpreted as $\sin^2 2\theta_{12}$ and Δm^2_{21} of the standard parametrization (2.35), respectively, in a good approximation. It is found that there were four allowed regions with matter effect [31], namely the small mixing angle solution (SMA: $\Delta m^2 \simeq 8 \times 10^{-6}\mathrm{eV}^2$, $\tan^2\theta \simeq 4 \times 10^{-5}$), the large mixing angle solution (LMA: $\Delta m^2 \simeq 5 \times 10^{-5}\mathrm{eV}^2$, $\tan^2\theta \simeq 0.3$), the low Δm^2 solution (LOW: $\Delta m^2 \simeq 1 \times 10^{-7}\mathrm{eV}^2$, $\tan^2\theta \simeq 0.8$), and the vacuum oscillation solution (VAC: $\Delta m^2 \simeq 5 \times 10^{-10}\mathrm{eV}^2$, $\tan^2\theta \simeq 2.5$). Although large deficit of solar neutrino indicates that the mixing angle is large, matter effect gives a possibility for the mixing to

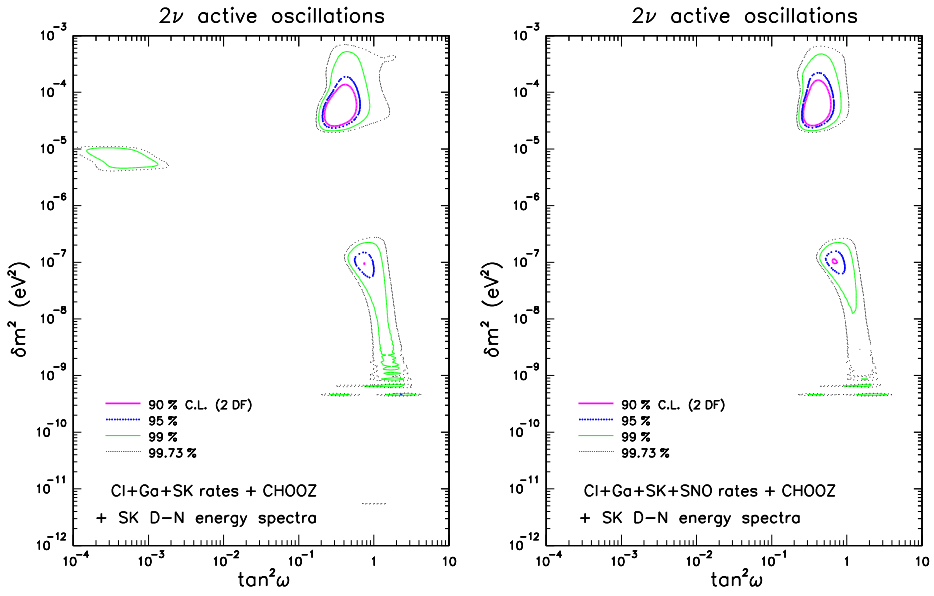

Figure 3.5: The results of solar neutrino observations are combined for two active neutrino approximation. In terms of 3ν scheme, $\tan^2\omega$ and δm^2 is understood as $\tan^2\theta_{12}$ and Δm^2_{21}, respectively. The left figure is before the first result of SNO CC measurement, and the right figure is after the result. (Taken from the first reference in [72].) Note that the small mixing angle (SMA) solution disappears in the right figure by virtue of SNO result.

be small. Here, $\tan^2\theta < 1$ corresponds to $m_1^2 < m_2^2$ due to matter effect in the sun.

SNO (Sudbury Neutrino Observatory) [11] observed solar neutrino with a very ingenious way. The experiment use 1kt heavy water (D_2O) instead of light water (H_2O). By virtue of deuteron, SNO can observe not only elastic scattering (ES: $\nu_e + e^- \to \nu_e + e^-$), which can be observed by light water as SK, but also charged-current reaction (CC: $\nu_e + d \to 2p + e^-$) and neutral-current reaction (NC: $\nu_e + d \to \nu_e + n + p$). The events of Those reactions are distinguished kinematically. The CC reaction is observed by Cherenkov light from the emitted electron while produced protons almost keep resting because of the large mass; The threshold of signal detection in SNO experiment is $T_e \geq 6.75$MeV for the electron kinetic energy. In the energy range of solar neutrino, this reaction is sensible only to e-flavor one because the energy is not enough to produce heavier charged leptons. It was found that the observed solar ν_e flux by CC reaction is less significantly than the precisely measured flux that caused ES events at SK. Remembering that ES can be caused by μ- and τ-flavor neutrinos also, the deviation is an evidence for the presence of non-electron-flavor neutrinos in the flux from the sun while only ν_e deficits were observed before. Despite attempts to obtain small mixing which is the case of quark sector, the result of SNO strongly disfavored the SMA solution as we see in Fig. 3.5 which is taken

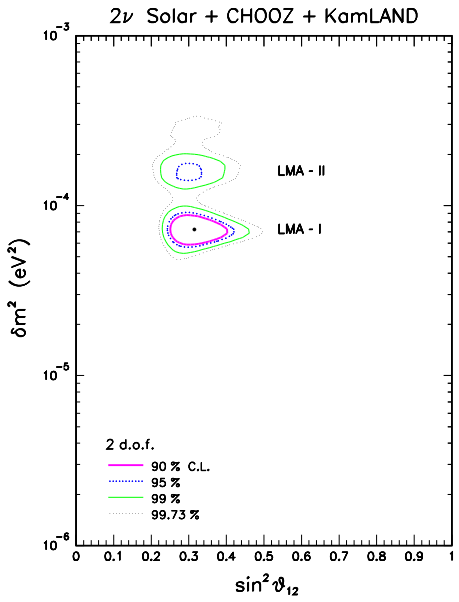

Figure 3.6: A 2ν global analysis of solar neutrino, CHOOZ, and KamLAND results. (Taken from second one of [74].) In 3ν case, δm^2 is understood as Δm^2_{21}. Note that only the large mixing angle (LMA) solution remains. Global best fit (so-called LMA-I) is $\Delta m^2_{21} = 7.3 \times 10^{-5}\mathrm{eV}^2$ and $s^2_{12} = 0.315$. Second best fit (so-called LMA-II) is $\Delta m^2_{21} = 15.4 \times 10^{-5}\mathrm{eV}^2$ and $s^2_{12} = 0.300$.

from the first reference in [72]. We understood that the mixing angles for atmospheric and solar neutrino oscillations are both large and the flavor mixing in the lepton sector is very different from that in the quark sector. Next, the NC reaction also can be observed due to gamma rays emitted when the recoil neutron is captured by a nucleus. Since capture efficiency of deuterium ($\simeq 20\%$) is not so large, SNO added ^{35}Cl as 2t NaCl (common salt) in the heavy water for their second phase referred to as the salt phase. The efficiency of neutron capture by ^{35}Cl is $\simeq 80\%$. Needless to say, NC interaction is blind to neutrino flavor. SNO showed that total flux is consistent with the prediction of the Standard Solar Model, which is an evidence for the flavor transition of solar ν_e whose deficit had already been understood. After the salt phase, SNO plans to use ^{3}He-filled proportional counters for event-by-event detection of NC reaction with the neutron capture: $^3\mathrm{He} + n \to p + {}^3\mathrm{H}$.

3.2.2 KamLAND experiment

Although global analyses [73] of solar neutrino experiments preferred the LMA parameter region over the others, it was not conclusive because e.g. the LOW solution agreed acceptably with the experimental results. The evidence for the LMA solution was presented by KamLAND experiment (Kamioka Liquid scintillator Anti-Neutrino Detector) [12] with

neutrino sources on the ground. In most cases, Δm^2_{21} which corresponds to solar neutrino oscillation is too small to observe the oscillation with terrestrial sources of neutrinos because $\sin^2(\Delta m^2_{21}L/4E) \simeq 1$ requires long baseline length and low energy neutrino beam. Both of the requirements make number of events very small due to $1/L^2$ suppressed flux and small cross section for low energy neutrinos. A miracle is, however, occurred at Kamioka site. There are 16 nuclear power plants whose total thermal power is $130\mathrm{GW_{th}}$ for the maximum operation of all of them and which provide the total flux $13.1 \times 10^5 \overline{\nu}_e/\mathrm{cm}^2/\mathrm{s}$ at Kamioka site.[3] Since the energy of reactor $\overline{\nu}_e$ is of the order of MeV, the baseline for the first maximum oscillation with $\Delta m^2_{21} \sim 10^{-5}\mathrm{eV}^2$ (LMA) is

$$L \sim \frac{\pi}{1.27 \times 2} \frac{1(\mathrm{MeV})}{10^{-5}(\mathrm{eV}^2)} \sim 100\mathrm{km} \tag{3.7}$$

Conveniently, 80% of the flux at Kamioka site comes from the reactors whose baselines are 138-214km. KamLAND is placed in the cavity where Kamiokande was located, and the detector is 1kt liquid scintillator (408t fiducial mass) which can be approximately regarded as CH_2. KamLAND detects reactor $\overline{\nu}_e$ by the inverse beta decay reaction on a free proton (the nucleus of H in CH_2)

$$\overline{\nu}_e + p \to e^+ + n \tag{3.8}$$

whose energy threshold is 1.8MeV. The produced e^+ gives the prompt signal and the capture of thermalized neutron by a proton does the secondary 2.2MeV signal about 210μs after the prompt one. (See also Sect. 3.3 of short baseline reactor experiments.) KamLAND observed the disappearance of reactor $\overline{\nu}_e$ and the result pinned down the LMA region as the solution of solar ν_e disappearance [74] assuming CPT invariance:

$$\Delta m^2 = 7.3 \times 10^{-5}\mathrm{eV}^2,\ \sin^2\theta = 0.315\ (\tan^2\theta = 0.46). \tag{3.9}$$

The so-called LMA-II solution which has high-Δm^2_{21} is now excluded at 99% CL by the one with SNO salt phase data [75], and at 3σ CL by the global analysis of all data with reanalyzed day-night variation of flux at SK [76]. The best fit values with global analysis by SK group are

$$\Delta m^2 = 7.1 \times 10^{-5}\mathrm{eV}^2,\ \tan^2\theta = 0.45. \tag{3.10}$$

[3]The largest contribution (32%) to the total flux comes from Kashiwazaki-Kariwa nuclear power plant which is used in Chapter 5 and 6.

3.3 The 1-3 Sector

3.3.1 CHOOZ experiment

The mixing angle θ_{13} of the standard parametrization for 3ν case (2.35) has not been measured yet, and we do not know whether θ_{13} is zero or not. The present upper bound on θ_{13} was obtained by the CHOOZ experiment [13]. The CHOOZ experiment measured $\overline{\nu}_e$'s that were yielded by the nuclear fission in reactors. The peak energy of reactor $\overline{\nu}_e$ event spectrum without oscillation is $E_\nu \simeq 4$MeV. The power plant at the Chooz village has two reactors, and the total thermal power is 8.5GW_{th}.[4] A reactor of 1GW_{th} yields about $1.6 \times 10^{20}\,\overline{\nu}_e$ in each second. The experiment was able to measure the number of background events in the reactor-off period. The liquid scintillator detector contains a 5ton of mineral oil loaded with 0.09% Gd (Gadolinium). It was placed about 1km away from the reactors and in underground of 300mwe (meters water equivalent) as schematically shown in Fig. 3.7, where the cosmic muon flux of $\sim 10^{-2}\text{cm}^{-2}\text{s}^{-1}$ at surface is reduced to $0.4 \times 10^{-4}\text{cm}^{-2}\text{s}^{-1}$.

The $\overline{\nu}_e$'s were detected by the inverse β decay

$$p + \overline{\nu}_e \to n + e^+. \tag{3.11}$$

Since the reactor neutrinos have low energy, the inverse β decay occurs only with free protons (hydrogen nuclei) in the liquid scintillator which is approximately regarded as CH_2. The energy threshold of the reaction is $E_\nu = 1.8$MeV. The produced e^+ is detected by prompt signal with 1-8MeV energy which consists of the scintillation light and the energy of its annihilation with e^-. Then, about 30μs ($\simeq 6$cm) after the prompt signal the secondary signal of about 8MeV energy occurs due to the neutron capture by Gd and its subsequent decay by emitting gamma rays. The $\overline{\nu}_e$ events are identified accurately by those two signals and the time difference; The procedure is referred to as "delayed coincidence" which was used with Cd (cadmium) loaded scintillator at the time of the neutrino discovery [77]. The 1km baseline makes the experiment focus on

$$\Delta m^2 = \frac{\pi}{2}\,\frac{4(\text{MeV})}{1.27 \times 1000(\text{m})} \simeq 5 \times 10^{-3}\text{eV}^2. \tag{3.12}$$

The CHOOZ experiment searched for the deficit of $\overline{\nu}_e$ is analyzed with the disappearance probability which can be written in a good approximation in 3ν scheme as

$$1 - P(\overline{\nu}_e \to \overline{\nu}_e) = \sin^2 2\theta_{13}\,\sin^2\left(\frac{\Delta m^2_{31} L}{4E}\right). \tag{3.13}$$

The matter effect is neglected because of the short base line and the low energy. There was no deficit in the measurement of about one year exposure[5] accumulating $\simeq 2500\ \overline{\nu}_e$ signal

[4] The electrical power is about 0.33 times the thermal power.

[5] It corresponds to about 100day exposure with the full power of the reactors.

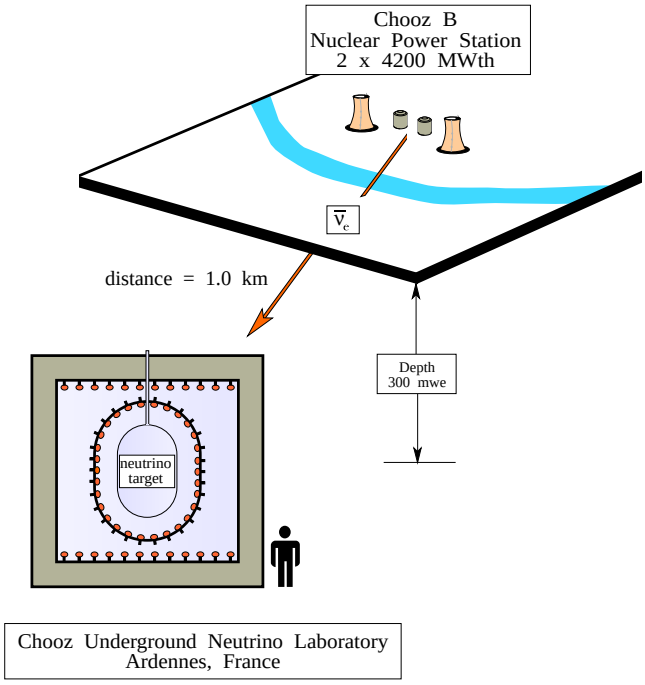

Figure 3.7: A schematic figure of the configuration of the CHOOZ experiment. The detector will be the prototype of the detector for proposed Japanese reactor experiment which is explained in Chapters 5 and 6.

which means $1/\sqrt{2500} = 2\%$ statistical error and the number of signal events is enough for the sensitivity with 2.7% systematic error to saturate. Fig. 3.8 shows the excluded region on the $\sin^2 2\theta_{13}$-$|\Delta m^2_{31}|$ plane at 90% CL for 2 degrees of freedom. The upper bound on θ_{13} at 90% CL by only the CHOOZ experiment is roughly

$$\sin^2 2\theta_{13} \lesssim 0.1. \tag{3.14}$$

The Palo Verde reactor experiment [78] gave a consistent result with the CHOOZ result.

Since solar neutrino and KamLAND results shows that Δm^2_{21} is very small and Δm^2_{31} is similar to Δm^2_{32} which is measured by atmospheric neutrino and K2K experiments, we need to constrain only $\sin^2 2\theta_{13}$ by reactor experiments. Therefore, we can rely on the analysis for 1 degree of freedom, which gives more stringent bound than the analysis for 2 degrees of freedom. The most recent global analysis for 1 degree of freedom [79] results in at 90% CL

$$\sin^2 2\theta_{13} \lesssim 0.15. \tag{3.15}$$

3.3.2 Bugey experiment

The Bugey experiment [80] is another interesting reactor experiment. It is in fact a prototype for the future reactor experiment with multi-detector to be discussed in Chapter 5. The Bugey experiment used two detectors which consist of three identical modules. Those detectors were placed very short distances from a $2.8\mathrm{GW_{th}}$ reactor; The baselines[6] are 15m and 40m. The detectors are of 600 liters liquid scintillator with H/C ratio of 1.4 and loaded with ^{6}Li of 0.15% in mass, which emits gamma rays of 4.8MeV total energy as the secondary signal due to a neutron capture. The experiment also could measure in the reactor off period, and is was possible to estimate background events to subtract.

In 2ν case, the $\Delta\chi^2$ for the sensitivity to nonzero θ of disappearance experiments at the oscillation maximum is roughly described as

$$\Delta\chi^2_{da} \equiv \frac{\left(N_0 \ \sin^2 2\theta\right)^2}{N_0(1-\sin^2 2\theta) + N_{\rm BG} + \sigma^2_{\rm sys}\{N_0(1-\sin^2 2\theta)\}^2 + \sigma^2_{\rm BG}N^2_{\rm BG}}, \tag{3.16}$$

where N_0 is the number of events without oscillation, $N_{\rm BG}$ is the number of background events, and $\sigma_{\rm sys}$ ($\sigma_{\rm BG}$) is the systematic error for signal (background) events. The small mixing makes the sensitivity dominated by $\sigma_{\rm sys}$ because the statistical error and background fraction are suppressed by the large number of signal events ($\sim 10^4$ events for

[6] Actually, the Bugey nuclear power plant has four reactors. The near detector position (15m) is also 90m far from the next nearest reactor.

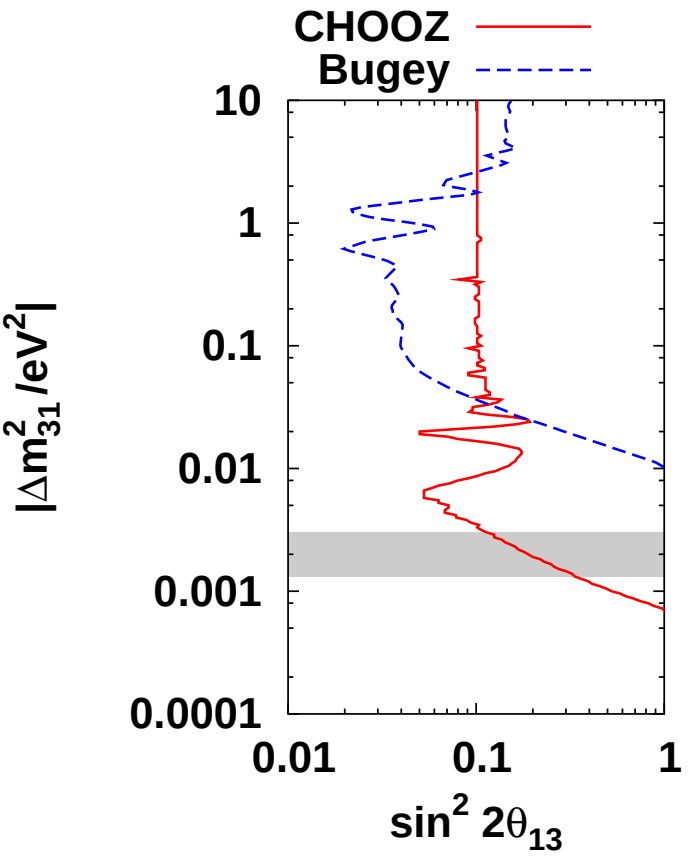

Figure 3.8: The CHOOZ and the Bugey results at 90% CL for 2 degrees of freedom are presented by solid and dashed lines, respectively. The right side of each lines is excluded by those experiments. The 90% allowed region, $1.3 \times 10^{-3}\,\mathrm{eV}^2 < |\Delta m_{31}| < 3.0 \times 10^{-3}\,\mathrm{eV}^2$, of the SK atmospheric neutrino measurement is superimposed by a shaded band.

Bugey). Thus, the systematic errors on the number of signal events is the key point for the precision measurement of small $\sin^2 2\theta_{13}$ in reactor experiments. The advantage of reactor θ_{13} experiments is that it requires rather short time and/or small detectors to obtain the final result by virtue of the large amount of the observed events due to the small disappearance probability and the short distance.[7] The Bugey experiment reduced the 5% systematic errors on the normalization to 2% by comparing the total numbers of events at near and far detectors. The 2% error is smaller than 2.7% of the CHOOZ experiment. The result did not show significant $\overline{\nu}_e$ deficit, and the excluded parameter region is presented in Fig. 3.8. Unfortunately, the relevant bound on $\sin^2 2\theta_{13}$ is looser than that of the CHOOZ in the Δm^2 region of $\sim 10^{-3}\mathrm{eV}^2$ where SK favored later despite their smaller systematic error because the baseline was too short to probe the region.

[7]Conversely, it can be shown that larger number of signal events does not help us to improve the sensitivity without any improvement of the systematic errors.

Chapter 4

Future Long Baseline Experiments and the Problem of Parameter Degeneracy

4.1 Future Long Baseline Experiments

4.1.1 An overview

A conventional way to measure θ_{13} is the appearance measurement in the long baseline (LBL) neutrino oscillation experiments. This subsection is devoted to a brief overview of the future LBL experiments. The LBL experiments will explore neutrino oscillations with respect to Δm^2_{31}, which relates to the atmospheric neutrino oscillation. The baseline lengths are $\sim 10^2$-10^3km, and the large detector and the intense beam are necessary. and intense neutrino beam. The mixing angle θ_{13} can be observed by the measurement of the oscillation probability $P(\nu_\mu \to \nu_e)$, for example. Then, if θ_{13} is not too small, precise measurement of $P(\nu_\mu \to \nu_e)$ and its CP transform $P(\overline{\nu}_\mu \to \overline{\nu}_e)$ will give us the value of CP phase δ.

MINOS experiment (Main Injector Neutrino Oscillation Search) [81] will start in December 2004, and it will be the first one of the next generation LBL experiment. The detector is 5.4kt of magnetized (1.5T) iron-scintillator sandwich calorimeters at the Soudan mine. The magnetized detector enable us to distinguish particles and anti-particles and to check CPT invariance. The neutrino beam (ν_μ or $\overline{\nu}_\mu$) is produced at Fermilab by NuMI (Neutrinos at the Main Injector) whose power is 0.4MW providing 4×10^{13} protons of 120GeV for each 1.9s within 8.1μs spill. The neutrino beam is the wide band beam, and the mean energy of neutrinos can be tuned to 3-18GeV. Unfortunately, since the baseline is 735km, the neutrino energy is larger than that of the first oscillation maximum for

$|\Delta m^2_{31}| \simeq 2.5 \times 10^{-3}\mathrm{eV}^2$:

$$E \simeq 1.27 \times \frac{2}{\pi} \times 735(\mathrm{km}) \times 2.5 \times 10^{-3}(\mathrm{eV}^2) \simeq 1.5\mathrm{GeV}. \tag{4.1}$$

MINOS will be able to reduce the error on $|\Delta m^2_{31}|$, whose recent error is about 40%, to 10% at 90% CL by ν_μ disappearance measurement. The result will be helpful for succeeding LBL experiments to tune precisely their beam energy to the oscillation maximum. The longer baseline length than 250km of K2K may give some information about matter effect, namely about the sign of Δm^2_{31}. The experiment seems, however, to be rather far from optimal one for ν_e appearance search in the present state of affairs because the search with wide band beam suffers from large number of background,

NuMI beam is planed to be used as off-axis beam also [82]. Off-axis beam is a better option for ν_e appearance search as described in the next subsection. The NuMI off-axis experiment is proposed to use 50kt detector at the direction of 0.8° off-axis, and the baseline is 810km. The experiment can probe smaller θ_{13} ($\simeq 10^{-2}$) than MINOS experiment by $\nu_\mu \to \nu_e$ oscillation search.

CNGS (CERN Neutrinos to Gran Sasso) project aims to observe ν_τ appearance due to $\nu_\mu \to \nu_\tau$ oscillation. The baseline is 732km. The neutrino beam is produced by the 400GeV super proton synchrotron, and the mean energy of the neutrinos ($\simeq$ 17GeV) is large enough to produce τ ($m_\tau = 1.776$GeV) by charged-current interaction of ν_τ. There are two proposed detectors, OPERA (Oscillation Project with Emulsion-tRacking Apparatus) and ICARUS (Imaging Cosmic And Rare Underground Signals). OPERA uses 1.8kt detector composed of Pb plates and emulsion firms. Emulsion detectors can record particle tracks precisely, and the high spatial resolution enable us to see the track of τ who has very short lifetime $\simeq 2.9 \times 10^{-14}$s. The expected result of the number of τ events is 10.3 for 5 year run (2.25×10^{20} protons on target) assuming $|\Delta m^2_{31}| = 2.5 \times 10^{-3}\mathrm{eV}^2$ and $\theta_{23} = \pi/4$; The expected number of background is 0.65. The ν_e appearance search of OPERA can probe $\sin^2 2\theta_{13} \simeq 0.06$ at 90% CL. On the other hand, ICARUS detector is 3kt time projection chamber filled with liquid argon. ICARUS selects out τ events kinematically from backgrounds. The expected result of the number of τ events is 11.9 for 5 year run (2.25×10^{20} protons on target) with $|\Delta m^2_{31}| = 2.5 \times 10^{-3}\mathrm{eV}^2$ and $\theta_{23} = \pi/4$, and the number of expected background is 0.7. The sensitivity of ICARUS to $\sin^2 2\theta_{13}$ is expected to be $\simeq 0.04$ at 90% CL.

J-PARC to Kamioka experiment [19] will use off-axis 2° ν_μ beam from J-PARC (Japan Proton Accelerator Research Complex) at Tokai village, and the neutrinos will be detected by the existing Super-Kamiokande (50kt total mass) in its phase I. The baseline is 295km and the peak energy of the beam is about 0.7GeV which corresponds approximately to the first oscillation maximum for the baseline and $|\Delta m^2_{31}| = 3.0 \times 10^{-3}\mathrm{eV}^2$. The $\nu_m u$

disappearance measurement in the experiment can measure $|\Delta m^2_{31}|$ and $\sin^2 2\theta_{23}$ with the errors of $\lesssim 10^{-4}\mathrm{eV}^2$ (10%) and $\lesssim 0.01$ (1%) at 90% CL, respectively. By searching for ν_e appearance, J-PARC experiment is expected to probe $\sin^2 2\theta_{13}$ down to $\simeq 0.006$ at 90% CL. In its phase II, beam power is expected to be upgraded from 0.75MW to 4MW, and a much large detector Hyper-Kamiokande (1Mt total mass) is to be build. By using $\overline{\nu}_\mu$ beam after the exposure with ν_μ one, the experiment can observe CP violating phase δ at 3σ CL if it is larger than 20° and $\sin^2 2\theta > 0.01$. In the following parts of this thesis, we focus on J-PARC experiment because it has the largest reality and the highest sensitivity to θ_{13} and δ among various proposals. The next subsection is devoted to explain the experiment more for better understanding of the discussions in the later sections.

The experiments described above use the so-called conventional super-beam. Other possibilities are also proposed. One is the so-called neutrino factory [86] which produces intense ν_e or $\overline{\nu}_e$ beam by the decay of muons in the storage ring. In order to observe $\nu_e \to \nu_\mu$ oscillation, charge discrimination of final state leptons is necessary because muon decay produces not only e-flavor neutrino but also wrong sign μ-flavor neutrino: $\mu^+ \to e^+ + \nu_e + \overline{\nu}_\mu$. The other possibility is referred to as the beta beam [87] which is obtained by the beta decay of accelerated nucleons, ^{18}Ne for ν_e and ^{6}He for $\overline{\nu}_e$. Note that each beam is pure without contaminations of other neutrinos. The mean energies of ν_e and $\overline{\nu}_e$ beams are 0.36 and 0.24GeV, respectively. Those energies are close to the first oscillation maximum one for $|\Delta m^2_{31}| = 2.5 \times 10^{-3}\mathrm{eV}^2$ and about 150km which corresponds to the baseline of 130km between CERN and Fréjus. Although the neutrino factory and the beta beam experiments are expected to have extremely high sensitivity to θ_{13} and δ, the realization of such experiments seems, however, to require long time for the research and the development.

4.1.2 J-PARC to Kamioka experiment

Hereafter, we concentrate our attention to the J-PARC to Kamioka experiment [19] among future LBL experiments. The J-PARC at Tokai village is a research complex with 50GeV proton synchrotron as a principal machine whose intensity is 3.3×10^{14} protons per pulse of 0.285Hz; The design beam power is 0.75MW and the beam spill is $\simeq 5.2\mu$s. The accelerator is to deriver 10^{21} protons on target (POT) in each year which corresponds to 123 days operation with the full power. The proton bombardment on target yields pions and the decay of π^+ (π^-) produces ν_μ ($\overline{\nu}_\mu$) beam. The selection of ν_μ or $\overline{\nu}_\mu$ is achieved by the magnetic horn with the right polarity to eliminate wrong sign pions. The intensity of low energy neutrino is approximately proportional to the proton beam power. The proton beam power may be upgraded to 4MW in the future. On the other hand, the detector is the existing Super-Kamiokande with fully reconstructed 11,146 photo-multiplier tubes,

whose fiducial mass is 22.5kt of the 50kt total mass. The baseline length is 295km.

The signal in the appearance (disappearance) measurement is the single ring e-like (μ-like) events due to final state charged leptons produced by charged-current quasi-elastic interaction with nucleons in the water, $\nu_e n \to e^- p$ ($\nu_\mu n \to \mu^- p$). The background comes from pions produced by inelastic interactions of high energy neutrinos, $\nu N \to \nu N' \pi$ or $\nu N \to l N' \pi$. The main background for the ν_μ disappearance measurement is caused by charged pions because they can imitate muon produced by the charged-current quasi-elastic interaction of lower energy ν_μ. On the other hand, the background in the ν_e appearance search is due to π^0; They decay into two γ, and it can be misidentified as a electron when one γ is missed. Here, we should take into account also that ν_μ beam is not pure due to ν_e contamination[1] which mimics perfectly the signal of $\nu_\mu \to \nu_e$ oscillation.

An possibility to reduce high energy neutrinos, which give low energy background, and the ν_e contamination is to use the narrow band beam (NBB) instead of the wide band beam (WBB). The NBB is obtained by selecting parent pions with bending magnets. The peak energy of the neutrino beam is controlled by the pion energy selection as we see in Fig. 4.2(a). NBB 1.5GeVπ and NBB 3GeVπ mean NBB with 1.5 and 3GeV pions, respectively. On the other hand, ν_e contamination is reduced also by using off axis beam (OAB) [88], namely by placing the detector in the direction of a few degrees off the direction of the parent $\pi^\pm$ beam. The daughter neutrino energy E_ν of $\pi \to \nu\mu$ decay relates to the off axis angle ϕ as

$$E_\nu = \frac{m_\pi^2 - m_\mu^2}{2\left(E_\pi - \sqrt{(E_\pi^2 - m_\pi^2)}\cos\phi\right)}, \tag{4.2}$$

where E_π denotes the parent pion energy, and $m_\pi \simeq 0.14$GeV and $m_\mu \simeq 0.1$GeV are $\pi^\pm$ and muon masses, respectively. The peak energy of neutrinos is adjustable by taking an appropriate off axis angle ϕ.(See Fig. 4.1 and Fig. 4.2.) In order to maximize the oscillation of ν_μ and $\overline{\nu}_\mu$ into other flavor neutrinos, the neutrino beam energy is tuned to

$$E = \frac{2}{\pi} \times 1.27 \times L(\text{km}) \times |\Delta m_{31}^2|(\text{eV}^2) \simeq 0.6\text{GeV}, \tag{4.3}$$

where $|\Delta m_{31}^2| \simeq 2.5 \times 10^{-3}\,\text{eV}^2$. Thus, NBB 1.5GeV$\pi$ and the off axis 2° beam may be appropriate for the value of $|\Delta m_{31}^2|$. The OAB2° has, however, higher intensity and lower ν_e contamination at the peak energy than those for NBB 1.5GeVπ as we see in Table 4.1. Therefore, OAB2° may be the better choice. Roughly speaking, the 0.2% ν_e contamination in OAB2° at the energy of the oscillation maximum shows that 0.2% is the sensitivity limit to the measurement of the ν_e appearance probability. Remaining backgrounds by pions are reduced by stringent event selections. (See also Sect. 6.3.1.)

[1]The low energy ν_e is due to $\mu^+ \to e^+ \nu_e \overline{\nu}_\mu$, and high energy one to $K^+ \to \pi^0 e^+ \nu_e$ or $K_L^0 \to \pi^- e^+ \nu_e$.

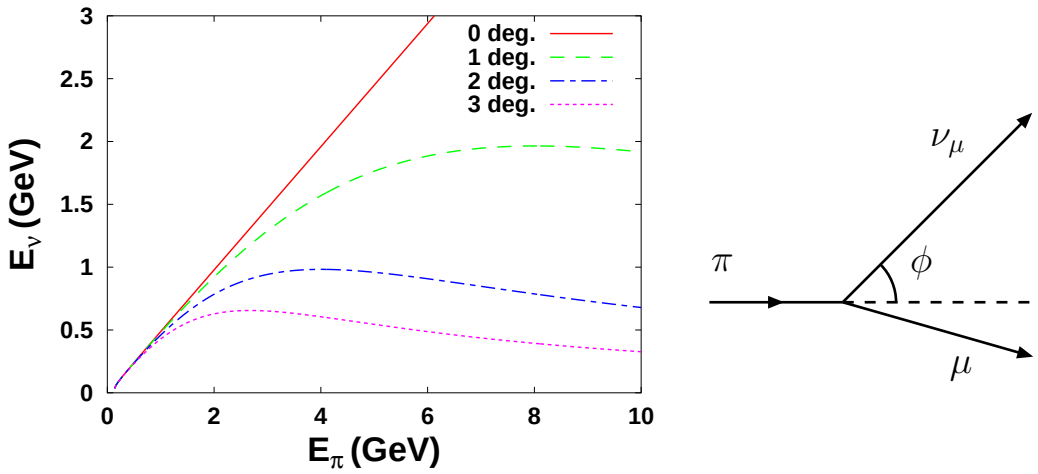

Figure 4.1: The relation between the parent pion energy E_π and the energy E_ν of the daughter neutrino emitted to the direction of off axis angle ϕ degree. It is seen that high energy pions produce neutrinos of similar E_ν. Thus, neutrino beam of narrow spectrum is obtained. The off-axis beam hardly includes high energy neutrinos which cause background.

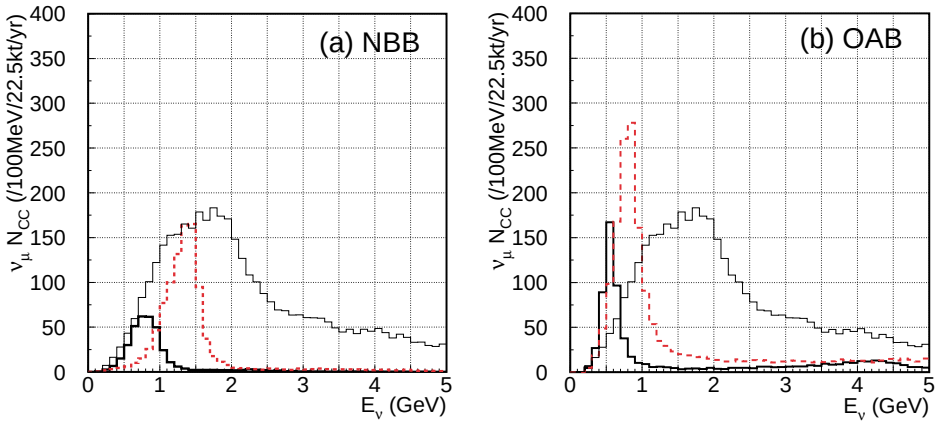

Figure 4.2: Energy spectra for the number of ν_μ charged-current events within 100MeV bins. No oscillation and one year exposure (10^{21} POT) with SK are assumed. (a): The spectrums for NBB 1.5GeVπ and NBB 3GeVπ are presented with solid and dashed lines, respectively. The thin line is for the spectrum of WBB. (b): The spectra for OAB3° and OAB2° are presented with normal and dashed lines, respectively. The thin line is for the spectrum of WBB.

		flux		ν_e/ν_μ (%)		# of interact.	
beam	$E_{\rm peak}$ (GeV)	ν_μ	μ_e	total	$E_{\rm peak}$	ν_μ	ν_e
WBB	1.1	25.5	0.19	0.74	0.34	7000	78
NBB 1.5GeVπ	0.7	5.3	0.05	1.00	0.39	510	5.7
NBB 3GeVπ	1.4	8.0	0.05	0.65	0.16	1400	9.3
OA3°	0.55	10.6	0.13	1.21	0.20	1100	29
OA2°	0.7	19.2	0.19	1.00	0.21	3100	60

Table 4.1: Beam properties. The unit of the flux is $10^6/\mathrm{cm}^2/\mathrm{yr}$. The "total" column shows the ratio of the fluxes integrated over neutrino energy, and the "$E_{\rm peak}$" column of the ratio shows the ratio at $E_{\rm peak}$. The number of interactions is the sum ($0 \le E_\nu \le 50$GeV) of the expected numbers of CC and NC events without oscillation in the unit of /22.5kt/yr.

There are three aims of the oscillation experiment. The first is the precise determination of $|\Delta m^2_{31}|$ and $\sin^2 2\theta_{23}$ by the measurement of ν_μ disappearance probability in 2ν approximation:

$$1 - P(\nu_\mu \to \nu_\mu) \simeq \sin^2 2\theta_{23} \, \sin^2 \frac{\Delta m^2_{31} L}{4E}. \tag{4.4}$$

We ignore the Earth matter effect in this discussion for clarity of explanation of the essential features. In fact, the matter effect in J-PARC neutrino project is smaller than that in most of the other LBL experiments by virtue of the rather short baseline (295km). For the survival probability of ν_μ, correction to (4.4) due to matter effect and other oscillation parameters is actually negligible because of the large value of the main term. The expected precisions of $\sin^2 2\theta_{23}$ and $|\Delta m^2_{31}|$ are ~ 0.01 and $\sim 10^{-4}\,\mathrm{eV}^2$ at 1σ CL. I would like to mention that this oscillation is very unique because it is almost maximal disappearance. The feature of the statistical analysis for the measurement is similar to that for appearance experiments. Therefore, applying severe selection on signal events and accumulation of selected events may improve the accuracy of small $\cos 2\theta_{23}$ measurement similarly to the following ν_e appearance measurement.

The second is the measurement of $\sin^2 2\theta_{13}$, whose value is not yet known, by searching for ν_μ oscillation to ν_e:

$$P(\nu_\mu \to \nu_e) \simeq s^2_{23} \sin^2 2\theta_{13} \, \sin^2 \frac{\Delta m^2_{31} L}{4E}. \tag{4.5}$$

Is is found that the precision of $\sin^2 2\theta_{23}$ measurement is important for the $\sin^2 2\theta_{13}$ sensitivity. The exposure time with ν_μ beam for above two aims (simultaneous) is assumed to be 5 years. In 2ν case, $\Delta\chi^2$ for the sensitivity to nonzero θ_{13} at the oscillation maximum

is roughly understood by

$$\Delta\chi_a^2 \equiv \frac{\left(N_0\, s_{23}^2 \sin^2 2\theta_{13}\right)^2}{N_0\, s_{23}^2 \sin^2 2\theta_{13} + N_{\rm BG} + \sigma_{\rm S}^2 (N_0\, s_{23}^2 \sin^2 2\theta_{13})^2 + \sigma_{\rm BG}^2 N_{\rm BG}^2}, \tag{4.6}$$

where N_0 is the number of events for $s_{23}^2 \sin^2 2\theta_{13} = 1$, $N_{\rm BG}$ is the number of background events, and $\sigma_{\rm S}$ ($\sigma_{\rm BG}$) is the systematic error for signal (background) events. The first and second terms in the denominator of the right-hand side are statistical errors which are negligible for large exposure. Then, we obtain the sensitivity in the limit of large statistics

$$(s_{23}^2 \sin^2 2\theta_{13})^2 \simeq \frac{\sigma_{\rm BG}^2 \Delta\chi_a^2}{1 - \sigma_{\rm S}^2 \Delta\chi_a^2} \frac{N_{\rm BG}^2}{N_0^2}, \tag{4.7}$$

where $\Delta\chi_a^2$ is fixed for the corresponding CL. Therefore, the key points for high sensitivity are to perform stringent event selections to make $N_{\rm BG}/N_0$ small, and to accumulate large number of selected signal events to make statistical errors small. It is an advantage of appearance experiments that those improvements of the sensitivity can be achieved by rather brute force without improvements of systematic errors ($\sigma_{\rm S}$ and $\sigma_{\rm BG}$). The sensitivity to $\sin^2 2\theta_{13}$ in the J-PARC neutrino project is expected to reach to 0.006 at 90% CL for 5 years exposure with $\sigma_{\rm BG} \leq 10\%$. There are, however, rather large additional ambiguities from the terms ignored in (4.6) due to unknown δ, matter effect, and $\theta_{23} \leftrightarrow \pi/2 - \theta_{23}$ ambiguity (if $\theta_{23} \neq \pi/4$), because $\sin^2 2\theta_{13}$ is so small as we will see in the next subsection.

On the other hand, the accuracy of θ_{13} determination in appearance experiments is roughly understood by

$$\Delta\chi_{a2}^2 \equiv \frac{\left(N_0\, s_{23}^2 \sin^2 2\theta_{13} - N_0\, s_{23}^2 \sin^2 2\theta_{13}^{\rm best}\right)^2}{N_0\, s_{23}^2 \sin^2 2\theta_{13}^{\rm best} + N_{\rm BG} + \sigma_{\rm S}^2 (N_0\, s_{23}^2 \sin^2 2\theta_{13}^{\rm best})^2 + \sigma_{\rm BG}^2 N_{\rm BG}^2}, \tag{4.8}$$

where $\theta_{13}^{\rm best}$ is the best fit value of θ_{13} determined by experiments. Thus, the larger $\theta_{13}^{\rm best}$ gives less accuracy due to larger value of the denominator of $\Delta\chi_{a2}^2$. while the accuracy in $\overline{\nu}_\mu$ disappearance experiments (reactor experiments) is almost independent of $\theta_{13}^{\rm best}$. (See Chapter 5.)

The third is the observation of the leptonic CP violation due to the CP phase δ. Since the terms ignored in (4.6) include CP violating one, the observation needs the precise measurement of ν_e and $\overline{\nu}_e$ appearance probabilities ($P(\nu_\mu \to \nu_e)$ and $P(\overline{\nu}_\mu \to \overline{\nu}_e)$) with ν_μ and $\overline{\nu}_\mu$ beams, respectively. It is necessary for the observation of CP violation that θ_{13} is not very small because δ appears with θ_{13} in the mixing matrix (2.35). Since the CP violating effect is extremely small, the beam power and the detector volume are expected to be upgraded to 4MW and 540kt fiducial mass of the Hyper-Kamiokande, respectively. The exposure time of $\overline{\nu}_\mu$ beam must be about 3 times longer than that of ν_μ beam because of smallness of antineutrino cross sections (See Fig. 4.3.); The periods are expected to be

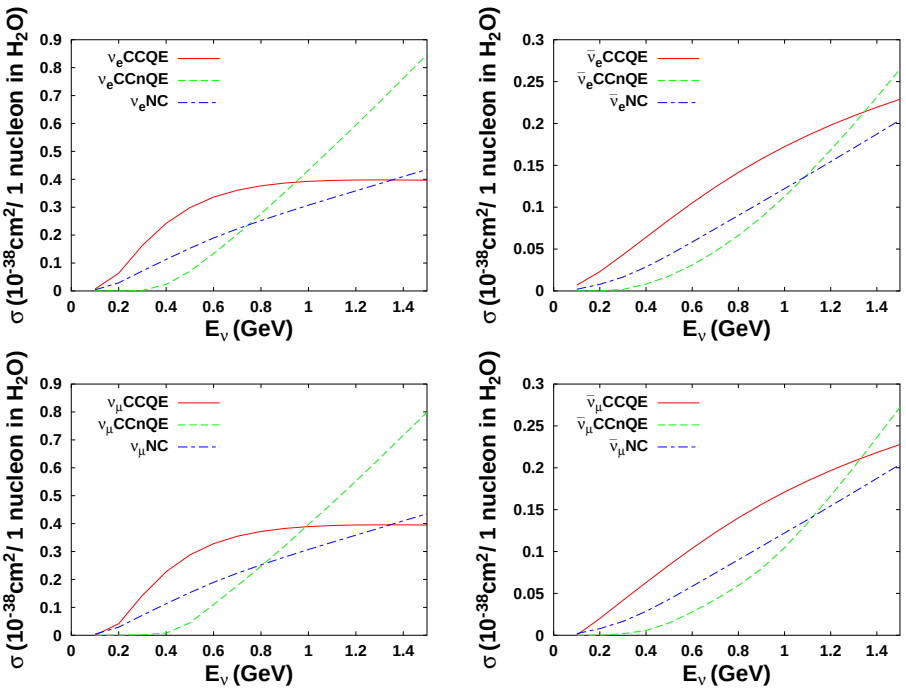

Figure 4.3: Cross sections with one averaged nucleon in H_2O [89]. Solid lines are of charged-current quasi-elastic interaction (CCQE). Dashed lines are of charged-current non-quasi-elastic interaction (CCnQE). Dash-dotted lines are of neutral-current interaction (NC).

2 years and 6.8 years for ν_μ and $\overline{\nu}_\mu$ beams, respectively. The observation is affected by the parameter degeneracy problem [15, 16, 17, 18] as described in Sect. 4.2. The confusion between CP conservation and violation due to the intrinsic degeneracy is, however, avoided by tuning the neutrino energy to the oscillation maximum energy ($E \simeq 0.6$GeV) [18, 20]. The sensitivity limit to CP violation (non-zero δ) is expected to be $\delta \simeq 20^\circ$ at 3σ CL for $\sin^2 2\theta_{13} > 0.01$.

4.2 The Problem of Parameter Degeneracy

4.2.1 An overview of the problem

The most important goal of neutrino oscillation experiment is to measure CP violating phase δ. Naively, it can be determined by measurement of $P(\nu_\mu \to \nu_e)$ and $P(\overline{\nu}_\mu \to \overline{\nu}_e) = CP[P(\nu_\mu \to \nu_e)]$ in long baseline (LBL) experiments. The measurement of δ has, however, a notorious problem so-called "parameter degeneracy" which prevents us from determining uniquely the values of oscillation parameters [15, 16, 17, 18]. There are three kinds of the degeneracy, and I will give a brief review of the problem below.

In LBL experiments, we should take the matter effect into account because the neutrino beams pass through the Earth matter in a long distance. The oscillation probabilities $P_{\mu e} \equiv P(\nu_\mu \to \nu_e)$ and $\overline{P}_{\mu e} \equiv P(\overline{\nu}_\mu \to \overline{\nu}_e)$ in matter are complicated functions of the oscillation parameters. Fortunately, there are small expansion parameters $\epsilon \equiv \Delta m^2_{21}/\Delta m^2_{31}$ and $\sin^2 2\theta_{13}$ by which the probabilities can be expanded: $|\epsilon| \simeq 0.03$, $\sin^2 2\theta_{13} \lesssim 0.1$. Then, the probabilities up to second order in ϵ and $\sin 2\theta_{13}$ are obtained [91, 92] as

$$\begin{aligned} P_{\mu e} &= \left| X \sin 2\theta_{13} + Z\, e^{i(\delta + \Delta_{31}/2)} \right|^2 \\ &= X^2 \sin^2 2\theta_{13} + 2XZ\, \sin 2\theta_{13} \cos\left(\delta + \frac{\Delta_{31}}{2}\right) + Z^2, \end{aligned} \tag{4.9}$$

$$\begin{aligned} \overline{P}_{\mu e} &= \left| \overline{X} \sin 2\theta_{13} + Z\, e^{i(\delta - \Delta_{31}/2)} \right|^2 \\ &= \overline{X}^2 \sin^2 2\theta_{13} + 2\overline{X}Z\, \sin 2\theta_{13} \cos\left(\delta - \frac{\Delta_{31}}{2}\right) + Z^2, \end{aligned} \tag{4.10}$$

where

$$\Delta_{jk} \equiv \frac{\Delta m^2_{jk} L}{2E}, \tag{4.11}$$

$$X \equiv f s_{23}, \quad \overline{X} \equiv \overline{f} s_{23}, \tag{4.12}$$

$$Z \equiv \epsilon\, c_{23}\, \sin 2\theta_{12}\, \frac{\sin(\hat{A}\Delta_{31}/2)}{\hat{A}}, \tag{4.13}$$

$$f, \overline{f} \equiv \frac{\sin((1 \mp \hat{A})\Delta_{31}/2)}{1 \mp \hat{A}}, \quad \hat{A} \equiv \frac{2\sqrt{2}\, G_{\rm F} N_e E_\nu}{\Delta m^2_{31}}. \tag{4.14}$$

	case I	case II	case III	case IV
θ_{23}	$< \pi/4$	$< \pi/4$	$> \pi/4$	$> \pi/4$
$\mathrm{sign}(\Delta m^2_{31})$	$+$	$-$	$+$	$-$

Table 4.2: Possible cases of discrete undetermined values relate with the parameter degeneracy problem. In each case, the intrinsic degeneracy (See Fig. 4.4.) occurs.

For simplicity, let us first deal with the case of one sign of Δm^2_{31} and fix parameter values except for $\sin^2 2\theta_{13}$ and δ. In this case, when a value of $P_{\mu e}$ is given, we can obtain $\sin 2\theta_{13}$ as unique function of δ:

$$\begin{aligned}\sin 2\theta_{13} &= -\frac{Z}{X}\cos\left(\delta + \frac{\Delta_{31}}{2}\right) \\ &\quad + \sqrt{\left\{\frac{Z}{X}\cos\left(\delta + \frac{\Delta_{31}}{2}\right)\right\}^2 + \frac{1}{X^2}\left(P_{e\mu} - Z^2\right)}. \end{aligned} \tag{4.15}$$

The sign in front of the square-root is chosen so that $\theta_{13} \geq 0$ because mixing parameters are defined as $0 \leq \theta_{jk} \leq \pi/2$ and $0 \leq \delta \leq 2\pi$ without loss the generality [30]. The first term mainly determines the δ-dependence: $\sin 2\theta_{13} \sim \cos(\delta + \Delta_{31}/2)$. On the other hand, a given $\overline{P}_{\mu e}$ provides another constraint: $\sin 2\theta_{13} \sim \cos(\delta - \Delta_{31}/2)$. It is clear that those two cosine curves of experimental constraints intersect at two points in the δ-θ_{13} space. (See Fig. 4.4.) One of those intersections is the true solution, and another is the fake solution. We can not determine which is the true solution of $\{\delta, \theta_{13}\}$; This is the so-called "intrinsic degeneracy" which is a part of the parameter degeneracy problem.

The problem includes two discrete degeneracy problems also. The appearance probabilities (4.9) and (4.10) depend on s^2_{23} which is to be constrained stringently by the ν_μ disappearance measurement. The observable in the disappearance measurement is, however, not s^2_{23} but $\sin^2 2\theta_{23}$:

$$1 - P(\nu_\mu \to \nu_\mu) = \sin^2 2\theta_{23}\, \sin^2\left(\frac{\Delta m^2_{31} L}{4E}\right). \tag{4.16}$$

Thus, two values of s^2_{23} are allowed because θ_{23} and $\theta'_{23} \equiv \pi/2 - \theta_{23}$ give the same value of $\sin^2 2\theta_{23}$: $\sin 2\theta_{23} = \sin(\pi - 2\theta_{23})$. Furthermore, the sign of Δm^2_{31} have not been determined yet. The ambiguity affects the oscillation probabilities (4.9) and (4.10) in LBL experiments through the matter effect. Therefore, there are four allowed cases as listed in Table 4.2. Since the intrinsic degeneracy problem occurs for each case, there are eight solutions of $\{\delta, \theta_{13}\}$ in the end (eight-fold degeneracy).

The parameter degeneracy problem is very serious because $\delta = 0$ can be allowed even if the true value is $\delta = \pi/2$, and vice versa. It means that the confusion between CP

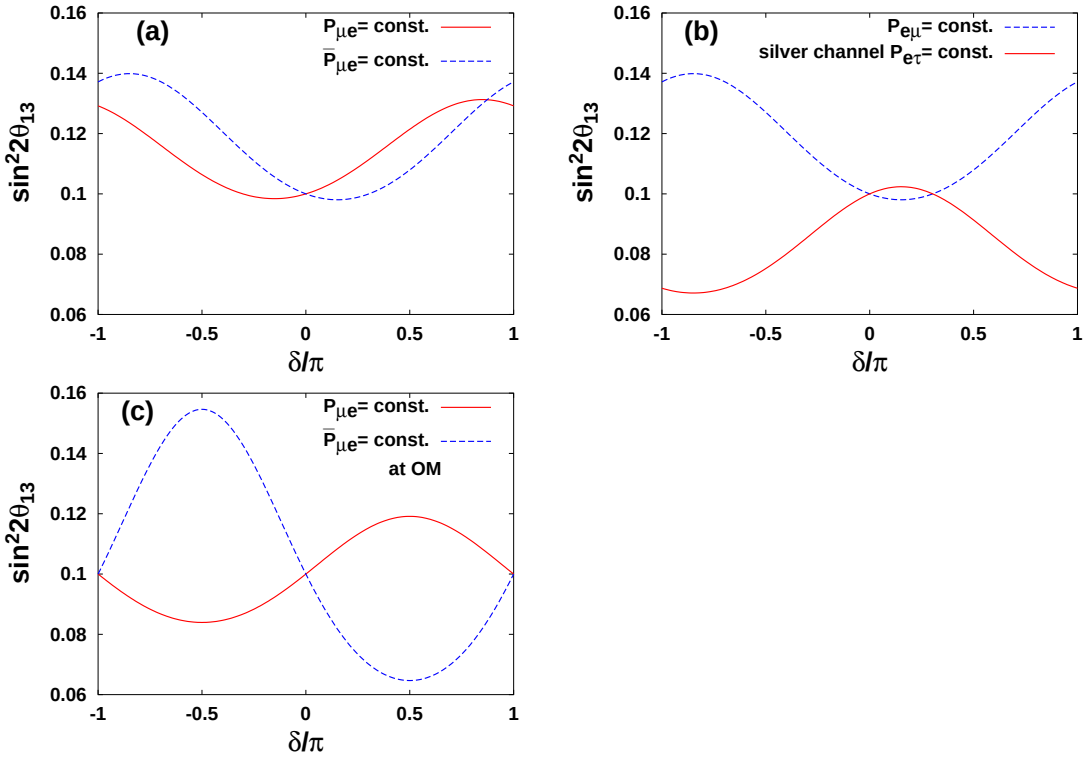

Figure 4.4: The situation of δ-$\sin^2 2\theta_{13}$ degeneracy problem by using $P_{\mu e}$ and $\overline{P}_{\mu e}$ or $P_{e\mu}$ and $P_{e\tau}$, namely (4.9) and (4.10) or (4.17) and (4.18). There are two intersections in each figure; One is the true solution and the other is a fake one. True values of parameters are chosen as $\delta = 0$, $\sin^2 2\theta_{13} = 0.1$, $\Delta m^2_{21} = 7.3 \times 10^{-5}\text{eV}^2$, $0 < \Delta m^2_{31} = 2.5 \times 10^{-3}\text{eV}^2$, $\tan^2\theta_{12} = 0.38$, $\sin^2 2\theta_{23} = 0.5$, $\rho = 2.3\text{g}\cdot\text{cm}^{-3}$, $Y_e = 0.5$. The measurement is assumed to be done with $L = 3000$km and $E_\nu = 20$GeV (mono-energetic beam) for figures (a) and (b). (a): The situation with $P_{\mu e}$ and $\overline{P}_{\mu e}$. This is similar to that with $P_{e\mu}$ and $\overline{P}_{e\mu}$. Since two curves in (a) are similar to each other, rather wide allowed region will be obtained by considering experimental errors. (b): This is the situation with $P_{e\mu}$ and $P_{e\tau}$ which is called the "silver channel". Note that two solutions have a value of θ_{13}. The difference between the central values of those cosine curves are due to the matter effect. (c): The situation with $P_{\mu e}$ and $\overline{P}_{\mu e}$, but differently from (a) the beam energy is tuned to the oscillation maximum energy ($\simeq 6$GeV). Note that two solutions give a set of $\{\sin\delta, \theta_{13}\}$ which does not cause the confusion between CP conservation and violation. The allowed region will concentrate well around the solution.

conservation and violation can arise. Moreover, even if we obtain rather large θ_{13}, it can be the fake solution of small true value. Since the problem is intrinsic to the nature of the neutrino oscillation, the problem can not be solved however accurate the measurement is.

A way to break the degeneracy is to combine information obtained with different oscillation modes or L/E. Actually, the eight-fold degeneracy exists for a measurement of three measurement: $P(\nu_\mu \to \nu_\mu)$, $P(\nu_\mu \to \nu_e)$, and $P(\overline{\nu}_\mu \to \overline{\nu}_e)$. The seven fake solutions do not necessarily explain results of LBL experiments using different E/L or oscillation channels. Since there are three types of degeneracy, the eight-fold degeneracy is resolved by three other results (totally five results) of LBL experiments even at the worst [93]. In principle, precise shape analysis of event spectrum helps us because the analysis is similar to using results of several LBL experiments with different energies.

Among other oscillation modes, the measurement of $P_{e\tau} \equiv P(\nu_e \to \nu_\tau)$ is interesting though ν_τ detection is rather difficult [94]. The oscillation is referred to as the "silver channel" in the neutrino factory in contrast to the "golden channel" $P_{e\mu}$. The oscillation probabilities up to second order in $\epsilon \equiv \Delta m^2_{21}/\Delta m^2_{31}$ and $\sin 2\theta_{13}$ are

$$P_{e\mu} = X^2 \sin^2 2\theta_{13} + 2XZ \sin 2\theta_{13} \cos\left(\delta - \frac{\Delta_{31}}{2}\right) + Z^2, \tag{4.17}$$

$$P_{e\tau} = X_\tau^2 \sin^2 2\theta_{13} - 2XZ \sin 2\theta_{13} \cos\left(\delta - \frac{\Delta_{31}}{2}\right) + Z_\tau^2, \tag{4.18}$$

where

$$X_\tau \equiv f c_{23}, \quad Z_\tau \equiv \epsilon\, s_{23} \sin 2\theta_{12} \frac{\sin(\hat{A}\Delta_{13}/2)}{\hat{A}}. \tag{4.19}$$

$P_{e\mu}$ is obtained from $\overline{P}_{\mu e}$ of (4.10) by replacing A with $-A$, namely $\overline{X}$ with X. Note that X_τ is obtained from X by exchanging s_{23} and c_{23}. Consequently, the difference between X and X_τ can help us to resolve the θ_{23} degeneracy if θ_{13} is rather large so that the terms of $\sin^2 2\theta_{13}$ in (4.17) and (4.18) dominate over other terms. Next, note that the δ-dependent term of (4.18) has the opposite sign to that of $P_{e\mu}$. Thus, although the intrinsic degeneracy arises also for the measurement of $P_{e\mu}$ and $P_{e\tau}$ with the same L/E, the two solutions of $\{\delta,\, \theta_{13}\}$ have the same value of θ_{13}. The opposite behavior of $P_{e\mu}$ and $P_{e\tau}$ with respect to δ has the advantage also in statistical analyses, namely it gives rather small allowed region (precise determination of parameter values) in the δ-θ_{13} space.

The intrinsic degeneracy in $P_{\mu e}$ and $\overline{P}_{\mu e}$ also can be tamed [18, 20]. Assuming the mono-energetic beam tuned the energy to the oscillation maximum energy ($|\Delta m_{31}|L/4E = \pi/2$), the oscillation probabilities (4.9) and (4.10) become

$$P_{\mu e} = X^2 \sin^2 2\theta_{13} - 2XZ \sin 2\theta_{13} \sin\delta + Z^2, \tag{4.20}$$

$$\overline{P}_{\mu e} = \overline{X}^2 \sin^2 2\theta_{13} + 2\overline{X}Z \sin 2\theta_{13} \sin\delta + Z^2. \tag{4.21}$$

Note that the phase of the δ-dependent term in (4.20) is different from that in (4.21) by just π. Thus, two solution of $\{\delta, \theta_{13}\}$ caused by intrinsic degeneracy collapse into a solution of $\{\sin\delta, \theta_{13}\}$ for the measurement of $P_{\mu e}$ and $\overline{P}_{\mu e}$ with mono-energetic beams at the oscillation maximum. It is remarkable that the way of determination of $\sin\delta$ never cause the confusion between CP conservation and violation. Of course, the large difference of δ dependence leads to rather precise determination of the parameters as the case of using $P_{e\tau}$. The essential point of the reduction is the elimination of $\cos\delta$ term from oscillation probabilities. Even for non-mono-energetic ν_μ beams, we can eliminate $\cos\delta$ term in principle from the predicted total number of signal ν_e events by tuning the beam energy so as to satisfy

$$\int_{E_{\rm min}}^{E_{\rm max}} \phi\,\sigma\,X Z \cos\frac{\Delta_{31}}{2} = 0, \tag{4.22}$$

where $E_{\rm min} < E_\nu < E_{\rm max}$ is the neutrino energy range in which signal events are counted, and ϕ and σ represent the beam flux and the cross section, respectively; The same argument holds for $\overline{\nu}_\mu$ beam also.

4.2.2 Another viewpoint of the problem

In this subsection, the eight-fold degeneracy is explained from another point of view with the $\sin^2 2\theta_{13}$-s^2_{23} space for convenience of understanding the discussion in Chapter 5.

Let us first define the symbols $x \equiv \sin^2 2\theta_{13}$ and $y \equiv s^2_{23}$. If $|\epsilon| \equiv |\Delta m^2_{21}/\Delta m^2_{31}|$ and $|\hat{A}| \equiv |A/\Delta m^2_{31}|$ are vanishing (or extremely small), $P_{\mu e}$ and $\overline{P}_{\mu e}$ become a vacuum oscillation probability of two generation neutrinos: $P_{\mu e} = \overline{P}_{\mu e} = xy$. A given value of $P_{\mu e}$ puts a constraint $xy = constant$. On the other hand, the disappearance probability $1 - P_{\mu\mu}$ with $\theta_{23} = \pi/4$ gives a constraint $y = constant$. Then, those constraints can determine a solution as shown in Fig. 4.5(a).

If the 2-3 mixing angle is not maximal one, $\theta_{23} \neq \pi/4$, the disappearance probability becomes two constraints $y = y_1$ and y_2, where $y_2 = 1 - y_1$ corresponding to the $\theta_{23} \leftrightarrow \pi/2 - \theta_{23}$ ambiguity. It is then obvious in Fig. 4.5(b) that there are two crossing points of these curves. This is the simplest version of the $(\theta_{13}, \theta_{23})$ degeneracy problem.

Next, We discuss what happens when finite $|\epsilon| \equiv |\Delta m^2_{21}/\Delta m^2_{31}|$ is took into account. In this case, $\overline{P}_{\mu e}$ is not necessarily the same as $P_{\mu e}$ due to CP phase δ. A given set of $P_{\mu e}$ and $\overline{P}_{\mu e}$ puts a contour that crosses two $y = constant$ lines at four points in general (Fig. 4.5(c)). It results in the four-fold degeneracy. Each point on the contour corresponds to a value of δ. Simultaneously, the two $y = constant$ lines are slightly bent and the splitting between those two curves becomes smaller at larger $\sin^2 2\theta_{13}$, though the effect is too tiny to be clearly seen.

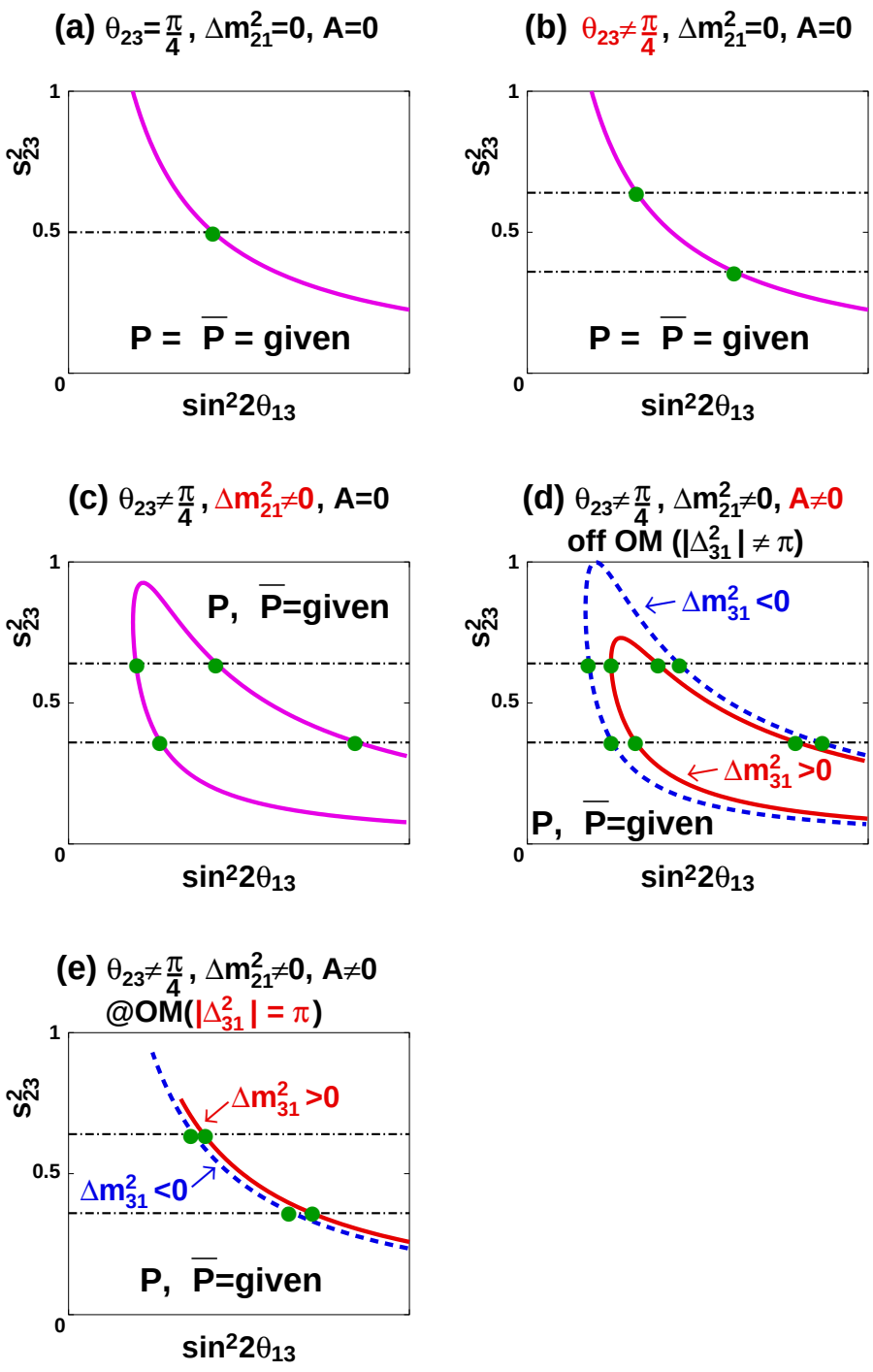

Figure 4.5: Schematic figures to see how the seven fake solutions arise (the eight-fold degeneracy) in the $\sin^2 2\theta_{13}$-s^2_{23} space. See the explanation in Sect. 4.2.2.

If the baseline distance is longer, the Earth matter effect $\hat{A} \equiv A/\Delta m^2_{31}$ comes in and splits each appearance contour into two, depending upon the sign of Δm^2_{31}. Then, there are eight solutions in general as displayed in Fig. 4.5(d). This is a simple pictorial representation of the maximal eight-fold parameter degeneracy with the $\sin^2 2\theta_{13}$-s^2_{23} space.

Additionally, if we tune the beam energy to that of the oscillation maximum $|\Delta_{31}| = \pi$ (strictly speaking, (4.22) should be satisfied), two appearance contours are collapsed as we see in Fig. 4.5(e). In this case, the eight-fold degeneracy becomes four-fold one in the $\sin^2 2\theta_{13}$-s^2_{23} space because there is a solution of $\sin^2 2\theta_{13}$ for each case of Table 4.2. (See also Fig. 4.4(c).) Furthermore, small matter effect makes the degeneracy simple two-fold one in the space, which is the fact that we use in Chapter 5.

Chapter 5

Reactor Measurement of θ_{13} and Its Complementarity to Long Baseline Experiments

5.1 Possibility to Measure θ_{13} by the Future Reactor Experiment

5.1.1 Reactor experiment as a clean laboratory for θ_{13} measurement

In this thesis, we explore the possibility of measuring θ_{13} by the disappearance measurement of $\overline{\nu}_e$ from nuclear reactors. Since the reactor $\overline{\nu}_e$ is low energy neutrino ($E \simeq 4$MeV), the oscillation becomes maximal at short distance, $\simeq 1$km for $|\Delta m^2_{31}| = 2.5 \times 10^{-3}\text{eV}^2$. Thus, the reactor experiment can accumulate large number of events with rather small detector and/or short time scale. In this thesis, it is emphasized that the reactor $\overline{\nu}_e$ disappearance experiment provides particularly clean environment for the measurement of θ_{13} while the measurement by the long baseline (LBL) experiment with only neutrino beam suffers from large uncertainty due to unknown CP phase δ.[1] Thus, the reactor measurement of θ_{13} will give us valuable information complementary to the one from LBL experiments. The complementary nature is discussed in later parts of this chapter, and let us first study in this section how clean the measurement of θ_{13} by the reactor experiments is. We examine possible "contamination" on the reactor θ_{13} measurement by δ, the matter effect, the sign of Δm^2_{31}, and the solar parameters one by one.

We first note that, due to its low neutrino energy of a few MeV, the reactor experiments are inherently disappearance experiments, which can measure only the survival probability

[1] Even for the long baseline experiment with neutrino and antineutrino beam, the determination of parameter values is disturbed by the parameter degeneracy problem which is discussed in Sect. 4.2.

$P(\bar{\nu}_e \to \bar{\nu}_e)$. It is well known that the survival probability does not depend on the CP phase δ in arbitrary matter densities [95].

In any reactor experiment on the Earth, short or long baseline, the matter effect is very small because the neutrino energy E is quite low and can be ignored to a good approximation. It can be seen by comparing the matter and the vacuum effects (as the matter correction comes in only through this combination in the approximate formula in [91])

$$\begin{aligned} |\hat{A}| &= \frac{2aE}{|\Delta m^2_{31}|} \\ &= 2.8 \times 10^{-4} \left(\frac{|\Delta m^2_{31}|}{2.5 \times 10^{-3}\,\mathrm{eV}^2} \right)^{-1} \left(\frac{E}{4\,\mathrm{MeV}} \right) \left(\frac{\rho}{2.3\,\mathrm{g \cdot cm^{-3}}} \right) \left(\frac{Y_e}{0.5} \right), \end{aligned} \quad (5.1)$$

where $a = \sqrt{2} G_F N_e$ denotes the index of refraction in matter with G_F being the Fermi constant, and N_e the electron number density in the Earth; N_e is related to the Earth matter density ρ as $N_e = Y_e \rho / m_p$ where Y_e is proton fraction and $m_p = 0.938$GeV is proton mass. Hereafter, the Earth matter density is taken to be $\rho = 2.3\,\mathrm{g \cdot cm^{-3}}$ based on the estimate given in [96]. The electron fraction Y_e is taken to be 0.5. The best fit value of $|\Delta m^2_{31}|$ is given by $|\Delta m^2_{31}| = 2.5 \times 10^{-3}\,\mathrm{eV}^2$ from the Super-Kamiokande (SK) atmospheric neutrino data [97], and we use this as the reference value for $|\Delta m^2_{31}|$ throughout this thesis.[2]

Since $|\hat{A}|$ is negligible for reactor experiments, the vacuum probability formula applies. The exact expression of $P(\bar{\nu}_e \to \bar{\nu}_e)$ for 3ν case in vacuum is given by

$$\begin{aligned} 1 - P(\bar{\nu}_e \to \bar{\nu}_e) &= 4 \sum_{j>k} |U_{ej}|^2 |U_{ek}|^2 \sin^2 \left(\frac{\Delta m^2_{jk} L}{4E} \right) \\ &= \sin^2 2\theta_{13} \sin^2 \frac{\Delta_{31}}{2} - \frac{1}{2} s^2_{12} \sin^2 2\theta_{13} \sin \Delta_{31} \sin \Delta_{21} \\ &\quad + c^4_{13} \sin^2 2\theta_{12} \sin^2 \frac{\Delta_{21}}{2} + s^2_{12} \sin^2 2\theta_{13} \cos \Delta_{31} \sin^2 \frac{\Delta_{21}}{2}, \end{aligned} \quad (5.2)$$

where the parametrization (2.35) has been used in the second line and we used $\Delta_{ij} \equiv \Delta m^2_{ij} L / 2E$. Note that only the second term in the last equality depends on the sign of Δm^2_{31}. Relatively to the main depletion term which is the first term in the last equality of (5.2), other three terms are suppressed by ϵ, $\epsilon^2 / \sin^2 2\theta_{13}$, ϵ^2, respectively, where $\epsilon \equiv \Delta m^2_{21} / \Delta m^2_{31}$. Assuming that $|\Delta m^2_{31}| = 1.3\text{-}3.0 \times 10^{-3}\,\mathrm{eV}^2$ [67], we obtain $|\epsilon| \simeq 0.1\text{-}0.01$ for the LMA MSW solar neutrino solution, $\Delta m^2_{21} = 3\text{-}9 \times 10^{-5}\,\mathrm{eV}^2$ [74]. Then, the second and the fourth terms in the last equality can be ignored, although the second term can be comparable to the main depletion term by $|\epsilon| \simeq 0.1$. (Notice that we are considering the

[2] $|\Delta m^2_{31}| = 2 \times 10^{-3}\,\mathrm{eV}^2$ is the most recent best fit value obtained by SK atmospheric neutrino analysis [67] but K2K data prefers larger value $|\Delta m^2_{31}| = 2.8 \times 10^{-3}\,\mathrm{eV}^2$ [97].

measurement of $\sin^2 2\theta_{13}$ in the range of 0.1-0.01.) Therefore, assuming that $|\Delta m^2_{31}|$ is determined precisely by LBL experiments, the reactor $\bar{\nu}_e$ disappearance experiment gives us a clean measurement of θ_{13} which is independent of any solar parameters except for the case of rather large $|\epsilon|$ and extremely small θ_{13}.

5.1.2 Near-far detector complex: basic concepts and estimation of sensitivity

In order to obtain a good sensitivity to $\sin^2 2\theta_{13}$, the selection of an optimized baseline and having small systematic errors are crucial. For instance, the baseline length that gives the first oscillation maximum for reactor $\bar{\nu}_e$'s which have typical energy 4MeV is about 1.7km for $\Delta m^2 \simeq 2.5 \times 10^{-3}\,\mathrm{eV}^2$. Along with this baseline selection, an order of magnitude improvement for the $\sin^2 2\theta_{13}$ sensitivity is possible at $\Delta m^2 \simeq 2.5 \times 10^{-3}\,\mathrm{eV}^2$ if the total systematic error can be reduced to 1% level which is 2.7 times better than the CHOOZ experiment [13]. In this section, we demonstrate that such kind of experiment is certainly possible.

The experiment with 1% systematic error should accumulate 10^4 $\overline{\nu}_e$ events in order to obtain 1% statistical error. Thus, we consider the Kashiwazaki-Kariwa nuclear power plant which is the most powerful in the world at this moment and whose maximum energy generation is $24.3\mathrm{GW}_{\mathrm{th}}$. Although the power plant consists of seven reactors we take the approximation of one reactor of $24.3\mathrm{GW}_{\mathrm{th}}$ thermal power in this thesis. A CHOOZ-like detector of Gd loaded liquid scintillator, is assumed to be placed with 1.7km baseline $\simeq$ 200m underground near the single reactor.

The major part of systematic errors is caused by the uncertainties in the neutrino flux calculation, number of protons (including the uncertainty of the detector volume), and the detection efficiency. For instance, in the CHOOZ experiment, the uncertainty of the neutrino flux is 2.1%, that of number of protons is 0.8%, and that of detection efficiency 1.5% as is shown in the Table 5.1. The uncertainty of the neutrino flux includes ambiguities of the reactor thermal power generation, the reactor fuel composition, the neutrino spectra from fissions, and so on. The uncertainty of the detection efficiency includes the ambiguity of the cross section of the inverse beta decay ($\overline{\nu}_e + p \to e^+ + n$). These systematic uncertainties, however, cancel out if we compare data taken by the detectors placed near and far from the reactor because these systematic uncertainties are correlated ones between the detectors. Furthermore, if the detectors are identical, many other errors such as the errors on the number of protons will be correlated ones and cancel out also. Therefore, it is better that the near detector is identical to the far detector as much as possible. This is more or less the strategy taken in the Bugey experiment [80].[3]

[3]The Krasnoyarsk group also plans in their Kr2Det proposal [98] to construct two identical 50ton liquid

We assume that a near detector, which is identical to the far detector, is located at 300m away from the reactor we consider.[4] In the actual setting with the Kashiwazaki-Kariwa power plant, two near detectors may be necessary due to extended array of seven reactors.[5]

To estimate how good the cancellation will be, we study the case of the Bugey experiment, which uses two detectors of three identical modules to detect $\overline{\nu}_e$ at 15 and 40m from a reactor. For the Bugey case, the uncertainty of the neutrino flux were completely canceled out, the error on the detection efficiency improved from 3.5 % to 1.7 %, and the error on the solid angle (the error on the baseline length) remained the same (0.5 % $\rightarrow$ 0.5 %) because it is proper to each detector. If each ratio of the improvement of errors in the Bugey case is applicable to the case considered in this thesis, the total systematic error will improve from 2.7 % (the systematic error in CHOOZ experiment) to 0.8 % as shown in the Table 5.1. The error on the solid angle is neglected because it will be small enough due to much longer baselines (300m and 1.7km) than the Bugey one. In this chapter, we take 2 % and 0.8 % as the reference values of the relative systematic error $\sigma_{\rm rel.sys}$ for the total number of $\bar{\nu}_e$ events in our analysis. Let us examine the physics potential of such a reactor experiment assuming these reference values for the systematic error. We take the Kashiwazaki-Kariwa reactor of 24.3 $\mathrm{GW_{th}}$ thermal power and assume its operation with 80 % efficiency. Two identical liquid scintillation detectors are located at 300 m and 1.7 km away from the reactor and assumed to detect $\bar{\nu}_e$ by delayed coincidence with 70 % detection efficiency. The $\bar{\nu}_e$'s of 1-8 MeV visible energy, $E_{\rm visi} = E_{\bar{\nu}_e} - 0.782\,\mathrm{MeV}$, are used and the number of events are counted in 14 bins of 0.5 MeV.

In order to calculate theoretical numbers of $\overline{\nu}_e$ events, we need the energy spectrum of reactor $\overline{\nu}_e$ flux and the cross section for the inverse β decay. We use a phenomenological spectrum [100]

$$\frac{dN_{\rm react}}{dE_{\overline{\nu}_e}} = \exp\left(a_0 + a_1 E_{\overline{\nu}_e} + a_2 E_{\overline{\nu}_e}^2\right), \tag{5.3}$$

where the left-hand side denotes the number density of $\overline{\nu}_e$ emitted with $E_{\overline{\nu}_e}$ by a fission; The values of fitting parameter a's are obtained for each isotope [100] as listed in Table 5.2. A fission yields about 5 $\overline{\nu}_e$. The fissions in reactors are dominated by that of ^{235}U which is contained in the fuel uranium to the fraction of a few %. Our reference fission rates of each isotope to the total number of fissions are listed in Table 5.3. For simplicity, the rates are fixed in our analysis though the fuel composition varies during the reactor operation. In Table 5.3 the thermal powers that are generated by a fission of each isotope [101] are also

scintillators at 1100m and 150m away from the Krasnoyarsk reactor.

[4]The closer the near detector to reactor, the better the sensitivity in the single-reactor case because of smaller oscillation probability. The situation is, however, more subtle for multiple-reactor case [99].

[5]It is shown even in this case that an effective 1 reactor and 2 detector approximation can give a very good estimation of the sensitivity [99].

Bugey	absolute	relative	relative/absolute
flux	2.8%	0.0%	0
number of protons	1.9%	0.6%	0.32
solid angle	0.5%	0.5%	1
detection efficiency	3.5%	1.7%	0.49
total	4.9%	2.0%	

new experiment (Kashiwazaki-Kariwa)	absolute (CHOOZ)	relative (expected)	relative/absolute
flux	2.1%	0.0%	0
number of protons	0.8%	0.3%	0.38
detection efficiency	1.5%	0.7%	0.47
total	2.7%	0.8%	
for bins	8.1%	2.4%	

Table 5.1: Systematic errors in the Bugey experiment and a new experiment with two detectors similar to the CHOOZ one. In the Bugey experiments, absolute errors were reduced to relative errors by comparing events at near and far detectors. Relative errors in the new experiment are expectation with the same reduction rates of errors as those of Bugey. Bin-by-bin errors are estimated rather pessimistically as three times the errors for total numbers by (5.6).

isotope	^{235}U	^{239}Pu	^{238}U	^{241}Pu
a_0	0.870	0.896	0.976	0.793
a_1 (MeV^{-1})	-0.160	-0.239	-0.162	-0.080
a_2 (MeV^{-2})	-0.0910	-0.0981	-0.0790	-0.1085

Table 5.2: Parameters of the phenomenological spectra (5.3) of reactor $\overline{\nu}_e$ for each isotope [100].

isotope	^{235}U	^{239}Pu	^{238}U	^{241}Pu
fission rate	0.562	0.31	0.063	0.065
thermal power per fission (MeV)	201.7	205.0	210.0	212.4

Table 5.3: Contributions from each isotope to the thermal power of the reactor. The "fission rate" row shows an example of the values though the rates vary during the reactor operation; The main fuel ^{235}U decreases faster than other fuels, ^{239}Pu is produced easily from ^{238}U by a neutron capture and two times beta decay, and ^{241}Pu is produced from ^{239}Pu by a neutron capture twice. The values in the last row are taken from [101].

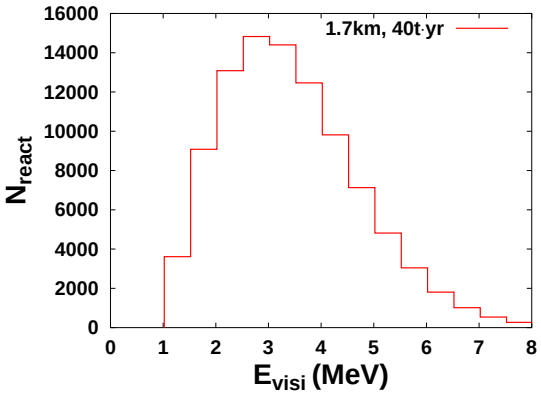

Figure 5.1: The spectrum of the number of events without oscillation expected in a 40 ton-year measurement at the distance of 1.7km from a 24.3GW$_{\rm th}$ reactor. $E_{\rm visi} = E_{\overline{\nu}_e} - 0.782$MeV is the energy of the prompt signal. The bin width is 0.5MeV. The total number of event within $E_{\rm visi}$ =1-8MeV is about 80,000 which corresponds to $1/\sqrt{80,000} = 0.35\%$ statistical error.

presented. On the other hand, the cross section [102] of $\overline{\nu}_e$ detection ($\overline{\nu}_e + p \to e^+ + n$) is

$$\sigma(E_{\overline{\nu}_e}) = 9.5 \times 10^{44}\, p_e(\text{MeV})\, E_e(\text{MeV})\ \text{cm}^2, \tag{5.4}$$

where p_e represents the positron momentum and $E_e = E_{\overline{\nu}_e} - 1.293$MeV is the positron energy. Without oscillation, a 10 (40) ton-year measurement at the far detector yields 20,000 (80,000) $\bar{\nu}_e$ events which is corresponds to a 0.7 (0.35) % statistical error. Fig. 5.1 shows the spectrum of the number of events expected in the 40 ton-year measurement.

The definition of $\Delta\chi^2$, which quantifies the deviation from the best fit point of the

"experimental data", is given by

$$\Delta\chi^2(|\Delta m^2_{31}|, \sin^2 2\theta_{13}) \equiv \sum_{i=1}^{14} \frac{\left\{ N_{fi} - \frac{N^{\rm best}_{fi}}{N^{\rm best}_{ni}} N_{ni} \right\}^2}{N^{\rm best}_{fi} + \left(\frac{N^{\rm best}_{fi}}{N^{\rm best}_{ni}} \right)^2 N^{\rm best}_{ni} + (\sigma^{\rm bin}_{\rm rel.sys})^2 \left(N^{\rm best}_{fi} \right)^2}. \tag{5.5}$$

$\sigma^{\rm bin}_{\rm rel.sys}$ is the relative systematic error for each bin which is assumed to be the same for all bins; N_{ai} denotes the theoretical number of $\bar{\nu}_e$ events at a-detector (near or far) within the ith energy bin, and $N^{\rm best}_{ai}$ does the number of events with the best fit values of parameters. The derivation of the $\Delta\chi^2$ is briefly explained in Appendix A.2. Assuming that the relative systematic error is uncorrelated among bins and distributed equally into bins, $\sigma^{\rm bin}_{\rm rel.sys}$ is estimated from the relative systematic error $\sigma_{\rm rel.sys}$ for the total number of events by

$$(\sigma^{\rm bin}_{\rm rel.sys})^2 = \sigma^2_{\rm rel.sys} \frac{\left(\sum_i N^{\rm best}_{fi} \right)^2}{\sum_i \left(N^{\rm best}_{fi} \right)^2}, \tag{5.6}$$

since the uncertainty squared of the total number of events is obtained by adding up the squared values of the bin-by-bin systematic uncertainties $\sigma^{\rm bin}_{\rm rel.sys} N^{\rm best}_{fi}$; The ratio $\sigma^{\rm bin}_{\rm rel.sys}/\sigma_{\rm rel.sys}$ is about 3 in our analysis. In order to compare two numbers of events, we use not the ratio N_{fi}/N_{ni} but a liner combination of the numbers of events $N_{fi} - (N^{\rm best}_{fi}/N^{\rm best}_{ni})N_{ni}$ because the statistical analysis with ratios is not well defined.[6](See, e.g., [103].) We assume that the value of $|\Delta m^2_{31}|$ is known to a precision of $10^{-4}\,{\rm eV}^2$ by the J-PARC $\rightarrow$ SK (hereafter, it is referred to as JPARC-SK). Then, $|\Delta m^2_{31}|$ can be regarded as a given number in the analysis of the reactor experiment. Therefore, we can rely on the analysis for 1 degree of freedom where we can obtain more stringent bound on θ_{13} than that for 2 degrees of freedom by protecting the information from outflowing to the other dimension of $|\Delta m^2_{31}|$. In practice, a consistency check will be necessary between $|\Delta m^2_{31}|$ obtained by LBL and reactor experiments with the analysis for 2 degrees of freedom before the analysis for 1 degree of freedom of the reactor experiment.

First, let us calculate how severely we can constrain $\sin^2 2\theta_{13}$ from above. For this purpose, we assume $\theta^{\rm best}_{13} = 0$. The 90% CL exclusion limits, which corresponds to $\Delta\chi^2 = 2.7$ for 1 degree of freedom, are presented in Fig. 5.2 for two cases: a 10 ton-year measurement with the 2 % systematic error in the total number of events and a 40 ton-year measurement with the 0.8 % error. The figure shows that it is possible to measure $\sin^2 2\theta_{13}$ down to 0.02 at the maximum sensitivity with respect to $|\Delta m^2_{31}|$, and to 0.04 for larger $|\Delta m^2_{31}|$ by a 40 ton-year measurement, provided the quoted values of the systematic errors are realized.

[6]The ratios or products of two provability variables that follow Gaussian probability distribution functions (p.d.f.) do not follow Gaussian p.d.f. while any liner combination of the original two variables does.

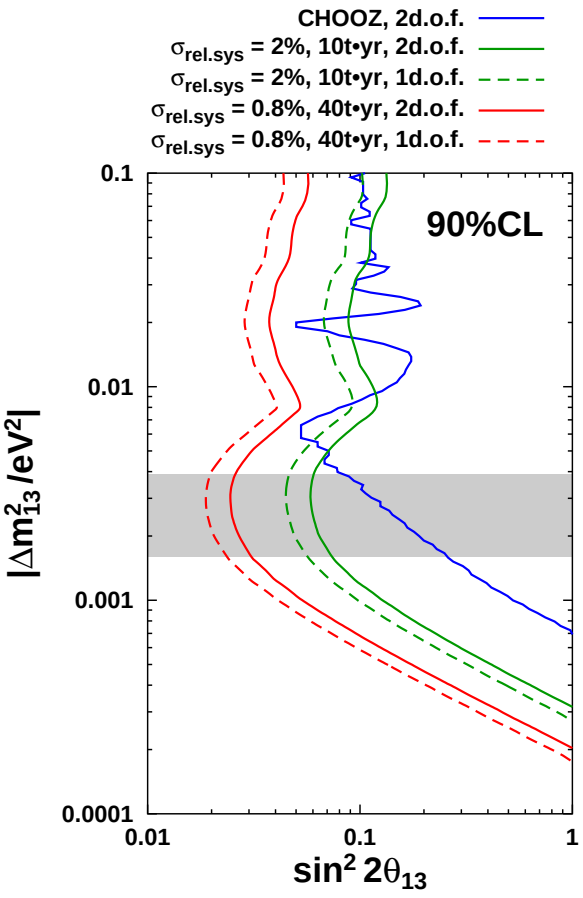

Figure 5.2: Shown are the 90% CL exclusion limits on $\sin^2 2\theta_{13}$ which can be placed by the reactor measurement as described in Sect. 5.1.2. From the left to right, the dash-dotted and the thin-dotted (the long-dashed and short-dashed) lines are based on analyses with 1 and 2 degrees of freedom, respectively, for $\sigma_{\mathrm{rel.sys}}$=0.8 %, 40 t·yr ($\sigma_{\mathrm{rel.sys}}$=2 %, 10 t·yr). The solid line is the CHOOZ result, and the 90 % CL interval $1.6\times10^{-3}\,\mathrm{eV}^2 \leq \Delta m^2_{31} \leq 3.9\times10^{-3}\,\mathrm{eV}^2$ of the Super-Kamiokande atmospheric neutrino data [97] is shown as a shaded strip.

The CHOOZ result [13] for 2 degrees of freedom is also depicted in Fig. 5.2. For a fair comparison with the CHOOZ contour, we also present in Fig. 5.2 the results of analysis with 2 degrees of freedom, which correspond to $\Delta\chi^2 = 4.6$ for 90 % CL, without assuming any precise knowledges on $|\Delta m^2_{31}|$ from other experiments.

Next, let us examine how precisely we could measure $\sin^2 2\theta_{13}$ around non-zero $\theta_{13}^{\rm best}$. We fixed $|\Delta m^2_{31}|$ as $|\Delta m^2_{31}|^{\rm best} = 2.5 \times 10^{-3}\,{\rm eV}^2$. The 90 % CL allowed regions of 1 degree of freedom, whose bounds correspond to $\Delta\chi^2 = 2.7$, are presented in Fig. 5.3 for the values of $\sin^2 2\theta_{13}^{\rm best}$ from 0.05 to 0.08 (0.02 to 0.08) in the unit of 0.01 in the case of a 10 ton-year (40 ton-year) measurement with systematic error $\sigma_{\rm rel.sys} = 2.0(0.8)$ %. We can read off the uncertainty at 90 % CL in $\sin^2 2\theta_{13}$ and it is almost independent of the central value $\sin^2 2\theta_{13}^{\rm best}$. Thus, we have

$$\begin{aligned} \sin^2 2\theta_{13} &= \sin^2 2\theta_{13}^{\rm best} \pm 0.043 \qquad (\text{at } 90\,\%\,\text{CL, d.o.f.} = 1) \\ &\quad \text{for} \quad \sin^2 2\theta_{13}^{\rm best} \gtrsim 0.05 \end{aligned}$$

in the case of $\sigma_{\rm rel.sys} = 2\,\%$ with a 10 ton-year measurement, and

$$\begin{aligned} \sin^2 2\theta_{13} &= \sin^2 2\theta_{13}^{\rm best} \pm 0.018 \qquad (\text{at } 90\,\%\,\text{CL, d.o.f.} = 1) \\ &\quad \text{for} \quad \sin^2 2\theta_{13}^{\rm best} \gtrsim 0.02 \end{aligned}$$

in the case of $\sigma_{\rm rel.sys} = 0.8\,\%$ with a 40 ton-year measurement.

5.2 Resolving the Parameter Degeneracy by Reactor Measurement of θ_{13}

While the reactor experiment is a pure measurement of θ_{13} as we see in Sect 5.1.1, LBL experiments are enriched with some other parameters which cause the complicate problem of parameter degeneracy. In this section we discuss how reactor experiments can contribute to resolve the parameter degeneracy. To make our discussion as concrete as possible we use the particular long-baseline experiment, the J-PARC neutrino project [19], to illuminate the complementary role played by reactor and long-baseline experiments. It is likely that the experiment will be carried out at around the first oscillation maximum ($|\Delta_{31}| = \pi$) for a number of reasons: the dip in energy spectrum in disappearance channel is the deepest, the number of appearance events are nearly maximal, and the two-fold degeneracy in δ becomes simple ($\delta \leftrightarrow \pi - \delta$) for each mass hierarchy [18, 20]. With the distance $L =$ 295km, the oscillation maximum is at around $E = 0.6$GeV. We assume, for definiteness, that a long-baseline disappearance measurement has resulted in $\sin^2 2\theta_{23} = 0.92$ and $\Delta m^2_{31} = 2.5 \times 10^{-3}\,{\rm eV}^2$. For the LMA solar neutrino parameters we take $\tan^2\theta_{12} = 0.38$

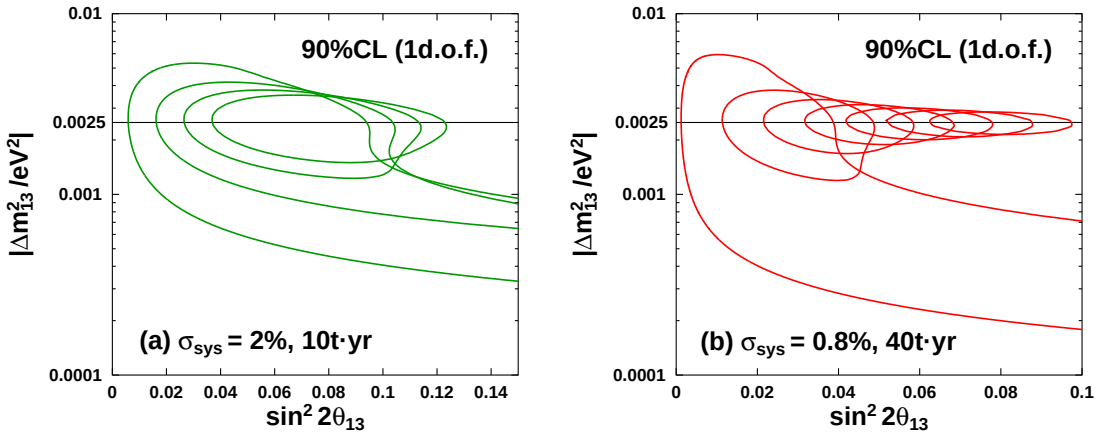

Figure 5.3: Shown is the accuracy of determination of $\sin^2 2\theta_{13}$ at 90 % CL for the case of positive evidence based on analysis with 1 degree of freedom, $\Delta\chi^2 = 2.7$. Figures (a) and (b) are for $\sigma_{\rm rel.sys}$=2%, 10 t·yr, and $\sigma_{\rm rel.sys}$=0.8%, 40 t·yr, respectively. The lines correspond to the best fit values of $\sin^2 2\theta_{13}$, from left to right, 0.05 to 0.08 in the unit of 0.01 in Fig. 5.3(a), and 0.02 to 0.08 in the unit of 0.01 in Fig. 5.3(b). The reference value of $|\Delta m^2_{31}|^{\rm best}$ is taken to be $2.5 \times 10^{-3}{\rm eV}^2$, which is indicated by a gray line.

and $\Delta m^2_{21} = 6.9 \times 10^{-5}\,{\rm eV}^2$ [10]. We use the values of these parameters throughout this chapter unless otherwise stated.

5.2.1 Illustration of how reactor measurement helps resolve the $\{\theta_{13}, \theta_{23}\}$ degeneracy

Let us first give an illustrative example showing how reactor experiments could help to resolve the $\{\theta_{13}, \theta_{23}\}$ degeneracy. If θ_{23} is not maximal, we have two solutions for θ_{23} (θ_{23} and $\theta'_{23} = \pi/2 - \theta_{23}$), even though we ignore the uncertainty in the determination of $\sin^2 2\theta_{23}$. For example, if $\sin^2 2\theta_{23} = 0.95$, which is perfectly allowed by the most recent atmospheric neutrino data [67], then s^2_{23} can be either 0.39 or 0.61. Since the dominant term in the appearance probability depends upon s^2_{23} instead of $\sin^2 2\theta_{23}$, it leads to ± 20 % difference in the number of appearance events in this case. On the other hand, even in the case of maximal mixing, it still leaves a rather wide range of θ_{23}, despite such fantastic accuracy of the measurement. 1 % accuracy in $\sin^2 2\theta_{23}$ implies about 10 % uncertainty in s^2_{23}. Thus, whenever we try to determine $\sin^2 2\theta_{13}$ from the appearance measurement, we have to face the ambiguity due to the two-fold nature of the solution for s^2_{23}.

To present a clear step-by-step explanation of the relationship between LBL and reactor experiments, we first plot in Fig. 5.4 the allowed regions in the $\sin^2 2\theta_{13}$–s^2_{23} plane by measurements of $P(\nu_\mu \to \nu_e)$ alone and $P(\bar{\nu}_\mu \to \bar{\nu}_e)$ alone separately. The former is

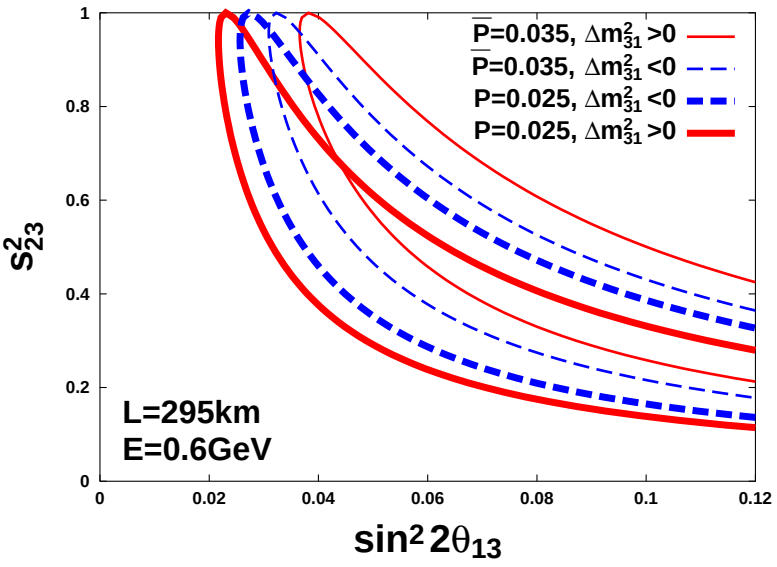

Figure 5.4: The allowed regions are shown in the $\sin^2 2\theta_{13}$–s^2_{23} plane determined with a given value of $P \equiv P(\nu_\mu \to \nu_e)$ alone (in this case $P = 0.025$), or $\bar{P} \equiv P(\bar{\nu}_\mu \to \bar{\nu}_e)$ alone (in this case $\bar{P} = 0.035$) at the oscillation maximum $|\Delta_{31}| = \pi$ of the J-PARC experiment. Each allowed region is the area bounded by the black solid (for $\Delta m^2_{31} > 0$ with P only), the black dashed (for $\Delta m^2_{31} < 0$ with P only), the gray solid (for $\Delta m^2_{31} > 0$ with $\bar{P}$ only), the gray dashed (for $\Delta m^2_{31} < 0$ with $\bar{P}$ only), respectively, where the line with a definite value of the CP phase δ sweeps out each region as δ varies from 0 to 2π. The oscillation parameters are taken as follows: $\Delta m^2_{31} = 2.5 \times 10^{-3}\text{eV}^2$, $\Delta m^2_{21} = 6.9 \times 10^{-5}\text{eV}^2$, $\tan^2\theta_{12} = 0.38$. The Earth density is taken to be ρ=2.3 g/cm^3.

indicated by the regions bounded by black lines and the latter by gray lines. The solid and dashed lines are used for cases with positive and negative Δm^2_{31}. The values of disappearance and appearance probabilities are chosen arbitrarily for illustrative purpose and are given in the caption of Fig. 5.4. Notice that the negative Δm^2_{31} curve is located right (left) to the positive Δm^2_{31} curve in neutrino (antineutrino) channel. A plot with only measurement in neutrino mode goes beyond academic interest because the J-PARC experiment is expected to run only with the neutrino mode in its first phase. We observe that there is large intrinsic uncertainty in the θ_{13} determination due to unknown δ, the problem addressed in [20]. The two regions corresponding to positive and negative Δm^2_{31} heavily overlap due to small matter effect. When two measurements of ν and $\bar{\nu}$ channels are combined, the allowed solution becomes a line which lies inside of the overlap of the ν and $\bar{\nu}$ regions for each sign of Δm^2_{31} in Fig. 5.4. In Fig. 5.5 we have plotted such solutions as two lines, one for positive Δm^2_{31} (the solid curve) and the other for negative Δm^2_{31} (the dashed curve) at the first oscillation maximum $|\Delta_{31}| = \pi$. It may appear curious that the two curves with positive and negative Δm^2_{31} almost overlap with each other in Fig. 5.5. In fact, a slight splitting between the solid ($\Delta m^2_{31} > 0$) and dashed ($\Delta m^2_{31} < 0$) lines is due to the fact that both $|\epsilon| \equiv \Delta m^2_{21}/|\Delta m^2_{31}|$ and the matter effect in the case of the J-PARC experiment are small. Thus, the degeneracy in the set $\{\theta_{13}, \theta_{23}\}$ is effectively two-fold in this case.

To have a feeling on whether the reactor experiment described in Sect. 5.1.2 will be able to resolve the degeneracy, we plot in Fig. 5.5 two sets of degenerate solutions by taking a particular value of θ_{23}, $\sin^2 2\theta_{23} = 0.92$, the lower end of the region allowed by Super-Kamiokande. We denote the true and fake solutions as $(\sin^2 2\theta_{13}, s^2_{23})$ and $(\sin^2 2\theta'_{13}, s^{2\,\prime}_{23})$, respectively, assuming the true θ_{23} satisfies $\theta_{23} < \pi/4$. We overlay in Fig. 5.5 a shadowed region to indicate the accuracy to be achieved by the reactor measurement of θ_{13}. If the experimental error $\delta_{\rm re}(\sin^2 2\theta_{13})$ in the reactor measurement of $\sin^2 2\theta_{13}$ is smaller than the difference

$$\delta_{\rm de}(\sin^2 2\theta_{13}) \equiv |\sin^2 2\theta'_{13} - \sin^2 2\theta_{13}| \tag{5.7}$$

due to the $\{\theta_{13}, \theta_{23}\}$ degeneracy, then the reactor experiment may resolve the degeneracy. Notice that once the θ_{23} degeneracy is lifted one can easily obtain four allowed sets of $\{\delta, \Delta m^2_{31}\}$ (though they are still degenerate at almost the same point on the $\sin^2 2\theta_{13}$–s^2_{23} plane) because the relationship between them is given analytically in a completely general setting [90].

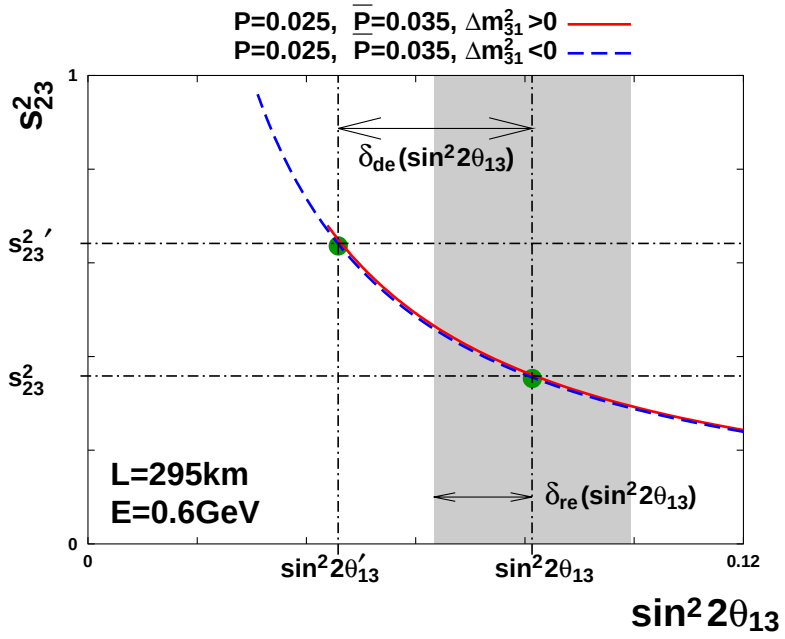

Figure 5.5: The allowed region in the $\sin^2 2\theta_{13}$–s^2_{23} plane becomes a line when both $P(\nu_\mu \to \nu_e)$ and $P(\bar{\nu}_\mu \to \bar{\nu}_e)$ are given (in this case $P(\nu_\mu \to \nu_e) = 0.025$, $P(\bar{\nu}_\mu \to \bar{\nu}_e) = 0.035$) at the oscillation maximum ($|\Delta_{31}| = \pi$, $E = 0.6$ GeV for the J-PARC experiment), as indicated in the figure. The solid and the dashed lines are for $\Delta m^2_{31} > 0$ and $\Delta m^2_{31} < 0$ cases, respectively. Assuming $\theta_{23} \neq \pi/4$, two solutions of ($\sin^2 2\theta_{13}$, s^2_{23}) are plotted; In this figure $\sin^2 2\theta_{23}$ is taken as 0.92. It is assumed arbitrarily that the solution of θ_{23} in the first octant ($\theta_{23} < \pi/4$) is the genuine one, while the one in the second octant ($\theta_{23} > \pi/4$) with primes is the fake one. Superimposed in the figure as a shaded region is the anticipated error in the reactor measurement of θ_{13} estimated in Sect. 5.1.2. If the error $\delta_{\rm re}(\sin^2 2\theta_{13})$ is smaller than the difference $\delta_{\rm de}(\sin^2 2\theta_{13}) \equiv |\sin^2 2\theta'_{13} - \sin^2 2\theta_{13}|$ due to the degeneracy, then the reactor experiment may be able to resolve it.

5.2.2 Resolving power of the $\{\theta_{13}, \theta_{23}\}$ degeneracy by a reactor measurement

Let us make a semi-quantitative estimate of how powerful the reactor method is for resolving the $\{\theta_{13}, \theta_{23}\}$ degeneracy.[7] For this purpose, we compare in this section the difference of the two θ_{13} solutions due to the degeneracy with the resolving power of the reactor experiment. We consider, for simplicity, the special case $|\Delta_{31}| = \pi$, i.e., energy tuned at the first oscillation maximum. The simplest case seems to be indicative of features of more generic cases.

As we saw in the previous section, there are two solutions of θ_{13} due to doubling of θ_{23} for a given $\sin^2 2\theta_{23}$ in each sign of Δm^2_{31}. Then, we define the fractional difference due to the degeneracy

$$\frac{\delta_{\rm de}(\sin^2 2\theta_{13})}{\sin^2 2\theta_{13}}. \tag{5.8}$$

It is to be compared with $\delta_{\rm re}(\sin^2 2\theta_{13})/\sin^2 2\theta_{13}$ of the reactor experiment, where $\delta_{\rm re}(\sin^2 2\theta_{13})$ denotes the experimental uncertainty estimated in Sect. 5.1.2, i.e., 0.043 or 0.018. In Fig. 5.6(a) we plot the normalized error $\delta_{\rm re}(\sin^2 2\theta_{13})/\sin^2 2\theta_{13}$ which is expected to be achieved in the reactor experiment described in Sect. 5.1.2. We restrict ourselves to the analysis with 1 degree of freedom, because we expect that the JPARC-SK will provide us accurate information on Δm^2_{31} by the time when the issue is really addressed. The fractional difference (5.8) can be computed from the relation [18]

$$\begin{aligned} \sin^2 2\theta'_{13} &= \sin^2 2\theta_{13} \tan^2\theta_{23} + \left(\frac{\Delta m^2_{21}}{\Delta m^2_{31}}\right)^2 \frac{\tan^2(aL/2)}{(aL/\pi)^2} \\ &\times \left[1 - (aL/\pi)^2\right] \sin^2 2\theta_{12} \left(1 - \tan^2\theta_{23}\right), \end{aligned} \tag{5.9}$$

and the result for $\delta_{\rm de}(\sin^2 2\theta_{13})/\sin^2 2\theta_{13}$ is plotted in Fig. 5.6(b) as a function of $\sin^2\theta_{23}$ for two typical values of ϵ. We notice that the fractional differences differ by up to a factor of ~ 2 in small $\sin^2 2\theta_{23}$ region between the first ($\theta_{23} < \pi/4$) and the second octant ($\theta_{23} > \pi/4$). For the best fit value of the two mass squared differences Δm^2_{21} ($6.9\times10^{-5}\,{\rm eV}^2$) and $|\Delta m^2_{31}|$ ($2.5\times10^{-3}\,{\rm eV}^2$), for which $|\epsilon| \equiv \Delta m^2_{21}/|\Delta m^2_{31}| = 0.028$, there is little difference between the case with $\sin^2 2\theta_{13} = 0.03$ and the one with $\sin^2 2\theta_{13} = 0.09$. In this case they are all approximated by the first term in (5.9) and $\delta_{\rm de}(\sin^2 2\theta_{13})/\sin^2 2\theta_{13}$ depends approximately only on θ_{23}, making the analysis easier. On the other hand, if the ratio $|\epsilon| \equiv \Delta m^2_{21}/|\Delta m^2_{31}|$ is much larger than that at the best fit point, then the second term in (5.9) is not negligible. In Fig. 5.6(b), $\delta_{\rm de}(\sin^2 2\theta_{13})/\sin^2 2\theta_{13}$ is plotted in an extreme case of $|\epsilon| = 1.9\times10^{-4}\,{\rm eV}^2/1.6\times10^{-3}\,{\rm eV}^2 = 0.12$, which is allowed at 90% CL

[7] An alternative way to resolve the ambiguity is to look at $\nu_e \to \nu_\tau$ channel because the main oscillation term in the probability $P(\nu_e \to \nu_\tau)$ depends upon c^2_{13}.

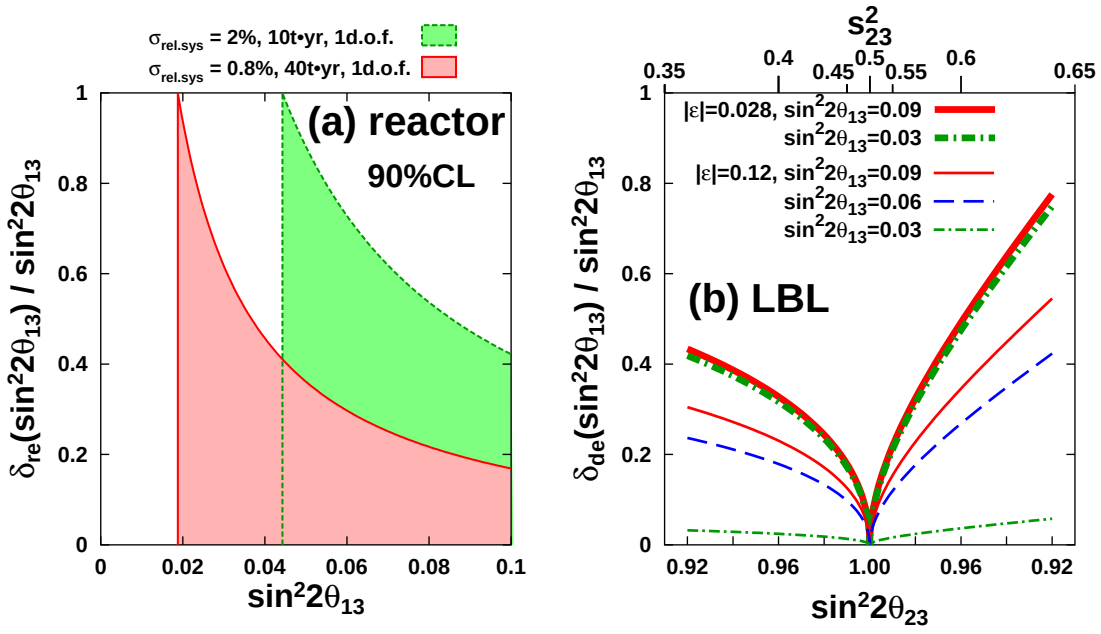

Figure 5.6: (a): The normalized error at 90 % CL in the reactor measurement of θ_{13} is given for $\sigma_{\rm rel.sys}$=2 %, 10 t·yr (d.o.f.=1, $\delta_{\rm re}(\sin^2 2\theta_{13}) = 0.043$) and for $\sigma_{\rm rel.sys}$=0.8 %, 40 t·yr (d.o.f.=1, $\delta_{\rm re}(\sin^2 2\theta_{13}) = 0.018$), respectively. Notice that the degrees of freedom becomes 1 once the value of $|\Delta m^2_{31}|$ is known from JPARC-SK. (b): The fractional difference $\delta_{\rm de}(\sin^2 2\theta_{13})/\sin^2 2\theta_{13}$ due to the degeneracy is plotted as a function of $\sin^2 2\theta_{23}$. Here, $\delta_{\rm de}(\sin^2 2\theta_{13}) \equiv |\sin^2 2\theta'_{13} - \sin^2 2\theta_{13}|$ stands for the difference between the true solution $\sin^2 2\theta_{13}$ and the fake one $\sin^2 2\theta'_{13}$, and $\epsilon \equiv \Delta m^2_{21}/\Delta m^2_{31}$; $|\epsilon| = 6.9 \times 10^{-5}\,{\rm eV}^2/2.5 \times 10^{-3}\,{\rm eV}^2 = 0.028$ is for the best fit and an extreme case with $|\epsilon| = 1.9 \times 10^{-4}\,{\rm eV}^2/1.6 \times 10^{-3}\,{\rm eV}^2 = 0.12$, which is allowed at 90 % CL (atmospheric) or 95 % CL (solar), is also shown for illustration. The horizontal axis is suitably defined so that it is linear in $\sin^2 2\theta_{23}$, where the left half is for $\theta_{23} < \pi/4$ whereas the right half is for $\theta_{23} > \pi/4$. The solar mixing angle is taken as $\tan^2\theta_{12} = 0.38$. $\sin^2 2\theta_{23} \geq 0.92$ has to be satisfied due to the constraint from the Super-Kamiokande atmospheric neutrino data. If the value of $\cos^2 2\theta_{23}$ is large enough, the value of $\delta_{\rm de}(\sin^2 2\theta_{13})/\sin^2 2\theta_{13}$ increases and lies outside of the normalized error of the reactor experiment, then the reactor result may resolve the θ_{23} ambiguity.

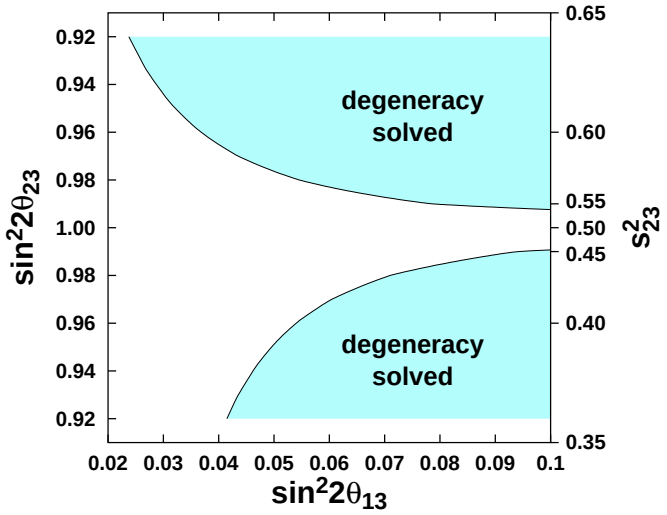

Figure 5.7: The shadowed area stands for the region in which $\delta_{\rm re}(\sin^2 2\theta_{13}) < \delta_{\rm de}(\sin^2 2\theta_{13})$ is satisfied for $\sigma_{\rm rel.sys}$=0.8 %, 40 t·yr, d.o.f.=1 and for the best fit values of the solar and atmospheric oscillation parameters. In this shadowed region, the (θ_{13}, θ_{23}) degeneracy may be solved. The vertical axis is the same as the horizontal axis of Fig. 5.6(b).

(atmospheric) or 95% CL (solar), with $\sin^2 2\theta_{13} = 0.03, 0.06, 0.09$. From this, we observe that the suppression in the first term in (5.9) is compensated by the second term for $\sin^2 2\theta_{13} = 0.03$, i.e., the degeneracy is small and therefore resolving the degeneracy is difficult in this case. To clearly illustrate the resolving power of the degeneracy by the reactor measurement, assuming the best fit value $|\epsilon| = 0.028$, we plot in Fig. 5.7 the region where the degeneracy can be lifted in the $\sin^2 2\theta_{13}$–$\sin^2 2\theta_{23}$ plane. It is evident that the reactor measurement will be able to resolve the (θ_{13}, θ_{23}) degeneracy in a wide range inside its sensitivity region, in particular for θ_{23} in the second octant.

Chapter 6

Exploring Leptonic CP Violation by Reactor and Neutrino Superbeam Experiments

6.1 Measurement of CP Violation in Long Baseline Experiments

Detecting leptonic CP violation is one of the most challenging goals in particle physics. In this chapter we raise the possibility that leptonic CP violation may be explored by combining the reactor experiment with $\nu_\mu \to \nu_e$ measurement of the long baseline (LBL) accelerator experiment. It constitutes the core part of this thesis. Let us start by recalling some basic features of the detection of CP violation in LBL experiments. A conventional way of measuring the CP violating phase δ is by LBL experiments with not only neutrino but also antineutrino beams. (See Sect. 4.1 for a review of LBL experiments.) These measurement would allow us to determine the CP-violating phase δ with a certain accuracy by measuring $P(\nu_\mu \to \nu_e)$ and $P(\overline{\nu}_\mu \to \overline{\mu}_e)$. For instance, J-PARC neutrino project with upgraded 4MW beam of 50GeV accelerator at J-PARC and Hyper-Kamiokande (hereafter abbreviated as JPARC-HK) is expected to observe CP violation at 3σ CL if $\delta \gtrsim 20^\circ$ [19].

Running the experiment with antineutrino mode is, however, possible only by overcoming a variety of grater difficulties than those in neutrino mode operation. Even if we ignore the issue of slightly less intense π^- beam compared to π^+ beam, the antineutrino cross sections are smaller by factor of $\simeq 3$ than neutrino cross sections, which results in three times longer period of data taking, 6 years of $\overline{\nu}$-mode compared to 2 years of ν-mode operation in JPARC-HK experiment. Moreover, the background in $\overline{\nu}_e$ appearance detection, according to the current estimate, are larger by factor of $\simeq 2$ compared with

those in ν_e detection because of 3 times longer running and 3 times larger cross section for the background due to wrong sign final-state leptons. Hence, antineutrino-mode measurement may be better characterized as an independent experiment rather than the in-situ measurement. Considering three times longer running time, it is certainly worthwhile to think about an alternative that can run simultaneously with neutrino-mode long baseline experiments. In this thesis, it is pointed out that a reactor experiment can serve for such purpose. The treatment in this chapter strengthen our viewpoint of the LBL-reactor complementarity discussed in Chapter 5. See Ref. [98, 104, 105, 106] for detailed description of possible designs of reactor experiments to measure θ_{13}.

6.2 Reactor-LBL Combined Measurement of CP Violation

The principle of detection of leptonic CP violation in a reactor-LBL combined measurement is very simple. As we have discussed in length in Sect. 5.1.1, reactor experiment can serve for pure measurement of θ_{13} assuming that Δm^2_{31} is accurately determined by disappearance measurement of $P(\nu_\mu \to \nu_\mu)$ in LBL experiments. Namely, it is not contaminated by uncertainties due to unknown CP phase δ, the matter effect, and possibly to the octant ambiguity $\theta_{23} \to \pi/2 - \theta_{23}$ from which ν_e appearance measurement by LBL experiment suffers.

Now LBL ν_e appearance experiment will observe the neutrino oscillation probability $P(\nu_\mu \to \nu_e)$. In second order in $\sin 2\theta_{13}$, $\Delta m^2_{21}/\Delta m^2_{31}$, and Δ_{21}/aL, it takes the form [91]

$$P_{\mu e} \equiv P(\nu_\mu \to \nu_e) = X^2 \sin^2 2\theta_{13} + 2XZ \sin 2\theta_{13} \cos\left(\delta + \frac{\Delta_{31}}{2}\right) + Z^2, \tag{6.1}$$

where we used the standard parametrization (2.35) of MNS matrix. The coefficients X and Z are given by

$$X \equiv s_{23} \frac{\Delta_{31}}{B} \sin\left(\frac{B}{2}\right), \tag{6.2}$$

$$Z \equiv c_{23} \sin 2\theta_{12} \frac{\Delta_{21}}{aL} \sin\left(\frac{aL}{2}\right) \tag{6.3}$$

with

$$\Delta_{jk} \equiv \frac{\Delta m^2_{jk} L}{2E} \quad \text{and} \quad B \equiv \Delta_{31} - aL, \tag{6.4}$$

where $a = \sqrt{2} G_F N_e$ denotes the index of refraction in matter with G_F being the Fermi constant and N_e a constant electron number density in the Earth. The mass squared difference of neutrinos is defined as $\Delta m^2_{jk} \equiv m^2_j - m^2_k$ where m_j is the mass of the j-th eigenstate.

There exist number of reasons for tuning the beam energy to the oscillation maximum $|\Delta_{13}| = \pi$ in doing the appearance and the disappearance measurement in LBL experiments, as listed in [20]. In this case, $X\cos\left(\delta + \frac{\Delta_{13}}{2}\right) = |X|\sin\delta$ and (6.1) can be solved for $\sin\delta$ as

$$\sin\delta = \frac{P_{\mu e} - Z - X^2\sin^2 2\theta_{13}}{|X|Z\sin 2\theta_{13}}. \tag{6.5}$$

We note that, since θ_{13} can be measured by reactor experiments, the right-hand side of (6.5) consists solely of experimentally measurable quantities. Therefore, the measurement of $P(\nu_\mu \to \nu_e)$ by LBL experiments, when combined with the reactor experiment, implies measurement of $\sin\delta$.

In the rest of this Chapter, we try to elaborate our treatment by including suitably estimated experimental uncertainties of both LBL and the reactor experiments. As indicated in (6.5), the accuracy of measurement of $\sin\delta$ solely depends upon how precisely $P_{\mu e}$ and $\sin 2\theta_{13}$ in the right-hand side of (6.5) can be determined in LBL and reactor experiments, respectively. We take the best possible case among the concrete proposals of long baseline experiments currently available in the community, the JPARC-HK experiment assuming 4MW beam power and 540 kton as the fiducial volume of the detector. However, most probably our conclusion does not heavily depend on any detailed experimental setting in the particular experiment, once the accuracy of measurement of the ν_e appearance probability reaches to that level and if the baseline is not too long. For the reactor experiment, we present all results in units of $\mathrm{GW_{th}}\cdot\mathrm{ton}\cdot\mathrm{year}$ exposure to allow application to wider class of experiments. The results may be useful to indicate what condition must be met to uncover the leptonic CP violation in such reactor-LBL combined measurement.

6.3 Treatment of Errors in LBL and Reactor Experiments

To carry out quantitative analyses of the sensitivity to CP violation, we must first establish the method for statistical treatment of long baseline and reactor experiments.

6.3.1 Treatment of errors in the JPARC-HK experiment

We consider neutrino-mode appearance measurement for 2 years in the JPARC-HK experiment. For definiteness, we use the neutrino flux estimated for the off-axis 2° beam [19]. We define $\Delta\chi^2$ for the experiment as

$$\Delta\chi^2_{\text{J-PARC}\nu} \equiv \frac{\left(N_\nu - N_\nu^{\text{best}}\right)^2}{N_\nu^{\text{best}} + N_{\text{BG}} + \sigma_{\text{S}}^2 (N_\nu^{\text{best}})^2 + \sigma_{\text{BG}}^2 (N_{\text{BG}})^2}, \tag{6.6}$$

where N_ν and N_{BG} represent the expected number of signal and background events, respectively, computed with the cross section in [89]. N_ν^{best} is defined as the number of signal

OAB2° ν_μ beam	ν_e signal	ν_μCC BG	ν_μNC BG	ν_eBG
LOI	301.6	10713.6	4080.3	292.1
ours (0-50GeV)	309.1	10751.5	4072.4	293.2

Table 6.1: Comparison of our results with those in the letter of intent (LOI) [19] as a consistency check of our calculations. The column of ν_e signal is for the numbers of oscillated ν_e charged-current interaction (CC) events with $s^2_{23}\sin^2 2\theta_{13} = 0.05$ and $|\Delta m^2_{31}| = 3\times 10^{-3}\mathrm{eV}^2$. The column of ν_μCC BG is without oscillation. CC events include charged-current quasi-elastic (CCQE) and charged-current non-quasi-elastic (CCnQE) events. The column of ν_μNC BG is for the numbers of $\nu_\mu \to \nu_x$NC BG, namely unoscillated ν_μNC BG because of flavor blindness of NC interaction. The column of ν_eBG is for the numbers of CC+NC events of ν_e contaminates initial flux. Other parameters are fixed as $\Delta m^2_{21} = 0$ and $\rho = 0$.

OAB2° ν_μ beam	ν_e signal	ν_μBG	$\overline{\nu}_\mu$BG	ν_eBG	$\overline{\nu}_e$BG
0-5GeV CC	4139.9	139434.8	22195.7	7553.8	836.7
NC	1577.5	161251.5	11628.5	2543.7	328.9
total	5717.7	300686.2	33824.1	10097.5	1165.6

Table 6.2: The numbers of events before cut in our calculation. The numbers correspond to those in Fig. 6.1.

event N_ν calculated with the best-fit values of the "experimental data", which is to be tested against the CP conserving hypothesis, $\delta = 0$. σ_{S} and σ_{BG} represent the fractional uncertainties of the estimation of the number of signal and background events, respectively. Following the letter of intent of J-PARC neutrino project [19], we use $\sigma_{\mathrm{S}} = \sigma_{\mathrm{BG}} = 2\%$ in our analysis. (See Sect. 6.4 for more about how to use $\Delta\chi^2$ in our procedure to determine the sensitivity region to CP violation.)

While we do not use the spectral information in a direct way in our analysis, we need to estimate how the experimental event selection affects the spectrum to calculate the numbers of signal and background events. The most important cut is to suppress the background events due to π^0 which is produced by charged-current non-quasi-elastic interaction (CCnQE) or neutral-current interaction (NC) and whose daughter gamma rays can mimic ν_e signal event. We use the simulated spectra after the cut, N_{ac}, calculated by the J-PARC experiment group [107] with $\delta = \pi/4$ and $\sin^2 2\theta_{13} = 0.03$ in each energy bin of 50MeV width. Those spectra are presented in Fig. 6.2. (See also Table 6.3.) On the other hand, we can calculate the number of events before cut, $N_{bc}(\delta, \sin^2 2\theta_{13})$, for

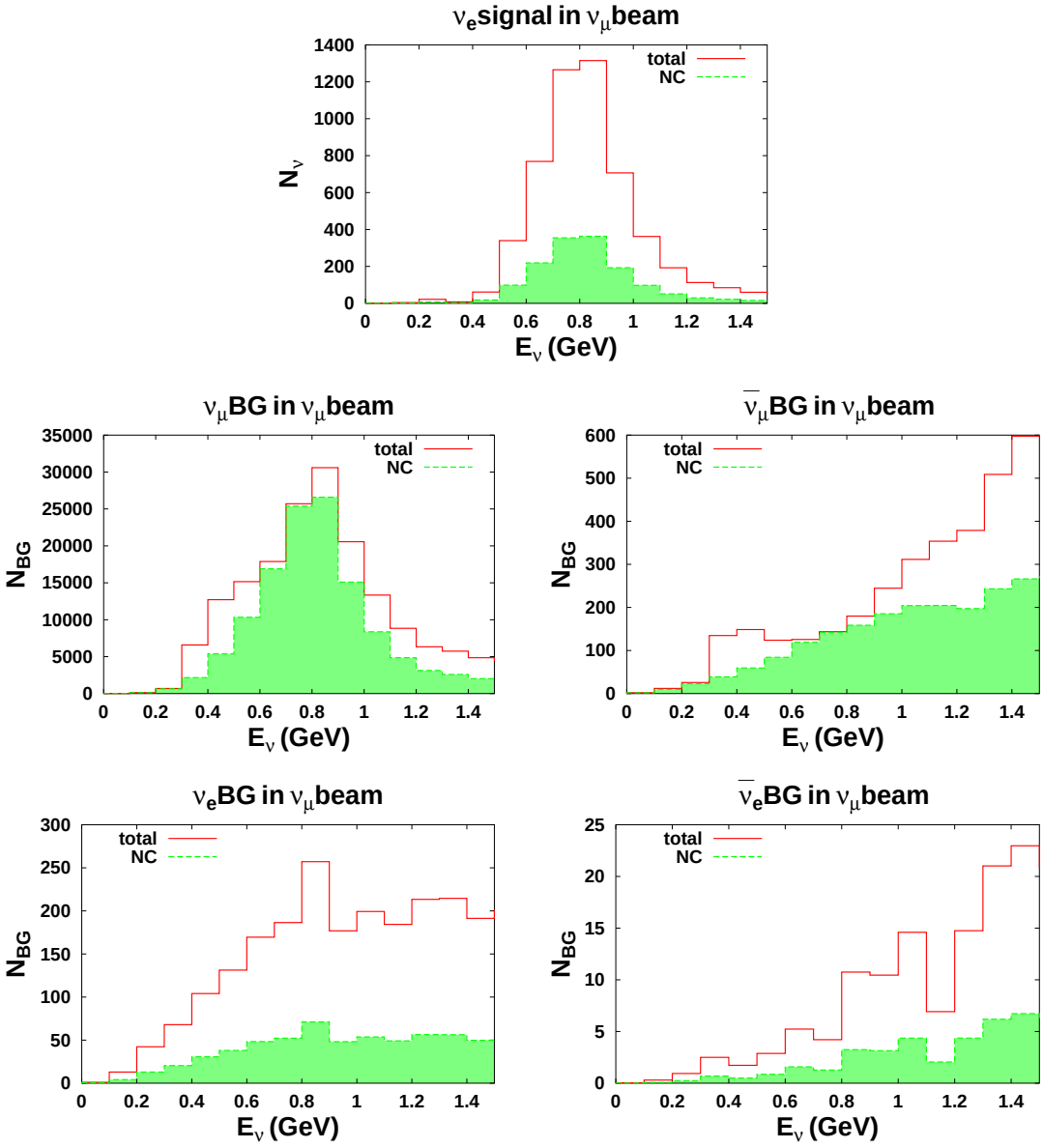

Figure 6.1: Event spectra in our calculation before event selections. Assumed values of parameters are same as those of Fig. 6.2. The histograms with solid line are of total number of CC and NC events while those with dashed line are for the number of NC events. In low energy region $\lesssim$ 0.3GeV, our calculation seems to be not accurate because of high frequency of the oscillation probability. Most of the error may be, however, canceled by the ratio in the right-hand side of (6.7).

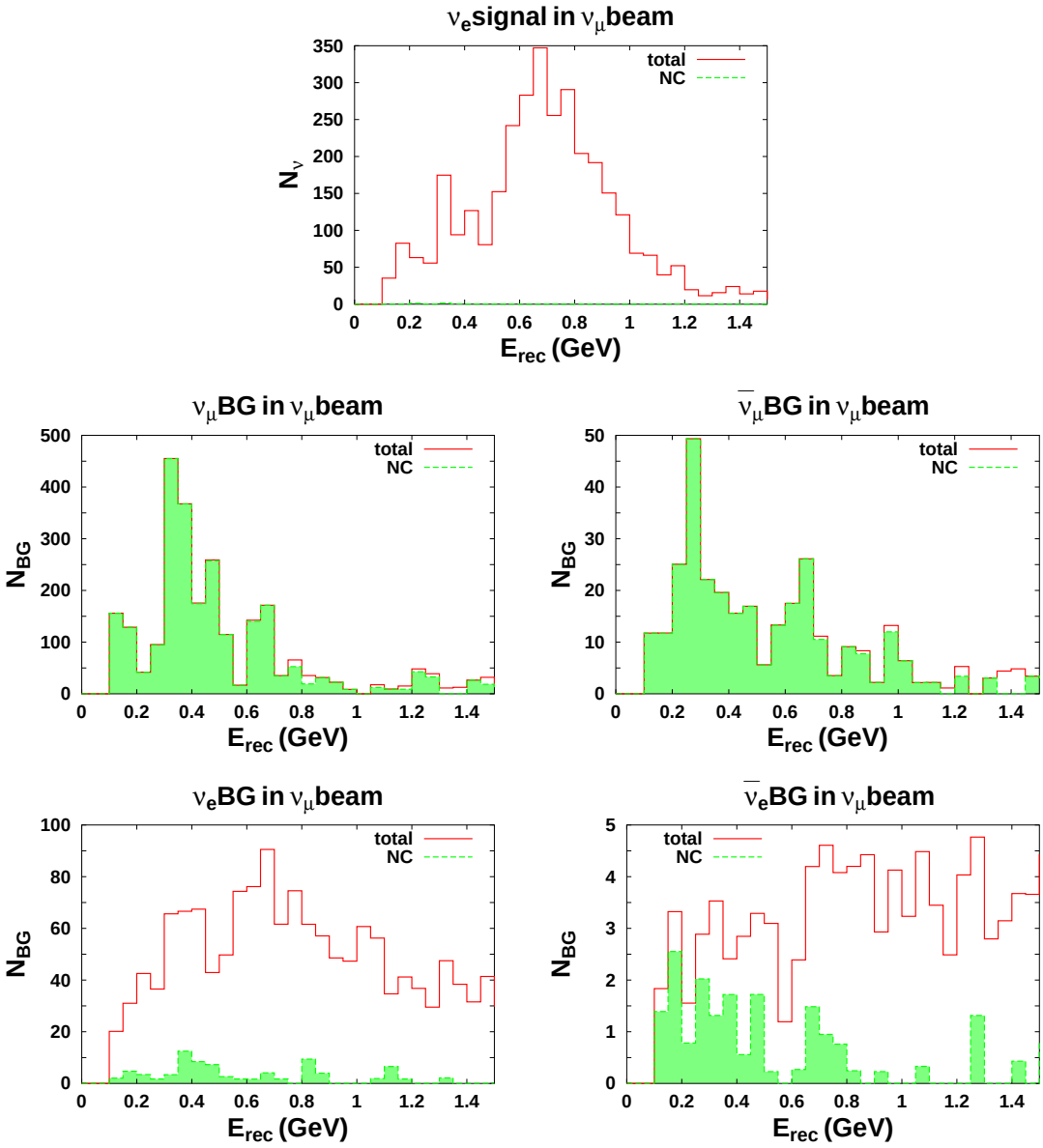

Figure 6.2: The spectra are calculated with Monthe-Carlo simulation by J-PARC experiment group [107]. Those are spectra after event selections except for the energy window restriction ($0.4\text{GeV} \leq E_{\text{rec}} \leq 1.2\text{GeV}$); E_{rec} is reconstructed energy by assuming CCQE interaction. The histograms with solid line are of total number of CC and NC events while those with dashed line are for the number of NC events. We use approximated relations $E_{\text{rec}} = E_\nu$ for CC events and $E_{\text{rec}} = E_\nu - 300\text{MeV}$ for NC events. The assumed values are 4MW accelerator power, OAB2°, 1Mt fiducial mass, 2yr exposure, $\Delta m^2_{21} = 5 \times 10^{-5}\text{eV}^2$, $\Delta m^2_{31} = 3 \times 10^{-3}\text{eV}^2$, $\sin^2 2\theta_{12} = 0.8$, $\sin^2 2\theta_{13} = 0.03$, $\sin^2 2\theta_{23} = 1$, $\delta = \pi/4$, and $\rho = 2.8\text{g} \cdot \text{cm}^{-3}$.

OAB2° ν_μ beam	ν_e signal	ν_μBG	$\overline{\nu}_\mu$BG	ν_eBG	$\overline{\nu}_e$BG
0-5GeV CC	3323.6	121.5	22.5	1762.8	120.2
NC	5.7	2802.1	321.8	88.7	20.1
total	3329.3	2923.6	344.3	1851.6	140.3
0.4-1.2GeV CC	2670.4	45.2	3.6	893.5	48.3
NC	2.0	1075.3	151.0	51.1	6.8
total	2672.4	1120.5	154.5	944.6	55.0

Table 6.3: The numbers of events after event cuts, which correspond to the spectrum of Fig. 6.2 calculated by the J-PARC experiment group [107]. The lower three rows are final results of event cuts including the energy cut (0.4-1.2GeV).

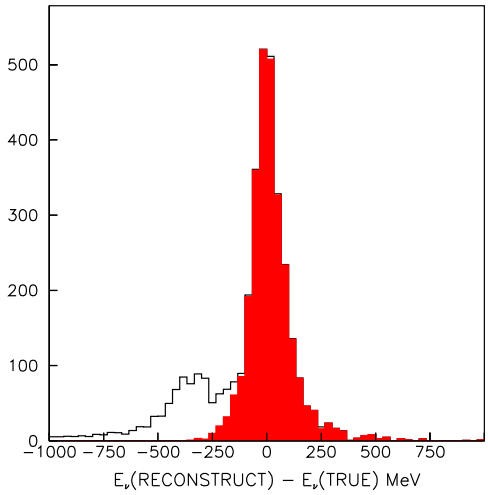

Figure 6.3: Energy resolution of ν_μ events [19]. The shaded histogram is of true CCQE events. We assume that the resolution for ν_e events is similar to this histogram, and we use $E_{\rm rec} = E_\nu$ for CC events and $E_{\rm rec} = E_\nu - 300$MeV for NC background events.

any parameter values in each energy bin of 100MeV width. Table 6.1 presents the result of comparison between our calculation and the numbers in the letter of intent (LOI) of J-PARC experiment as a consistency check. It is found that our calculation reproduces well the numbers calculated by the J-PARC experiment group. Fig. 6.1 shows the spectra with the same parameter values as those of Fig. 6.2. (See also Table 6.2.) Then, we estimate the number of signal events within each 100MeV bin after the cut for any values of mixing parameters as

$$N_{ac}(\delta, \sin^2 2\theta_{13}) = \frac{N_{bc}(\delta, \sin^2 2\theta_{13})}{N_{bc}(\pi/4, 0.03)} N_{ac}(\pi/4, 0.03). \tag{6.7}$$

Since reconstructed energy $E_{\rm rec}$ for background events is less than true neutrino energy E_ν for signal events by about 300MeV (Fig. 6.3), we use the prescription that the energy of NC background events before cut is sifted to 300MeV smaller value in (6.7). In this way, the total numbers of signal and background (μ-like and e-like) events within energy range 0.4-1.2GeV are estimated and used in our analysis. Note that bin-by-bin conversion through (6.7) is necessary because shape of the event spectrum before the cut depends on δ and θ_{13}.

6.3.2 Treatment of errors in the reactor experiment

Similarly to Chapter 5, we consider the case of single reactor and two (near and far) detector complex. The far detector is placed 1.7km away from the reactor, the optimal distance for $|\Delta m^2_{31}| = 2.5 \times 10^{-3}\,\mathrm{eV}^2$. We assume that a near detector identical with the far detector is placed 300m away from the reactor to reduce systematic errors.

We consider four types of systematic errors: $\sigma_{\rm DB}$, $\sigma_{\rm Db}$, $\sigma_{\rm dB}$, and $\sigma_{\rm db}$. The subscript D (d) represents the fact that the error is correlated (uncorrelated) between detectors. The subscript B (b) represents that the error is correlated (uncorrelated) among bins. To indicate nature of these respective errors, we list below some examples of the errors in each category:

$\sigma_{\rm DB}$: error in estimation of reactor power

$\sigma_{\rm Db}$: error in estimation of detection cross sections

$\sigma_{\rm dB}$: error in estimation of fiducial volume of each detector

$\sigma_{\rm db}$: errors inherent to detectors such as artificial firing of photomultiplier tubes

Although the values of $\sigma_{\rm dB}$ for far and near detectors, for example, can be different from each other, we neglect such difference for simplicity. The values of systematic errors we assume are listed in Table 6.4.

As will be briefly explained in Appendix A.2, the errors $\sigma_{\rm D}$ and $\sigma_{\rm d}$ for the total number

		between detectors		
		correlated	uncorrelated	single detector
between bins	correlated	$\sigma_{\rm DB} = 2.5\%$	$\sigma_{\rm dB} = 0.5\%$	$\sigma_{\rm B} \simeq 2.6\%$
	uncorrelated	$\sigma_{\rm Db} = 2.5\%$	$\sigma_{\rm db} = 0.5\%$	$\sigma_{\rm b} \simeq 2.6\%$
total number of events		$\sigma_{\rm D} \simeq 2.6\%$	$\sigma_{\rm d} \simeq 0.5\%$	$\sigma_{\rm sys} \simeq 2.7\%$

Table 6.4: Listed are assumed values of systematic errors $\sigma_{\rm DB}$, $\sigma_{\rm Db}$, $\sigma_{\rm dB}$, and $\sigma_{\rm db}$. The subscripts D (d) and B (b) are represent the correlated (uncorrelated) error among detectors and bins, respectively. Using those four values, the errors for the total number of events and for single detector are calculated.

of events are obtained as

$$\sigma_{\rm D}^2 = \sigma_{\rm DB}^2 + \sigma_{\rm Db}^2 \frac{\sum_i (N_{ai}^{\rm best})^2}{\left(\sum_i N_{ai}^{\rm best}\right)^2}, \quad \sigma_{\rm d}^2 = \sigma_{\rm dB}^2 + \sigma_{\rm db}^2 \frac{\sum_i (N_{ai}^{\rm best})^2}{\left(\sum_i N_{ai}^{\rm best}\right)^2}, \tag{6.8}$$

where $a = n, f$ are the index for near and far detectors, and i runs over number of bins. We use 14 bins of 0.5MeV width in 1-8MeV window of visible energy, $E_{\rm visi} = E_{\bar{\nu}_e} - 0.782$MeV. The coefficient of $\sigma_{\rm Db}^2$ and $\sigma_{\rm db}^2$ is about 1/9 in our analysis almost independently of a. Since relative normalization errors are $\sqrt{2}$ times of uncorrelated errors, $\sigma_{\rm d} \simeq 0.5\%$ is consistent with 0.8% relative error which is used in Chapter 5. In Chapter 5, the most pessimistic assumption $\sigma_{\rm DB} = \sigma_{\rm dB} = 0$ was taken for bin-by-bin distribution of errors. We adopted in this chapter rather even assumption, namely $\sigma_{\rm DB} = \sigma_{\rm Db}$ and $\sigma_{\rm dB} = \sigma_{\rm db}$. The value of $\sigma_{\rm sys}^2 \equiv \sigma_{\rm D}^2 + \sigma_{\rm d}^2$ is also consistent with the total systematic error of the CHOOZ experiment. In summary, it seems that the errors listed in Table 6.4 are not too optimistic ones and are likely to be realized by the setting discussed in [98, 104, 105, 106].

Our definition of $\Delta\chi^2_{\rm react}$ is

$$\Delta\chi^2_{\rm react} \equiv \min_{\alpha\text{'s}} \sum_{a=f,n} \left[\sum_{i=1}^{14} \left\{ \frac{\left(N_{ai} - (1 + \alpha_i + \alpha_a + \alpha) N_{ai}^{\rm best}\right)^2}{N_{ai}^{\rm best} + \sigma_{\rm db}^2 (N_{ai}^{\rm best})^2} + \frac{\alpha_i^2}{\sigma_{\rm Db}^2} \right\} + \frac{\alpha_a^2}{\sigma_{\rm dB}^2} \right] + \frac{\alpha^2}{\sigma_{\rm DB}^2}, \tag{6.9}$$

where N_{ai} represents the theoretical number of events at a-detector within i-th bin. Again, $N_{ai}^{\rm best}$ is defined as the number of signal event calculated with the best-fit parameters of the "experimental data". The minimization in (6.9) is achieved analytically, and then we obtain

$$\Delta\chi^2_{\rm react} = (\vec{x}^T, \vec{y}^T) V^{-1} \begin{pmatrix} \vec{x} \\ \vec{y} \end{pmatrix}, \tag{6.10}$$

$$\vec{x}^T \equiv \left(\frac{N_{f1} - N_{f1}^{\rm best}}{N_{f1}^{\rm best}}, \cdots \right), \ \vec{y}^T \equiv \left(\frac{N_{n1} - N_{n1}^{\rm best}}{N_{n1}^{\rm best}}, \cdots \right), \tag{6.11}$$

$$V \equiv \mathrm{diag}\left(\frac{1}{N_{f1}^{\mathrm{best}}}, \cdots, \frac{1}{N_{n1}^{\mathrm{best}}}, \cdots\right) + \sigma_{\mathrm{db}}^2 I_{28} + \sigma_{\mathrm{dB}}^2 \begin{pmatrix} H_{14} & 0 \\ 0 & H_{14} \end{pmatrix} + \sigma_{\mathrm{Db}}^2 \begin{pmatrix} I_{14} & I_{14} \\ I_{14} & I_{14} \end{pmatrix} + \sigma_{\mathrm{DB}}^2 H_{28}, \quad (6.12)$$

where I_n represents the $n \times n$ identity matrix and H_n represents the $n \times n$ matrix whose elements are all unity. Notice that an infinitely good sensitivity is obtained for infinite number of events if σ_{db} vanishes because $\det(V)$ goes to zero for the case. See [108] for more about the equivalence between the "pull" and the covariance matrix methods.

To indicate the expected sensitivity of the reactor experiment with the systematic errors listed in Table 6.4, we present in Fig. 6.4 the excluded region in $\sin^2 2\theta_{13}$-$|\Delta m^2_{31}|$ space in the absence of flux depletion ($\theta_{13}^{\mathrm{best}} = 0$) for 10^3, 4×10^3, and 10^4 $\mathrm{GW_{th}} \cdot \mathrm{ton} \cdot$ year exposure. The $\bar{\nu}_e$ detection efficiency of 70% is assumed. The number of events expected during these exposure are about 10^5, 4×10^5, 10^6 $\bar{\nu}_e$ events, respectively, at the far detector.[1] Notice that what we mean by numbers in units of $\mathrm{GW_{th}}$ is the thermal power actually generated from reactors and it should not be confused with the maximal thermal power of reactors. Assuming average 80% operation efficiency the above three cases correspond approximately to 0.5, 2, and 5 years running, respectively, for 100 ton detector at the Kashiwazaki-Kariwa nuclear power plant whose maximal thermal power is $24.3\mathrm{GW_{th}}$.

6.4 Estimation of Sensitivity of Reactor-LBL Combined Detection of CP Violation

To estimate the sensitivity of the reactor-LBL combined measurement to leptonic CP violation, we define the combined $\Delta\chi^2$ as

$$\begin{aligned} \Delta\chi^2_{\mathrm{CP1}}(\delta; \delta^{\mathrm{best}}, \sin^2 2\theta_{13}^{\mathrm{best}}) &\equiv \min_{\sin^2 2\theta_{13}} \Delta\chi^2_{\mathrm{CP}}(\delta, \sin^2 2\theta_{13}; \delta^{\mathrm{best}}, \sin^2 2\theta_{13}^{\mathrm{best}}) \\ &\equiv \min_{\sin^2 2\theta_{13}} \Big\{ \Delta\chi^2_{\text{J-PARC}\nu}(\delta, \sin^2 2\theta_{13}; \delta^{\mathrm{best}}, \sin^2 2\theta_{13}^{\mathrm{best}}) \\ &\qquad + \Delta\chi^2_{\mathrm{react}}(\sin^2 2\theta_{13}; \sin^2 2\theta_{13}^{\mathrm{best}}) \Big\}. \end{aligned} \quad (6.13)$$

We take the following procedure in the analysis. We pick up a point in the two-dimensional parameter space spanned by δ^{best} and $\sin^2 2\theta_{13}^{\mathrm{best}}$ and make the hypothesis test on whether the point is consistent with CP conservation within 90% CL. For this purpose, we use the projected $\Delta\chi^2$ onto one-dimensional δ space, $\Delta\chi^2_{\mathrm{CP1}}$, as defined in (6.13) and then

[1] In the rate-only analysis without binning, the sensitivity is saturated at around $10^5 \bar{\nu}_e$ events.

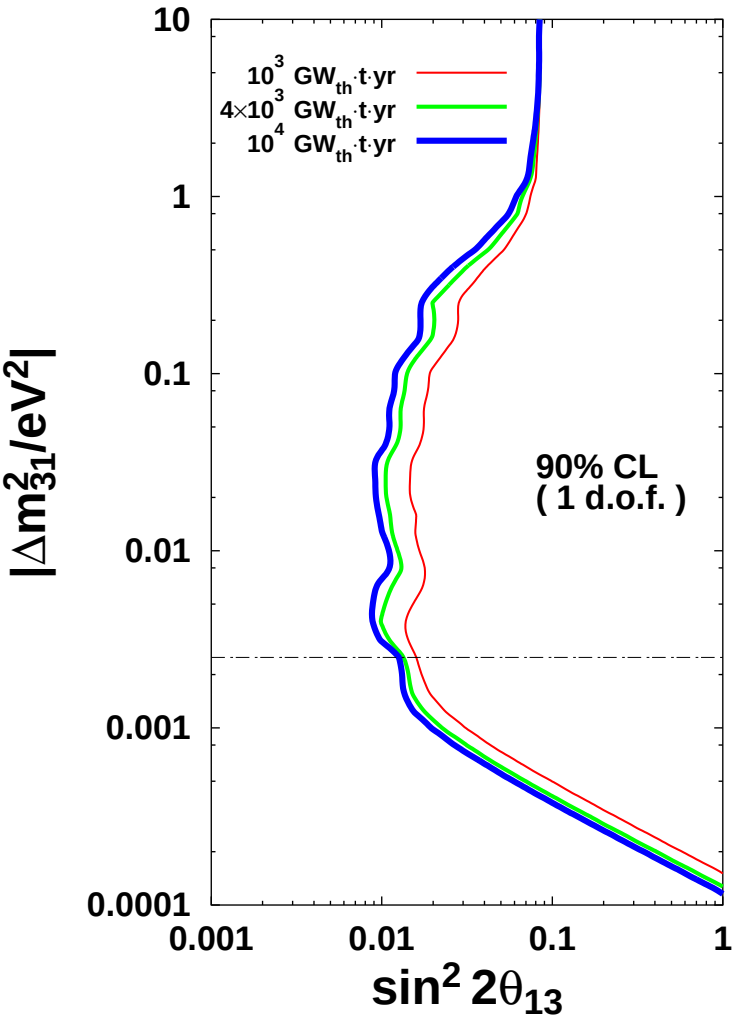

Figure 6.4: The excluded regions at 90% CL in the absence of $\bar{\nu}_e$ disappearance ($\theta_{13}^{\rm best} = 0$) are drawn for 10^3, 4×10^3, and 10^4 $\mathrm{GW_{th}} \cdot \mathrm{ton} \cdot \mathrm{year}$ exposure of a reactor experiment by thin-solid, solid, and thick-solid lines, respectively. The far (near) detector is placed 1.7km (300m) away from the reactor. We assume that $|\Delta m^2_{31}|$ is precisely measured by LBL experiments and adopt the analysis with one degree of freedom ($\Delta\chi^2_{\rm react} = 2.7$). We use the value $|\Delta m^2_{31}| = 2.5 \times 10^{-3}\mathrm{eV}^2$ as indicated by the dashed-doted line in the figure. In this analysis, we use 14 bins of 0.5MeV width in 1-8MeV window of visible energy with the systematic errors listed in Table 6.4.

the statistical criterion for 90% CL is $\Delta\chi^2_{\rm CP1} \leq 2.7$. Then, a collection of points in the parameter space which are consistent with CP conservation forms a region surrounded by a contour in the $\delta^{\rm best}$-$\sin^2 2\theta_{13}^{\rm best}$ space, as will be shown in Figs. 6.5-6.7 below.

The neutrino mixing parameters are taken as follows: $|\Delta m^2_{31}| = 2.5\times10^{-3}{\rm eV}^2$, $\Delta m^2_{21} = 7.3\times10^{-5}{\rm eV}^2$, $\tan^2\theta_{12} = 0.38$, and $\sin^2 2\theta_{23} = 1$. The Earth matter density is taken to be $\rho = 2.3\,{\rm g\cdot cm}^{-3}$ [96] and the electron number density is computed with electron fraction $Y_e = 0.5$.

6.4.1 CP sensitivity in the case of known sign of Δm^2_{31}

In Fig. 6.5, the regions consistent with CP conservation at 90% CL are drawn for $\Delta m^2_{31} > 0$ case in the region $-\pi/2 \leq \delta^{\rm best} \leq \pi/2$. The thin-solid, the solid, and the thick-solid lines are for 10^3, 4×10^3, and $10^4{\rm GW_{th}\cdot ton\cdot years}$, respectively, and the regions consistent with CP conservation are within the envelope of these contours.[2] We remark that the present constraint on θ_{13} becomes milder to $\sin^2 2\theta_{13} < 0.25$ at 3σ CL [79] by the smaller values of $|\Delta m^2_{31}|$ indicated by the reanalysis of atmospheric neutrino data [67]. Notice that the other half region of $\delta^{\rm best}$ gives the identical contours apart from tiny difference which arises because the peak energy of the off-axis 2° beam is slightly off the oscillation maximum.

If an experimental best fit point falls into outside the envelope of those regions, it gives an indication for leptonic CP violation because it is inconsistent with the hypothesis $\delta = 0$ at 90% CL. We observe from Fig. 6.5 that there is a chance for reactor-LBL combined experiment of seeing an indication of CP violation for relatively large $\theta_{13}^{\rm best}$, $\sin^2 2\theta_{13}^{\rm best} \geq 0.03$ at 90% CL. Then, this can be the first time that a possibility is raised for detecting leptonic CP violation based on a quantitative treatment of experimental errors by a method different from the conventional one of comparing neutrino and antineutrino appearance measurement in LBL experiments.

The sign of Δm^2_{31} is taken to be positive in Fig. 6.5 which corresponds to the normal mass hierarchy. If we flip the sign of Δm^2_{31} (the case of inverted mass hierarchy) we obtain almost identical CP sensitivity contours. It is demonstrated in Figs. 6.7a and 6.7b which serve also for the discussion in the next subsection. By comparing the contours depicted by thick-solid and thick-dashed lines in Figs. 6.7a ($\Delta m^2_{31} > 0$) and 6.7b ($\Delta m^2_{31} < 0$),

[2]Since we rely on hypothesis test with 1 degree of freedom (1 d.o.f.) the information of $\sin^2 2\theta_{13}$ is lost through the process of minimization in (6.13). The individual contours presented in Fig. 6.5 indicate the region $\Delta\chi^2_{\rm CP} \leq 2.7$ for eight assumed values of $\sin^2 2\theta_{13}$ which range from 0.02 to 0.16. In this way the figure is designed so that the envelope of the contours gives the region of CP conservation at 90% CL by 1 d.o.f. analysis, and at the same time carries some informations of how the sensitivity regions are determined by the interplay between the reactor and the LBL measurement.

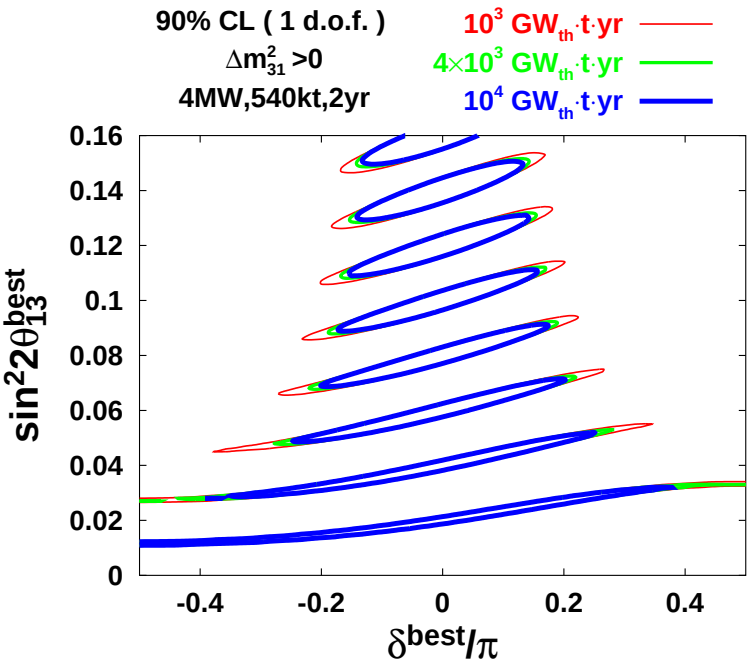

Figure 6.5: The contours are plotted for eight assumed values of $\sin^2 2\theta_{13}$ which range from 0.02 to 0.16 to indicate the regions consistent with the hypothesis $\delta = 0$ at 90% CL ($\Delta\chi^2_{\rm CP} = 2.7$) by the reactor-LBL combined measurement. If an experimental best fit point falls into outside the envelope of those regions, it gives an evidence for leptonic CP violation at 90% CL. The thin-solid, solid, and thick-solid lines are for 10^3, 4×10^3, and $10^4 {\rm GW_{th}} \cdot {\rm ton} \cdot {\rm year}$ exposure of a reactor experiment, respectively, corresponding to about 0.5, 2, and 5 years exposure of 100 ton detectors at the Kashiwazaki-Kariwa nuclear power plant. For the JPARC-HK experiment, 2 years measurement with off-axis 2° ν_μ beam is assumed. (See the text for more details.) The normal mass hierarchy, $\Delta m^2_{31} > 0$, is assumed.

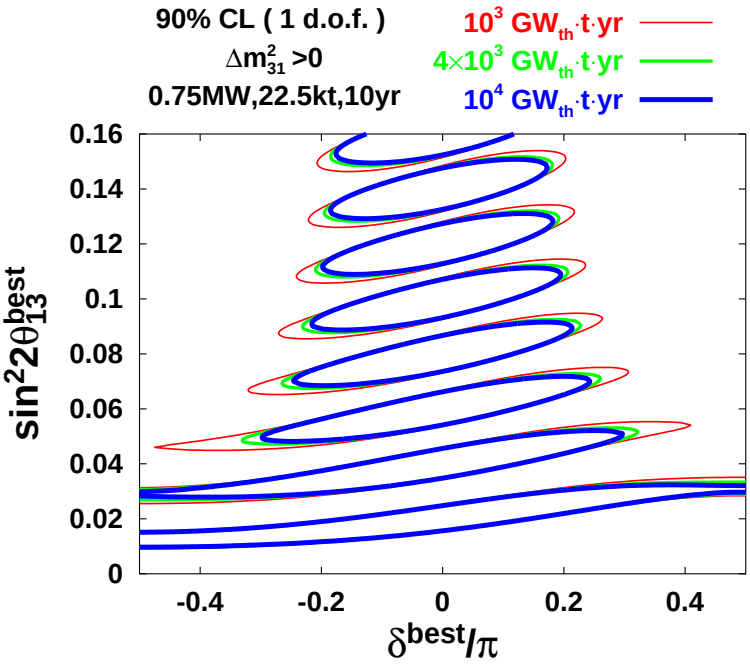

Figure 6.6: The same as in Fig. 6.5 but with measurement in 10 years running of the JPARC-SK experiment with 0.75MW beam power and 22.5kt detector (Super-Kamiokande). Although each contour becomes thicker because of a factor of $\simeq 25$ lower statistics of the experiment, the sensitivity to CP violation still exists at 90% CL.

respectively, it is clear that the CP sensitivity is almost identical between positive and negative Δm^2_{31}. The largest noticeable changes are shifts of the end points of the contours toward smaller (larger) δ in the first (fourth) quadrants by about 10% (a few %) at $\sin^2 2\theta_{13} = 0.1$. Namely, the both end points slightly move toward better sensitivities for the inverted mass hierarchy.

The sensitivity contour to CP violation is determined as an interplay between constraints from reactor and accelerator experiments. The former gives a rectangular box in the $\delta^{\rm best}$-$\sin^2 2\theta_{13}^{\rm best}$ space, whereas the latter gives the equal-$P_{\mu e}$ contour (See also Fig. 4.4.) determined by (6.1) under the hypothesis $\delta = 0$ with finite width due to errors, as indicated in Figs. 6.5 and 6.7. In region of parameter space where both of these two constraints are satisfied, the best fit parameter is consistent with CP conservation. Outside the region the CP symmetry is violated at 90% CL. The discovery potential for CP violation diminishes at small $\sin^2 2\theta_{13}^{\rm best}$ primarily because $P_{\mu e}$ becomes less sensitive to δ at smaller θ_{13}, while the reactor constraint on $\sin^2 2\theta_{13}$ is roughly independent of $\theta_{13}^{\rm best}$. (See Fig. 5.3.)

Let us examine a pessimistic scenario to run the JPARC-SK experiment with 0.75MW

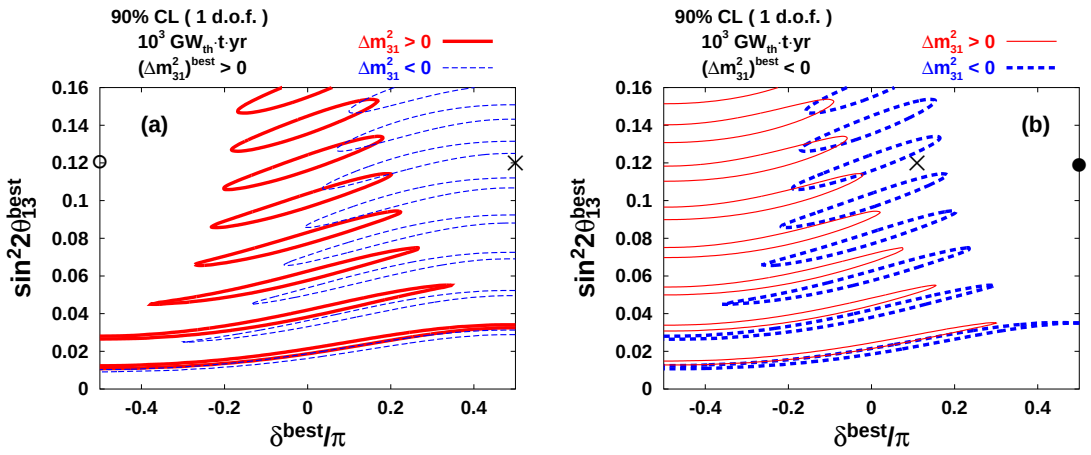

Figure 6.7: The contours which surround the region consistent with CP conservation are plotted in Fig. 6.7a (6.7b) by assuming $(\Delta m^2_{31})^{\rm best} > 0$ ($(\Delta m^2_{31})^{\rm best} < 0$) as nature's choice. If the right (wrong) sign is used as the hypothesis with $\delta = 0$, the contours indicated by the thick (thin) lines result in both figures. The three symbols, a cross, open and solid circles are placed on the figures as well as in Fig. 6.8 to indicate the relationship between observed numbers of events and the results of CP sensitivity analysis.

proton beam power and the fiducial volume of 22.5kt, while waiting for the construction of Hyper-Kamiokande. As is shown in Fig. 6.6, the sensitivity to CP violation becomes worse but still remains for its 10 years running.

6.4.2 CP sensitivity in the case of unknown sign of Δm^2_{31}

So far we have assumed that we know the sign of Δm^2_{31} prior to the search for CP violation by the reactor and the JPARC-HK experiments. But, it may not be the case unless LBL experiments with sufficiently long baseline start to operate in a timely fashion. In this subsection we assume the pessimistic situation of unknown sign of Δm^2_{31} and try to clarify the influence of our ignorance of the sign on the detectability of CP violation by our method.

If the sign of Δm^2_{31} is not known, the procedure of obtaining the sensitivity region for detecting CP violation has to be altered. It is because we have to allow such possibility as that we fit the data by using wrong assumption for the sign. In Fig. 6.7a (6.7b) we present the results of the similar sensitivity analysis for detecting CP violation as we did in the previous section by assuming that the sign of $(\Delta m^2_{31})^{\rm best}$, which is chosen by nature, is positive (negative). It is obvious from Fig. 6.7a (6.7b) that the contours of CP conservation moves to rightward (leftward) if the wrong sign is assumed in the hypothesis

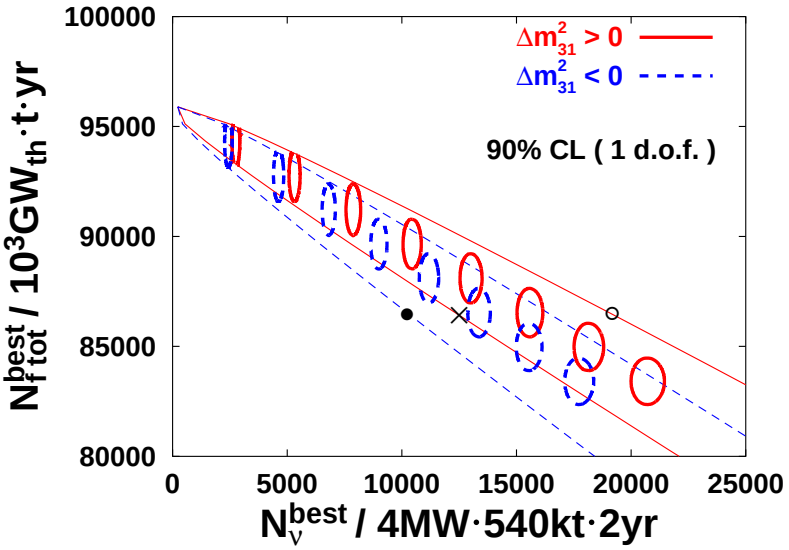

Figure 6.8: The contours which surround the region consistent with CP conservation are plotted in the number-of-events space of reactor and the LBL experiments. The thin lines correspond to $\delta^{\rm best} = \pm\pi/2$. The three symbols, a cross, open and solid circles are placed on the figures as well as in Fig. 6.7 to indicate the relationship between observed numbers of events and the results of CP sensitivity analysis.

test, essentially wiping out about half of the CP sensitive region of $\delta^{\rm best}$.

The results can be confusing and some of the readers might have naively interpreted, by combining Figs. 6.7a and 6.7b, that there is no sensitivity region in $\delta^{\rm best}$- $\sin^2 2\theta_{23}^{\rm best}$ plane. To resolve the puzzling feature we present in Fig. 6.8 the regions which are consistent with CP conservation by contours in the plane spanned by observable quantities, the number of events in the reactor and the JPARC-HK ν_e appearance experiments.[3] This plot indicates that the sensitivity region for detecting CP violation does not disappear but becomes about half. Which region of δ is CP sensitive depend upon the sign of Δm^2_{31}, or in other word on the location in bi-number of event plane in Fig. 6.8. For complete clarity, we have placed three different symbols in Fig. 6.8 and at the same time in Fig. 6.7 to indicate which points in the space of observable correspond to which points in the CP sensitivity plot. Note that the point indicated by a cross in Fig. 6.8 corresponds to two values of $\delta^{\rm best}$ because of unknown sign of Δm^2_{31}.

[3]Notice, however, that we have used binned data, not merely the total number of events, in analyzing reactor experiment to obtain the contours.

Chapter 7

Conclusion

In this thesis, we discussed the methods for determination of flavor mixing parameters in the lepton sector with use of reactor neutrinos.

In Chapter 5, we have explored in detail the possibility of measuring $\sin^2 2\theta_{13}$ by searching for the deficit of $\overline{\nu}_e$ from reactors. In order to realize the high sensitivity up to $\sin^2 2\theta_{13} \sim 0.01$, the statistical and systematic errors have to be $\lesssim 1\%$. For the small statistical error, large number of events should be accumulated by the large detector and/or the powerful reactor. Exploiting the more powerful reactor is advantageous than the larger detector option because it enable us to gain larger number of signal events while keeping background events unaltered. Therefore, the best site for the reactor experiment is the Kashiwazaki-Kariwa nuclear power plant whose total thermal power ($24.3\mathrm{GW_{th}}$) is the most powerful in the world. Under an effective single-reactor assumption, it was seen that 5 ton-year measurement at the baseline of 1.7km can accumulate about 10,000 $\overline{\nu}_e$ events which corresponds to 1% statistical error.

On the other hand, it was pointed out that placing near detector is crucial to reduce the systematic errors. We assumed that a near detector is placed 300m away from the reactor. By comparing the numbers of events observed at near and far detectors, we can cancel the correlated errors between detectors such as the error in the neutrino flux. We estimated that the systematic error can be reduced to 0.8%. It was shown in Fig. 5.2 that the sensitivity $\sin^2 2\theta_{13} = 0.018$ is obtained by 40 ton-year measurement with a $24.3\mathrm{GW_{th}}$ reactor by assuming that the systematic error is reduced to 0.8%.

It was stressed that this measurement is clean measurement of θ_{13} without any ambiguity from other parameters. The measurement of θ_{13} and δ by the long baseline experiment with ν and $\overline{\nu}$ beams suffer from the problem of parameter degeneracy; The long baseline experiment gives eight solutions in the worst case due to the problem no matter how accurate the measurement is. Therefore, it is understood that θ_{13} measurement by the reactor experiment is complementary to that by the long baseline experiments. In par-

ticular, we pursuit in this thesis the possibility of selecting out the true solution from fake solutions in the long baseline experiment by using reactor experiment. We focused on the J-PARC neutrino project as long baseline experiment; By tuning the beam energy to that of the oscillation maximum ($E_{\rm OM} = |\Delta m^2_{31}|L/2\pi \simeq 0.6$GeV), the potential eight solutions of θ_{13} in the experiment shrinks to two values which correspond to the ambiguity of $\theta_{23} \leftrightarrow \pi/2 - \theta_{23}$. We investigated the possibility to resolve the ambiguity of $\theta_{23} \leftrightarrow \pi/2 - \theta_{23}$ with clear determination of θ_{13} by the reactor experiment. We showed that it is possible if $\sin^2 2\theta_{13}$ and the difference of θ_{23} from $\pi/4$ are relatively large. For example, the degeneracy is resolved for $\sin^2 2\theta_{13} \gtrsim 0.05$ and $s^2_{23} \lesssim 0.39$ or $0.57 \lesssim s^2_{23}$ as we see in Fig. 5.7. Once the θ_{23} ambiguity vanishes, the value of θ_{13} is determined precisely by high sensitivity measurement of the LBL experiment.

We uncovered also a new method for detecting leptonic CP violation in Chapter 6. It is achieved by combining reactor measurement of θ_{13} with ν_e appearance measurement in the long baseline experiment. Each of those experiments must have high sensitivity because CP violating effect is so small due to the smallness of the Jarlskog factor. Therefore, as the long baseline experiment, we exploited 2yr measurement of ν_e appearance in the J-PARC phase II experiment with upgraded 4MW beam and Hyper-Kamiokande of 540Mt fiducial mass. On the other hand, precise spectral analysis and high statistics is required for the reactor experiment; The measurement was assumed at least to be of $10^3 \mathrm{GW_{th}} \cdot$ ton $\cdot$ year which corresponds to 50 ton-year measurement with the Kashiwazaki-Kariwa nuclear power plant. Then, it came to light that CP violation can be detected at 90% CL in the region of $\sin^2 2\theta_{13} \gtrsim 0.05$ and $|\delta| \gtrsim 0.3\pi(54^\circ)$. The sensitivity is less than that to be obtained with combining ν_e appearance measurement with $\overline{\nu}_e$ appearance in the J-PARC phase II because the latter enable us to observe CP violation at 3σ CL for $\sin^2 2\theta_{13} \gtrsim 0.01$ and $|\delta| \gtrsim 0.11\pi(20^\circ)$. The reactor-LBL combined method is, however, worth to do because it can exhibit the first information of the leptonic CP violation before the long-term measurement of $\overline{\nu}_e$ search in the J-PARC experiment. Even if the information is rather rough, it helps the experiments to optimize the settings (such as relative time sharing of ν and $\bar{\nu}$ modes in the LBL experiment with fixed total exposure time).

As a pessimistic situation without upgraded beam nor HK, we assumed also the J-PARC phase I with 0.75MW beam and existing Super-Kamiokande of 22.5kt fiducial mass. Even in this case, we found that CP violation can be detected by 10yr measurement of ν_e appearance, though slightly less sensitivities than that in the case with high-power beam and HK. The reactor-LBL combined method is very useful in the case of very long exposure with ν beam because the observation of CP violation requires the conventional method with $\overline{\nu}$ mode LBL experiment to run about three times longer than the exposure

with ν beam.

We should note that the sensitivity to CP violation is affected by uncertainties of other parameters because the CP violating effect is very small. Especially, the unknown sign of Δm^2_{31} has a serious consequence on the sensitivity as is shown in Figs. 6.7. Roughly speaking, the sensitivity region becomes half due to the uncertainty in this method. Actually, such a trouble occurs also, more or less, in the measurement of CP violation with antineutrino-mode LBL experiment. Hence, it became clear that knowing the sign of Δm^2_{31} is very important for any measurement of the leptonic CP violation.

From above discussions, we have understood that some valuable information will be extracted by the combined analyses of the reactor experiment with other experiments. Those are the benefits of the characteristic property of the reactor experiment as the pure measurement of of θ_{13}. Such a clean measurement is not only valuable by itself but also very useful as a tool for extracting new information of mixing parameters from results of other experiments. Thus, we conclude that the reactor experiment can play vital role for the determination of the values of neutrino mixing parameters.

Acknowledgments

I would like to express my deepest gratitude to my supervisor, H. Minakata, for bringing me into neutrino physics, his advice, useful discussions, and taking me sometimes for a coffee break. I am grateful to O. Yasuda for many valuable discussions especially on the statistical analysis and for his critical comments. I am grateful also to F. Suekane for many useful discussions on the reactor experiment and the analysis. I thank K. Inoue for his help and comments. N. Kitazawa encouraged me vary much and discussions with him was fruitful. I thank K. Kaneyuki, T. Kobayashi, and Y. Obayashi for correspondences and helpful discussions on J-PARC neutrino project. I thank S. Parke for valuable discussions on the problem of parameter degeneracy.

Appendix A

Statistical Analysis

A.1 χ^2 Analysis

In this thesis, our analyses are based on those of Gaussian probability distribution function (p.d.f.). The number of events, N', should obey Poissonian p.d.f. because the neutrino event is extremely rare. Furthermore, sufficiently accumulated number of events, $N = \sum N'$, becomes to obey Gaussian p.d.f.[1] with the Poissonian variance $\sigma_{\rm stat} = 1/\sqrt{N_0}$ which is the statistical error for observed number N_0. Then, we obtain the p.d.f.

$$f_{\rm stat}(N) = \frac{1}{\sqrt{2\pi N_0}} \exp\left\{-\frac{(N-N_0)^2}{2N_0}\right\}. \tag{A.1}$$

A systematic error $\sigma_{\rm sys}$, which will give the Gaussian noise (a random noise), can be introduced with a cascade of two Gaussian p.d.f. as

$$\begin{aligned} f(N) &= \frac{1}{2\pi\sigma_{\rm sys}\sqrt{N_0}} \int d\alpha \, \exp\left[-\frac{1}{2}\left\{\frac{(N-(1+\alpha)N_0)^2}{N_0} + \frac{\alpha^2}{\sigma_{\rm sys}^2}\right\}\right] & \text{(A.2)} \\ &= \frac{1}{\sqrt{2\pi(N_0+\sigma_{\rm sys}^2 N_0^2)}} \exp\left\{-\frac{1}{2}\frac{(N-N_0)^2}{N_0+\sigma_{\rm sys}^2 N_0^2}\right\}. & \text{(A.3)} \end{aligned}$$

In order to keep $f(N)$ being Gaussian p.d.f. for its simplicity, the auxiliary (noise) variable α should not be couple with the variable of $f(N)$. The overall normalization is not important. Note that the power in (A.3) is

$$\frac{(N-N_0)^2}{N_0+\sigma_{\rm sys}^2 N_0^2} = \min_{\alpha}\left\{\frac{(N-(1+\alpha)N_0)^2}{N_0} + \frac{\alpha^2}{\sigma_{\rm sys}^2}\right\}, \tag{A.4}$$

where the right-hand side is often used as the definition of χ^2.

The general form of (A.3) is the n-variable Gaussian p.d.f.

$$\frac{1}{\sqrt{(2\pi)^n \det V}} \exp\left(-\frac{1}{2}x^T V^{-1} x\right), \quad x^T \equiv \left(\frac{N-N_0}{N_0}, \cdots\right), \tag{A.5}$$

[1] Actually, this fact is independent of event-by-event p.d.f. by virtue of the central limit theorem.

d.o.f.	$1\sigma(68.3\%)$	$1.6\sigma(90\%)$	$2\sigma(95.4\%)$	$3\sigma(99.7\%)$
1	1	2.7	4	9
2	2.3	4.6	6.2	11.8
3	3.5	6.5	8.0	14.2

Table A.1: The values of χ^2 that corresponds to the confidence levels (CL) for some degrees of freedom (d.o.f.).

where V denotes the variance matrix which has the information of errors and x is independent of the errors. Here, χ^2 is defined as

$$\chi^2 \equiv x^T V^{-1} x. \tag{A.6}$$

Thus, χ^2 expresses the "statistical distance" to a point determined by N's from a point fixed by N_0's. Since we are interested in χ^2 only, other variables (the "solid angle") can be integrated out. Remembering that the area of a n-dimensional unit sphere is $2\pi^{n/2}/\Gamma(n/2)$, we obtain the χ^2 p.d.f. for n degrees of freedom

$$P(\chi^2, n) = \frac{2^{-n/2}}{\Gamma(n/2)} (\chi^2)^{n/2-1} e^{-\chi^2/2}. \tag{A.7}$$

The χ_b^2 which corresponds to the bound of $b\%$ CL can be defined such that

$$\frac{b}{100} = \int_0^{\chi_b^2} d\chi^2 \, P(\chi^2, n). \tag{A.8}$$

Some typical values of χ_b^2 are listed in Table A.1.

When we extract an allowed region in a parameter space, χ^2 is replaced with $\Delta\chi^2 \equiv \chi^2 - \chi^2_{\rm min}$, where $\chi^2_{\rm min}$ is obtained by minimizing χ^2 with respect to parameters of the model considered. Then, the degrees of freedom n is given by the number of parameters because $\Delta\chi^2$ is regarded approximately as a Gaussian p.d.f. for the parameters around the best fit point where χ^2 is minimized:

$$\Big(N(x) - N_0\Big)^2 - \Big(N(x^{\rm best}) - N_0\Big)^2 \simeq \frac{d^2 N(x^{\rm best})}{d(x^{\rm best})^2} \Big(N(x^{\rm best}) - N_0\Big)(x - x^{\rm best})^2. \tag{A.9}$$

For example, the d.o.f. for 2ν oscillation is two (θ and Δm^2) if we want to extract information of both parameters. If we need not, however, the information of some of parameters, we can minimize $\Delta\chi^2$ with respect to those parameters. Then, the d.o.f. is reduced by the number of unnecessary (minimized) parameters:

$$\min_y \left(\frac{(x-x_0)^2}{\sigma_x^2} + \frac{(x-x_0)(y-y_0)}{\rho_{xy}\sigma_x\sigma_y} + \frac{(y-y_0)^2}{\sigma_y^2} \right) = \left(1 - \frac{1}{4\rho_{xy}} \right) \frac{(x-x_0)^2}{\sigma_x^2}. \tag{A.10}$$

A.2 Cancellation of Errors by Near-Far Detector Comparison

This appendix is meant to be a pedagogical note in which we try to clarify the feature of cancellation of systematic errors by near-far detector comparison and the relationship between over-all and bin-by-bin errors.

The definition of $\Delta\chi^2$ for two detector system is

$$\begin{aligned}\Delta\chi^2_{nf} &\equiv \min_{\alpha} \Delta\chi^2_{nf}(\alpha) \\ &\equiv \min_{\alpha} \left[\frac{\left\{N_f - (1+\alpha)N_f^{\rm best}\right\}^2}{N_f^{\rm best} + \sigma_{\rm d}^2 (N_f^{\rm best})^2} + \frac{\left\{N_n - (1+\alpha)N_n^{\rm best}\right\}^2}{N_n^{\rm best} + \sigma_{\rm d}^2 (N_n^{\rm best})^2} + \frac{\alpha^2}{\sigma_{\rm D}^2} \right], \quad \text{(A.11)}\end{aligned}$$

where N_f (N_n) is the theoretical total number of events expected to be measured at far (near) detector. The quantities with superscript "best" are defined as the ones calculated with the best-fit values of the "experimental data", which are to be tested against the CP conserving case. $\sigma_{\rm D}$ and $\sigma_{\rm d}$ are correlated and uncorrelated errors between detectors, respectively.

We discuss statistical average of an observable $\mathcal{O}$ by the Gaussian probability distribution function as

$$< \mathcal{O} > \equiv C \int dN_f dN_n d\alpha \, \mathcal{O} \exp\left(-\frac{1}{2} \Delta\chi^2_{nf}(\alpha) \right), \quad \text{(A.12)}$$

where C is the normalization constant to make $< 1 >$ unity. Note that the integration with respect to α is equivalent to the minimization in (A.11). After the minimization, it takes the following form which is generic to the Gaussian distribution,

$$\Delta\chi^2_{nf} = (x, y) \begin{pmatrix} < x^2 > & < xy > \\ < yx > & < y^2 > \end{pmatrix}^{-1} \begin{pmatrix} x \\ y \end{pmatrix}, \quad \text{(A.13)}$$

$$x \equiv \frac{N_f - N_f^{\rm best}}{N_f^{\rm best}}, \quad y \equiv \frac{N_n - N_n^{\rm best}}{N_n^{\rm best}}. \quad \text{(A.14)}$$

In order to examine the feature of near-far cancellation of errors, it is valuable to transform[2] x and y as

$$X \equiv x - y = \frac{N_f}{N_f^{\rm best}} - \frac{N_n}{N_n^{\rm best}}, \quad Y \equiv x + y = \frac{N_f}{N_f^{\rm best}} + \frac{N_n}{N_n^{\rm best}} - 2. \quad \text{(A.15)}$$

[2]Such a transformation is not necessary for the numerical calculation of $\Delta\chi^2$ because it does not change the value of $\Delta\chi^2$.

Then, $\Delta\chi^2_{nf}$ can be written as

$$\Delta\chi^2_{nf} = (X,Y)\begin{pmatrix} <X^2> & <XY> \\ <YX> & <Y^2> \end{pmatrix}^{-1}\begin{pmatrix} X \\ Y \end{pmatrix}, \tag{A.16}$$

where

$$<X^2> = \frac{1}{N_f^{\rm best}} + \frac{1}{N_n^{\rm best}} + 2\sigma_{\rm d}^2, \tag{A.17}$$

$$<Y^2> = \frac{1}{N_f^{\rm best}} + \frac{1}{N_n^{\rm best}} + 2\sigma_{\rm d}^2 + 4\sigma_{\rm D}^2, \tag{A.18}$$

$$<XY> = <YX> = \frac{1}{N_f^{\rm best}} - \frac{1}{N_n^{\rm best}}. \tag{A.19}$$

It is evident in (A.17) that the correlated systematic errors cancel by the near-far comparison. The systematic error $\sqrt{2}\sigma_{\rm d}$ in $<X^2>$ is referred to as the relative normalization error in [80]. Note that (5.5) is $X^2/<X^2>$ of the normalization free analysis, and it dominates the sensitivity at the $|\Delta m^2_{31}|$ value we concern. The normalization is constrained by Y, and $<Y^2>$ determines the sensitivity to $\sin^2 2\theta_{13}$ at very large $|\Delta m^2_{31}|$ where X vanishes.

We briefly treat the case of two bins with infinite statistics to illustrate the importance of uncorrelated errors. In this case X subspace of $\Delta\chi^2_{nf}$ can be written as

$$X(2\sigma_d^2)^{-1}X \longrightarrow (X_1,X_2)\begin{pmatrix} 2\sigma^2_{\rm dB}+2\sigma^2_{\rm db} & 2\sigma^2_{\rm dB} \\ 2\sigma^2_{\rm dB} & 2\sigma^2_{\rm dB}+2\sigma^2_{\rm db} \end{pmatrix}^{-1}\begin{pmatrix} X_1 \\ X_2 \end{pmatrix}. \tag{A.20}$$

It is clear that $\sigma_{\rm db}=0$ leads to the diverge of $\Delta\chi^2_{nf}$ except for the best fit point ($X_i = Y_i = 0$), which means that the infinite precision can be achieved for the case. Thus, $\sigma_{\rm db}$ must be treated with great care.

Next we derive the relationship between over-all and bin-by-bin errors that was used in the text, (6.8). For simplicity, we consider the case of one detector with two bins. Then, $\Delta\chi^2$ for the case is defined as

$$\begin{aligned}\Delta\chi^2_{12} &\equiv \min_\alpha \Delta\chi^2_{12}(\alpha) \\ &\equiv \min_\alpha \left[\frac{\left\{N_1-(1+\alpha)N_1^{\rm best}\right\}^2}{N_1^{\rm best}+\sigma_{\rm b}^2(N_1^{\rm best})^2} + \frac{\left\{N_2-(1+\alpha)N_2^{\rm best}\right\}^2}{N_2^{\rm best}+\sigma_{\rm b}^2(N_2^{\rm best})^2} + \frac{\alpha^2}{\sigma_{\rm B}^2}\right],\end{aligned} \tag{A.21}$$

where N_1 and N_2 are the expected numbers of events within first and second bins, respectively, and $\sigma_{\rm B}$ ($\sigma_{\rm b}$) denotes the correlated (uncorrelated) error between bins.

To obtain the error for the total number of events, we define

$$x_{\rm tot} \equiv \sum_i \frac{N_i - N_i^{\rm best}}{N_{\rm tot}^{\rm best}}, \quad N_{\rm tot}^{\rm best} \equiv \sum_i N_i^{\rm best}. \tag{A.22}$$

Then, we obtain

$$\begin{aligned} < x_{\rm tot}^2 > &= C' \int dN_1 dN_2 d\alpha \, x_{\rm tot}^2 \exp\left(-\frac{1}{2}\Delta\chi_{12}^2(\alpha)\right) \\ &= \frac{1}{N_{\rm tot}^{\rm best}} + \sigma_{\rm B}^2 + \sigma_{\rm b}^2 \frac{\sum_i (N_i^{\rm best})^2}{(N_{\rm tot}^{\rm best})^2}. \end{aligned} \tag{A.23}$$

One can show that the same treatment goes though for arbitrary number of bins. The coefficient of $\sigma_{\rm b}^2$ is almost 1/9 in our analysis (14 bins). We see that (5.6) is obtained by $\sigma_{\rm B} = 0$ which is the most pessimistic case because of no correlated error to be reduced.

Bibliography

[1] S. Weinberg, Phys. Rev. Lett. **19**, 1264 (1967);
A. Salam, p.367 of *Elementary Particle Thepty*, ed. N. svartholm (Almwuist and Wiksells, Stockholm, 1969);
S.L. Glashow, J. Iliopoulos, and L. Maiani, Phys. Rev. **D2**, 1285 (1970).

[2] Y. Fukuda *et al.* [Super-Kamiokande Collaboration], Phys. Rev. Lett. **81**, 1562 (1998) [arXiv:hep-ex/9807003]; Phys. Rev. Lett. **85**, 3999 (2000) [arXiv:hep-ex/0009001].

[3] T. Yanagida, Prog. Theor. Phys. **64** 1103 (1980), and in *Proceedings of the Workshop on the Unified Theory and the Baryon Number of the Universe*, eds. O. Sawada and A. Sugamomto, KEK report No. 79-18, Tsukuba, Japan, 1979;
M. Gell-Mann, P. Ramond, and R. Slanski, in *Supergravity*, eds. P. van Nieuwenhuizen and D.Z. Freedman, North-Holland, Amsterdam, 1979.

[4] Z. Maki, M. Nakagawa, and S. Sakata, Prog. Theor. Phys. **28**, 870 (1962).

[5] S. H. Ahn *et al.* [K2K Collaboration], Phys. Lett. B **511**, 178 (2001) [arXiv:hep-ex/0103001].

[6] R. J. Davis, D. S. Harmer and K. C. Hoffman, Phys. Rev. Lett. **20**, 1205 (1968).
B. T. Cleveland *et al.*, Astrophys. J. **496**, 505 (1998).

[7] J. N. Bahcall, N. A. Bahcall and G. Shaviv, Phys. Rev. Lett. **20**, 1209 (1968);
J. N. Bahcall, the XXIII Physics in Collisions Conference (PIC03), 26-28 June 2003, Zeuthen, Germany [arXiv:astro-ph/0310030].

[8] J. N. Abdurashitov *et al.* [SAGE Collaboration], Phys. Rev. C **60**, 055801 (1999) [arXiv:astro-ph/9907113].

[9] W. Hampel *et al.* [GALLEX Collaboration], Phys. Lett. B **447**, 127 (1999).

[10] Y. Fukuda *et al.* [Super-Kamiokande Collaboration], Phys. Rev. Lett. **82**, 1810 (1999) [arXiv:hep-ex/9812009]; Phys. Lett. B **539**, 179 (2002) [arXiv:hep-ex/0205075].

[11] Q. R. Ahmad *et al.* [SNO Collaboration], Phys. Rev. Lett. **87**, 071301 (2001) [arXiv:nucl-ex/0106015]; Phys. Rev. Lett. **89**, 011302 (2002) [arXiv:nucl-ex/0204009];

[12] K. Eguchi *et al.* [KamLAND Collaboration], Phys. Rev. Lett. **90**, 021802 (2003) [arXiv:hep-ex/0212021];
Proposal for US Participation in KamLAND, [http://kamland.lbl.gov/KamLAND.US.Proposal.pdf]

[13] M. Apollonio *et al.* [CHOOZ Collaboration], Phys. Lett. B **466**, 415 (1999) [arXiv:hep-ex/9907037]; Eur. Phys. J. C **27**, 331 (2003) [arXiv:hep-ex/0301017].

[14] H. Minakata, H. Sugiyama, O. Yasuda, K. Inoue and F. Suekane, Phys. Rev. D **68**, 033017 (2003) [arXiv:hep-ph/0211111].

[15] G. L. Fogli and E. Lisi, Phys. Rev. D **54**, 3667 (1996) [arXiv:hep-ph/9604415].

[16] J. Burguet-Castell, M. B. Gavela, J. J. Gomez-Cadenas, P. Hernandez and O. Mena, Nucl. Phys. B **608**, 301 (2001) [arXiv:hep-ph/0103258].

[17] H. Minakata and H. Nunokawa, JHEP **0110**, 001 (2001) [arXiv:hep-ph/0108085]; Nucl. Phys. Proc. Suppl. **110**, 404 (2002) [arXiv:hep-ph/0111131].

[18] V. Barger, D. Marfatia and K. Whisnant, Phys. Rev. D **65**, 073023 (2002) [arXiv:hep-ph/0112119].

[19] Y. Itow *et al.*, arXiv:hep-ex/0106019;
For an updated version, see: http://neutrino.kek.jp/jhfnu/loi/loi.v2.030528.pdf

[20] T. Kajita, H. Minakata and H. Nunokawa, Phys. Lett. B **528**, 245 (2002) [arXiv:hep-ph/0112345].

[21] H. Minakata and H. Sugiyama, Phys. Lett. B **580**, 216 (2004) [arXiv:hep-ph/0309323].

[22] K. Hagiwara *et al.* [Particle Data Group Collaboration], Phys. Rev. D **66**, 010001 (2002).

[23] The Neutrino Oscillation Industry [http://neutrinooscillation.org/]

[24] [LEP Collaborations], arXiv:hep-ex/0103048.

[25] T. Affolder *et al.* [CDF Collaboration], Phys. Rev. D **64**, 052001 (2001) [arXiv:hep-ex/0007044];
B. Abbott *et al.* [D0 Collaboration], Phys. Rev. Lett. **84**, 222 (2000) [arXiv:hep-ex/9909030].

[26] P. Vilain *et al.* [CHARM-II Collaboration], Phys. Lett. B **335**, 246 (1994).

[27] N. Cabibbo, Phys. Rev. Lett. **10**, 531 (1963).

[28] M. Kobayashi and T. Maskawa, Prog. Theor. Phys. **49**, 652 (1973).

[29] L. L. Chau and W. Y. Keung, Phys. Rev. Lett. **53**, 1802 (1984);
H. Fritzsch and J. Plankl, Phys. Rev. D **35**, 1732 (1987);
F. J. Botella and L. L. Chau, Phys. Lett. B **168**, 97 (1986).

[30] H. Harari and M. Leurer, Phys. Lett. B **181**, 123 (1986).

[31] L. Wolfenstein, Phys. Rev. D **17**, 2369 (1978);
S. P. Mikheev and A. Y. Smirnov, Sov. J. Nucl. Phys. **42**, 913 (1985) [Yad. Fiz. **42**, 1441 (1985)]; Nuovo Cim. C **9**, 17 (1986).

[32] K. Kimura, A. Takamura and H. Yokomakura, Phys. Rev. D **66**, 073005 (2002) [arXiv:hep-ph/0205295].

[33] ALEPH homepage [http://aleph.web.cern.ch/aleph/].

[34] J. Bonn *et al.*, Nucl. Phys. Proc. Suppl. **91**, 273 (2001).

[35] V. M. Lobashev *et al.*, Nucl. Phys. Proc. Suppl. **91**, 280 (2001).

[36] A. Osipowicz *et al.* [KATRIN Collaboration], arXiv:hep-ex/0109033.

[37] H. V. Klapdor-Kleingrothaus *et al.*, Eur. Phys. J. A **12**, 147 (2001) [arXiv:hep-ph/0103062].

[38] C. E. Aalseth *et al.* [IGEX Collaboration], Phys. Rev. D **65**, 092007 (2002) [arXiv:hep-ex/0202026].

[39] W. C. Haxton, G. J. Stephenson and D. Strottman, Phys. Rev. D **25**, 2360 (1982).

[40] O. Civitarese, A. Faessler and T. Tomoda, Phys. Lett. B **194**, 11 (1987);
T. Tomoda and A. Faessler, Phys. Lett. B **199**, 475 (1987).

[41] J. Engel, P. Vogel, X. D. Ji and S. Pittel, Phys. Lett. B **225**, 5 (1989).

[42] A. Staudt, K. Muto and H. V. Klapdor-Kleingrothaus, Europhys. Lett. **13**, 31 (1990).

[43] E. Caurier, F. Nowacki, A. Poves and J. Retamosa, Phys. Rev. Lett. **77**, 1954 (1996) [arXiv:nucl-th/9601017].

[44] P. Vogel and M. R. Zirnbauer, Phys. Rev. Lett. **57**, 3148 (1986).

[45] H. V. Klapdor-Kleingrothaus, A. Dietz, H. L. Harney and I. V. Krivosheina, Mod. Phys. Lett. A **16**, 2409 (2001) [arXiv:hep-ph/0201231].

[46] C. E. Aalseth *et al.*, Mod. Phys. Lett. A **17**, 1475 (2002) [arXiv:hep-ex/0202018].

[47] H. V. Klapdor-Kleingrothaus, arXiv:hep-ph/0205228.

[48] H. L. Harney, arXiv:hep-ph/0205293.

[49] K. Zuber, Phys. Lett. B **519**, 1 (2001) [arXiv:nucl-ex/0105018].

[50] N. Ishihara *et al.*, Nucl. Instrum. Meth. A **443**, 101 (2000).

[51] X. Sarazin and D. Lalanne [NEMO Collaboration], 19th International Conference on Neutrino Physics and Astrophysics (Neutrino 2000), Sudbury, Canada, 16-21 June 2000, and 30th International Conference on High-Energy Physics (ICHEP 2000), Osaka, Japan, 27 July - 2 Aug. 2000 [arXiv:hep-ex/0006031].

[52] G. Bellini *et al.*, Eur. Phys. J. C **19**, 43 (2001) [arXiv:nucl-ex/0007012].

[53] T. Kishimoto [CANDLES Collaboration], The 4th Workshop on Neutrino Oscillations and their Origin (NOON2003), 10-14 Feb. 2003, Kanazawa, Japan.

[54] A. Alessandrello *et al.* [CUORE Collaboration], Phys. Atom. Nucl. **66**, 452 (2003) [Yad. Fiz. **66**, 480 (2003)] [arXiv:hep-ex/0201038].

[55] M. Danilov *et al.*, Phys. Lett. B **480**, 12 (2000) [arXiv:hep-ex/0002003].

[56] H. V. Klapdor-Kleingrothaus *et al.* [GENIUS Collaboration], arXiv:hep-ph/9910205.

[57] C. E. Aalseth *et al.* [Majorana Collaboration], 3rd International Conference on Nonaccelerator New Physics (NANP 01), 19-23 June 2001, Dubna, Russia [arXiv:hep-ex/0201021].

[58] M. Nomachi [MOON Collaboration], 8th International Workshop on Topics in Astroparticle and Underground Physics (TAUP2003), 5-9 Sept. 2003, Seattle, USA.

[59] M. Nakahata [XMASS Collaboration], IIIrd International Workshop on Low Energy Solar Neutrinos (LowNu 2002), 22-24 May 2002, Heidelberg, Germany.

[60] S. R. Elliott and P. Vogel, Ann. Rev. Nucl. Part. Sci. **52**, 115 (2002) [arXiv:hep-ph/0202264].

[61] H. Sugiyama, 4th Workshop on Neutrino Oscillations and their Origin (NOON2003), 10-14 Feb. 2003, Kanazawa, Japan [arXiv:hep-ph/0307311].

[62] K. S. Hirata *et al.* [KAMIOKANDE-II Collaboration], Phys. Lett. B **205**, 416 (1988); B **280**, 146 (1992).

[63] Y. Fukuda *et al.* [Kamiokande Collaboration], Phys. Lett. B **335**, 237 (1994);

[64] D. Casper *et al.*, Phys. Rev. Lett. **66**, 2561 (1991);
R. Becker-Szendy *et al.*, Phys. Rev. Lett. **69**, 1010 (1992).

[65] K. Daum [Frejus Collaboration.], Z. Phys. C **66**, 417 (1995).

[66] M. Aglietta *et al.* [The NUSEX Collaboration], Europhys. Lett. **8**, 611 (1989).

[67] Y. Hayato [Super-Kamiokande, K2K, and J-PARC ν collabolations], The International Europhysics Conference on High Energy Physics (HEP 2003), 17-23 July 2003, Aachen, Germany.

[68] M. Ambrosio *et al.* [MACRO Collaboration], Phys. Lett. B **566**, 35 (2003) [arXiv:hep-ex/0304037].

[69] M. Sanchez *et al.* [Soudan 2 Collaboration], Phys. Rev. D **68**, 113004 (2003) [arXiv:hep-ex/0307069].

[70] M. Altmann *et al.* [GNO Collaboration], Phys. Lett. B **490**, 16 (2000) [arXiv:hep-ex/0006034].

[71] Y. Fukuda *et al.* [Kamiokande Collaboration], Phys. Rev. Lett. **77**, 1683 (1996).

[72] G. L. Fogli, E. Lisi, D. Montanino and A. Palazzo, Phys. Rev. D **64**, 093007 (2001) [arXiv:hep-ph/0106247];
J. N. Bahcall, M. C. Gonzalez-Garcia and C. Pena-Garay, JHEP **0108**, 014 (2001) [arXiv:hep-ph/0106258];
A. Bandyopadhyay, S. Choubey, S. Goswami and K. Kar, Phys. Lett. B **519**, 83 (2001) [arXiv:hep-ph/0106264];
P. I. Krastev and A. Y. Smirnov, Phys. Rev. D **65**, 073022 (2002) [arXiv:hep-ph/0108177].

[73] M. B. Smy, in *Neutrino Oscillations and Their Origin (Kashiwa 2001)*, edited by Y. Suzuki *et al.* (World Scientific, Singapre, 2003), p. 40 [arXiv:hep-ex/0202020];

J. N. Bahcall, M. C. Gonzalez-Garcia and C. Pena-Garay, JHEP **0207**, 054 (2002) [arXiv:hep-ph/0204314];
V. Barger, D. Marfatia, K. Whisnant and B. P. Wood, Phys. Lett. B **537**, 179 (2002) [arXiv:hep-ph/0204253];
A. Bandyopadhyay, S. Choubey, S. Goswami and D. P. Roy, Phys. Lett. B **540**, 14 (2002) [arXiv:hep-ph/0204286];
P. C. de Holanda and A. Y. Smirnov, Phys. Rev. D **66**, 113005 (2002) [arXiv:hep-ph/0205241];
G. L. Fogli, E. Lisi, A. Marrone, D. Montanino and A. Palazzo, Phys. Rev. D **66**, 053010 (2002) [arXiv:hep-ph/0206162];
M. Maltoni, T. Schwetz, M. A. Tortola and J. W. Valle, Phys. Rev. D **67**, 013011 (2003) [arXiv:hep-ph/0207227].

[74] V. Barger and D. Marfatia, Phys. Lett. B **555**, 144 (2003) [arXiv:hep-ph/0212126];
G. L. Fogli, E. Lisi, A. Marrone, D. Montanino, A. Palazzo and A. M. Rotunno, Phys. Rev. D **67**, 073002 (2003) [arXiv:hep-ph/0212127];
M. Maltoni, T. Schwetz and J. W. F. Valle, Phys. Rev. D **67**, 093003 (2003) [arXiv:hep-ph/0212129];
A. Bandyopadhyay, S. Choubey, R. Gandhi, S. Goswami and D. P. Roy, Phys. Lett. B **559**, 121 (2003) [arXiv:hep-ph/0212146];
J. N. Bahcall, M. C. Gonzalez-Garcia and C. Pena-Garay, JHEP **0302**, 009 (2003) [arXiv:hep-ph/0212147];
H. Nunokawa, W. J. C. Teves and R. Zukanovich Funchal, Phys. Lett. B **562**, 28 (2003) [arXiv:hep-ph/0212202].

[75] S. N. Ahmed *et al.* [SNO Collaboration], arXiv:nucl-ex/0309004.

[76] M. B. Smy *et al.* [Super-Kamiokande Collaboration], arXiv:hep-ex/0309011.

[77] F. Reines and C.L. Cowan, Jr., Phys. Rev. **90**, 492 (1953); **92**, 830 (1953);
C.L. Cowan, Jr. *et al.*, Science **124**, 103 (1956).

[78] F. Boehm *et al.*, Phys. Rev. D **64**, 112001 (2001) [arXiv:hep-ex/0107009].

[79] G. L. Fogli, E. Lisi, A. Marrone, D. Montanino, A. Palazzo and A. M. Rotunno, arXiv:hep-ph/0308055.

[80] Y. Declais *et al.*, Nucl. Phys. B **434**, 503 (1995).

[81] The MINOS Collaboration, P. Adamson *et al.*, *MINOS Detectors Technical Design Report, Version 1.0*, NuMI-L-337, October 1998,

[http://www.hep.anl.gov/ndk/hypertext/minos_tdr.html].

[82] D. Ayres *et al.*, arXiv:hep-ex/0210005;
G. Feldman [NuMI Off-axis Collaboration], International Workshop on Neutrino Oscillations in Venice (NO-VE), 3-5 Dec. 2003, Venice, Italy.

[83] CNGS homepage [http://proj-cngs.web.cern.ch/proj-cngs/];
D. Duchesneau [OPERA Collaboration], eConf **C0209101**, TH09 (2002) [Nucl. Phys. Proc. Suppl. **123**, 279 (2003)] [arXiv:hep-ex/0209082];
M. Komatsu, P. Migliozzi and F. Terranova, J. Phys. G **29**, 443 (2003) [arXiv:hep-ph/0210043].

[84] I. Kreslo [OPERA collaboration], International Workshop on Neutrino Oscillations in Venice (NO-VE), 3-5 Dec. 2003, Venice, Itary.

[85] ICARUS homepage [http://pcnometh4.cern.ch/].

[86] C. Albright *et al.*, arXiv:hep-ex/0008064;
V. D. Barger, S. Geer, R. Raja and K. Whisnant, Phys. Rev. D **63**, 113011 (2001) [arXiv:hep-ph/0012017];
J. Pinney and O. Yasuda, Phys. Rev. D **64**, 093008 (2001) [arXiv:hep-ph/0105087];
P. Hernandez and O. Yasuda, Nucl. Instrum. Meth. A **485**, 811 (2002);
O. Yasuda, Nucl. Instrum. Meth. A **503**, 104 (2003) [arXiv:hep-ph/0111172]; 3rd Workshop on Neutrino Oscillations and Their Origin (NOON 2001), 5-8 Dec. 2001, Kashiwa, Japan [arXiv:hep-ph/0203273]; Conference on Physics Beyond the Standard Model: Beyond the Desert 02, 2-7 June 2002, Oulu, Finland [arXiv:hep-ph/0209127], and the references therein.

[87] P. Zucchelli, Phys. Lett. B **532**, 166 (2002) [arXiv:hep-ex/0107006];
J. Bouchez, M. Lindroos and M. Mezzetto, 5th International Workshop on Neutrino Factories and Superbeams (NuFact03), 5-11 June 2003, New York, USA [arXiv:hep-ex/0310059].

[88] D. Beavis *et al.*, Proposal of BNL AGS E-889 (1995).

[89] J. Kameda, *Detailed Studies of Neutrino Oscillation with Atmospheric Neutrinos of Wide Energy Range from 100 MeV to 1000 GeV in Super-Kamiokande*, Ph. D. thesis, University of Tokyo, September 2002.

[90] H. Minakata, H. Nunokawa and S. J. Parke, Phys. Rev. D **66**, 093012 (2002) [arXiv:hep-ph/0208163].

[91] A. Cervera, A. Donini, M. B. Gavela, J. J. Gomez Cadenas, P. Hernandez, O. Mena and S. Rigolin, Nucl. Phys. B **579**, 17 (2000) [Erratum-ibid. B **593**, 731 (2001)] [arXiv:hep-ph/0002108].

[92] M. Freund, Phys. Rev. D **64**, 053003 (2001) [arXiv:hep-ph/0103300].

[93] V. Barger, D. Marfatia and K. Whisnant, Phys. Rev. D **66**, 053007 (2002) [arXiv:hep-ph/0206038].

[94] A. Donini, D. Meloni and P. Migliozzi, Nucl. Phys. B **646**, 321 (2002) [arXiv:hep-ph/0206034];
A. Donini, 5th International Workshop on Neutrino Factories and Superbeams, 5-11 June 2003, New York, USA [arXiv:hep-ph/0310014].

[95] T. K. Kuo and J. Pantaleone, Phys. Lett. B **198**, 406 (1987);
H. Minakata and S. Watanabe, Phys. Lett. B **468**, 256 (1999) [arXiv:hep-ph/9906530];
H. Yokomakura, K. Kimura and A. Takamura, Phys. Lett. B **544**, 286 (2002) [arXiv:hep-ph/0207174].

[96] M. Koike and J. Sato, Mod. Phys. Lett. A **14**, 1297 (1999) [arXiv:hep-ph/9803212].

[97] T. Nakaya [Super-Kamiokande Collaboration], eConf **C020620**, SAAT01 (2002) [arXiv:hep-ex/0209036].

[98] Y. Kozlov, L. Mikaelyan and V. Sinev, Phys. Atom. Nucl. **66**, 469 (2003) [Yad. Fiz. **66**, 497 (2003)] [arXiv:hep-ph/0109277].

[99] H. Sugiyama, O. Yasuda, F. Suekane, and G. A. Horton-Smith, in preparation.

[100] P. Vogel and J. Engel, Phys. Rev. D **39**, 3378 (1989).

[101] F. Boehm and P. Vogel, *The Physics of Massive Neutrinos*, Cambridge University Press (New York) 1992.

[102] P. Vogel, Phys. Rev. D **29**, 1918 (1984).

[103] G. L. Fogli and E. Lisi, Phys. Rev. D **52**, 2775 (1995) [arXiv:hep-ph/9504287].

[104] F. Suekane, K. Inoue, T. Araki and K. Jongok, The 4th Workshop on Neutrino Oscillations and their Origin (NOON2003), 10-14 Feb. 2003, Kanazawa, Japan [arXiv:hep-ex/0306029].

[105] M. H. Shaevitz and J. M. Link, arXiv:hep-ex/0306031.

[106] T. Lasserre, Workshop on Future Low-Energy Neutrino Experiments, 9-11 Oct. 2003, Munich, Germany.

[107] T. Kobayashi, private communications.

[108] D. Stump *et al.*, Phys. Rev. D **65**, 014012 (2002) [arXiv:hep-ph/0101051].